UNIVERSITY OF OKLAHOMA

GRADUATE COLLEGE

TENDON TISSUE ENGINEERING USING MESENCHYMAL STEM CELLS, THE HUMAN UMBILICAL VEIN, AND MECHANICAL STIMULATION

A DISSERTATION

SUBMITTED TO THE GRADUATE FACULTY

in partial fulfillment of the requirements for the

Degree of

DOCTOR OF PHILOSOPHY

By

RITA ISSA ABOUSLEIMAN
Norman, Oklahoma
2008

TENDON TISSUE ENGINEERING USING MESENCHYMAL STEM CELLS, THE HUMAN UMBILICAL VEIN, AND MECHANICAL STIMULATION

A DISSERTATION APPROVED FOR THE
DEPARTMENT OF BIOENGINEERING

BY

_____
Dr. Vassilios Sikavitsas, Chair

_____
Dr. Matthias Nollert

_____
Dr. Peter McFetridge

_____
Dr. Rong Gan

_____
Dr. Gerald Miller

.

To My Husband and Children

I would like to dedicate this work to my little family.

My husband, Younane, who continues to show me how life is beautiful

"Life is What You Make Out Of It;"

My two little angels, Ghainaa and Nassib, who were always proud of their mommy and understanding when she could not spend time with them because she has to "write her book".

ACKNOWLEDGEMENTS

I wish to express my sincere gratitude and appreciation to my advisor, Dr. Vassilios Sikavitsas, for his valuable contributions to this study. Without his active involvement and thoughtful suggestions this work would not have been completed. I would like to extend my sincere appreciation to Dr. Peter McFetridge for his assistance, continuous guidance, and helpful comments. I am grateful for my committee members for their support, active interest and constructive criticism: Dr. Mathias U. Nollert, Professor Rong Gan, and Dr. Gerald Miller.

I am greatly thankful and in debt to Dr. Nancy L. Mergler, Senior Vice President and Provost, for the financial support she provided, in the form of a research assistantship, for the full duration of my doctorate studies at the University of Oklahoma. I would also like to acknowledge the Women's Center in Norman Regional Hospital, Norman, OK for supplying the umbilical cords used in the current study.

I appreciate all the help provided by the CBME staff: Donna King, Terri Colliver, Vernitta Farrow, Sherry Childress, and Renee Ogan. I am indebted to Mr. Alan Miles for his assistance in building all the experimental setups involved in this study, and for his skillful handling of all the different kinds of problems that we faced during testing. Special thanks to the undergraduate and graduate students whose assistance in the laboratory was so valuable and efficient: Laurence Rustom, Yuliana Reyes, Warren Yates, Hope Baumgarner, Ali Faramarzalian, and Shanna Sprinkle. I am grateful to my lab mates for their support and encouragements: Jose Alvarez, Zehra Tosun, Bonnie Landy, Erica Brown, and Sam VanGordon. I am in debt to my Mother,

Ghainaa, and Father, Issam, who encouraged me to pursue my doctorate degree and were always proud of my little accomplishments.

I keep the most special acknowledgements to last. I would like to express my deepest gratitude to my little family, the center of my life: My husband, Younane, who inspired me several times, and gave me strength and determination to achieve my academic goals. I appreciate all the words of encouragement, patience, kindness, and love he showed me. I would like to thank my precious kidos, Ghainaa and Nassib, for all the support and enthusiasm they showed. They came with me on numerous occasions to the Laboratory and helped me “feed the cells” by filling up pipette tip boxes.

TABLE OF CONTENTS

LIST OF TABLES

LIST OF FIGURES

ABSTRACT

The umbilical cord is a biological tissue that is readily available and is usually discarded. Previous studies suggested the use of the Human Umbilical Vein (HUV) as an acellular vascular grafting material. In this study, we attempt to develop a tissue engineered tendon model using HUVs as scaffolds coupled with Mesenchymal Stem Cell (MSC) therapy and with mechanical stimulation. HUV sections were dissected from fresh human umbilical cords, decellularized, and seeded with rat MSCs. A special bioreactor was designed to house and dynamically stimulate the constructs for periods of one and two weeks. Samples cultured without dynamic stimulation were used as controls. Dynamic stimulation resulted in 8 fold higher proliferation rates and significantly stronger (156%) and stiffer (109%) constructs compared to the controls. Microscopically, dynamically stimulated samples showed parallel orientation of collagen fibers and spindle-shaped cell nuclei mimicking the morphology of native tendons.

When higher seeding densities, of 5 and 10 million cells/ml were attempted extracellular matrix of the HUV significantly degraded, constructs had weaker mechanical properties, and cell bodies lysed after 2 weeks of culture. These results indicated that, for the current design, cells were not able to survive at original seeding concentrations higher than 5 million cells/ml. The limiting seeding density for unstimulated samples was calculated based on glucose consumption rates to be 3 million cells/ml. This value increases for stimulated constructs due to the enhancement of nutrients' transport through convective flow. The documented findings are limited by the design parameters and experimental protocols followed in this study.

Variation of these parameters, including HUV thickness, decellularization techniques, or stimulation scenarios, will significantly affect the results.

CHAPTER 1
GENERAL INTRODUCTION

Tendon injuries continue to affect a significant number of Americans yearly, and in many cases, prevent them from normal daily activities and work capabilities. The Bureau of Labor Statistics reported 44,504 tendinosis and/or carpal tunnel syndrome injuries in the private industry in the year 1999[1]. The same source reported that 57,420 total workers were affected from repetitive motion disorders in 2003[2]. Those who experienced tendonitis lost, on an average, 11 days of work.

Athletes are prone to Achilles tendon injuries more than the general public[3], with more than 232,000 injuries documented in 2002[4]. Athletes were prevented from participating in sports activities for up to one month in almost 50% of the cases, and for more than one month in another 25%. 66,000 patients were admitted to the emergency, hospitalized, or received therapy[4]. One quarter of Achilles tendon overuse injuries reported by athletes required surgery. Almost one fourth of those who underwent surgery required further future operations[4].

Tendons do not always heal, even with prolonged durations of rest and immobility. Common treatments include, strengthening, non-steroidal anti-inflammatory drugs, braces, and cryotherapy. When tendon replacement is inevitable, autografts and allografts are the available alternatives[5]. However, autografts are limited, require surgery in two different locations and result in donor site morbidity. Allografts are more readily available than autografts but in a significant number of cases they illicit an acute immune response[5]. Due to the limitations in the current tissue available for tendon replacements, there

is a need to engineer tendon-like tissue *in-vitro* that possesses comparable mechanical properties to the innate tissue and that would evade the immune response.

In this research a tissue engineered tendon model is developed by mechanically stimulating Mesenchymal Stem Cells (MSCs) seeded on decellularized Human Umbilical Veins (HUVs). The dissertation includes 8 chapters.

Chapter 1 is a general introduction that documents the aims of the research and summarizes the contents of the rest of the dissertation. **Chapter 2** includes and overview about tendon structure, biological composition and mechanical properties. Furthermore, tendon pathologies and available clinical treatments are documented. **Chapter 3** includes a literature review of tendon tissue engineering. The term "functional tissue engineering" is defined and the different aspects of this concept are documented including cells, scaffolds, seeding and stimulation techniques. The use of bioreactors in tendon tissue engineering is explored and the different stimulation techniques available are included. In **Chapter 4** the HUV is introduced as a potential scaffold for musculoskeletal tissue engineering in general and tendon tissue engineering in particular. The material properties of the HUV scaffold are documented including a comparison of the mechanical and morphometric properties among cellular, decellularized, and seeded HUVs. In **Chapter 5** the possibility of using the HUV as a scaffold for tendon tissue engineering is further investigated. A novel design of a bioreactor, termed as "Mechanical Stimulator for Tissue Engineering applications" (MSTE), is introduced. Constructs were stimulated in the MSTE

for 1 hour per day and cultured for periods of 1 and 2 weeks. The effect of stretching on the cellular, mechanical, and morphometric properties of the constructs was evaluated.

Mass transport limitation and diffusion of nutrients and growth factors through the wall of the HUV are explored in **Chapter 6**. The permeability of the HUV membrane to molecules with different molecular weights is computed, and a limiting molecule size beyond which particles are unable to diffuse through the HUV is estimated. In **Chapter 7** an attempt to optimize the seeding density of the tissue engineered constructs is demonstrated. HUVs with different seeding densities are tested and a potential optimal seeding density is reported. Finally, **Chapter 8** includes the conclusions of the research project, and future recommendations.

CHAPTER 2
TENDON PATHOLOGIES AND CURRENT CLINICAL TREATMENTS

2.1. INTRODUCTION

Most of total and partial tendon ruptures are due to occupational overloading and sporting activities involving lack of stretching, sudden exertion of force (examples include abrupt jumping or weight lifting) and sprinting movements[6,7]. In most sports and activities, overuse injuries, termed as "tendinopathies"[8], are the most common and challenging to diagnose and treat since the symptoms are often dispersed and non-specific[9]. Overuse of tendons causes continuous damage to the tissue that eventually escalates into a pathology when the repetitive strain overcomes the ability of the tendon to repair itself[9,10]. This might lead to tendinosis (tendon tissue degeneration without inflammatory response), tendinitis (tendon tissue degeneration with inflammatory response), edema, partial tears, or complete ruptures[8,11]. Some examples include tennis elbow, swimmer's shoulder, little league elbow, runner's knee, jumper's knee, and Achilles tendinitis[9,12].

In this chapter the biological composition and mechanical properties of tendons, different tendon pathologies and current available remedies are documented.

2.2. TENDON STRUCTURE

Tendons are collagenous anatomical tissues that transfer the load exerted on muscle into the bone[13,14]. The major type of cells in tendons are tenocytes; stellate cells scattered and sandwiched between parallel layers of

type I collagen fibers[15,16] (Figure 2.1). Tenocytes produce all the collagen and ground substance that composes this tissue.

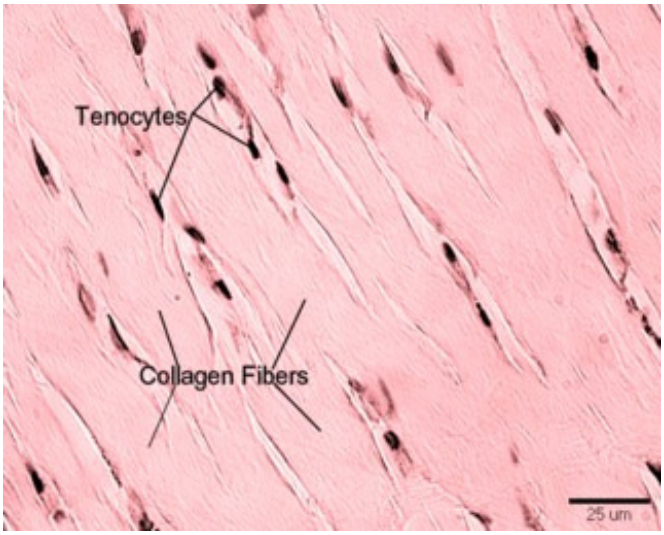

Figure 2.1: Histological longitudinal section of tendons.

Tendons are mainly composed of a tertiary hierarchal structure of parallel bundles of collagen fibers[17] (Figure 2.2) that are responsible for the tissue high tensile strength[18]. A collagen molecule, or tropocollagen, is composed of a right-handed triple helix α chains that include a glycine at every third position of the polypeptides and are rich in the amino acid proline[19]. Collagen fibrils are formed with packed tropocollagen molecules separated by a distance of 64 nm[19]. A collagen fiber is thus made up of a group of collagen fibrils.

A tendon primary fiber bundle, or subfascicle, is made up of parallel collagen fibers, following a wavy pattern, and tenocytes aligned with their longitudinal axes parallel to the collagen fibers (Figure 2.1)[20]. A bundle of subfascicles composes a secondary tendon fascicle. Similarly, a group of secondary fascicles forms a tendon tertiary fascicle. Covering the collagen subfascicles and fascicles is a layer of dense irregular connective tissue

termed endotenon[21]. The epitenon is the outermost layer of dense irregular connective tissue covering the whole tendon[17,21]. The paratenon is a loose connective tissue layer wrapping around the epitenon. The epitenon and paratenon could be lumped up in the term "peritendon"[17]. Tendons are not vascularised within the collagen bundles, however, large tendons are nourished by vasculature passing through the endotenon and epitenon layers[17,22,23]. Lacking an inclusive vascular network and composed of cells with low metabolism, tendons have poor intrinsic healing capabilities[8,24]. The healing tendon is more likely to deposit scar tissue in the injury site leading to a decrease in the strength of the healing tissue[25].

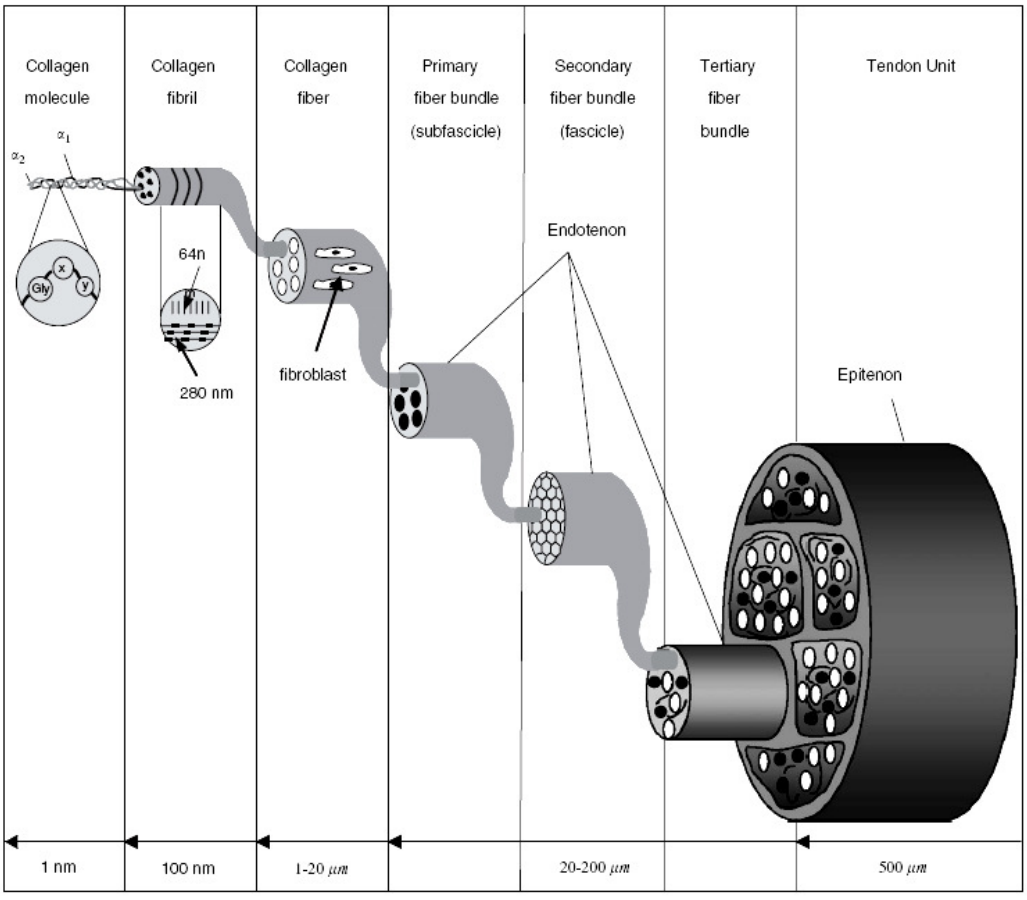

Figure 2.2: Hierarchal Arrangement of Tendon[26].

2.3. TENDON BIOLOGICAL COMPOSITION

The extracellular matrix (ECM) of tendons is mainly composed of collagen fibers[26]. Collagen type I is the most abundant and constitutes 95% of total tendon collagen content, 90% of the total tendon protein content[17], or 86% of the fat-free dry weight of tendons (DWT)[15,27]. Collagen type III, which is mostly present in the endotenon and epitenon[28,29], and collagen type V constitute most of the remaining 5% of collagen in tendons; however, minute amounts of collagen types II, VI, IX, X, and XI are also present[26]. Elastin only contributes 1% to 2% DWT[15,17]. It is suggested that the elastic fibers help the collagen fibers recover their configuration after stretching is ceased[30].

The ground substance of tendons include proteoglycans (1% - 5% DWT), glycosaminoglycans (GAGs) of which hyaluronic acid constitutes 6%[31], collagen type VI[27], and structural glycoproteins[15,17] such as Tenascin-C[26]. Proteoglycans mainly crosslink the collagen fibers together, forming the tendon subfascicles and fascicles[12]. The proteoglycan decorin is widely distributed in tendons[24,27]. It provides the structural support for the collagen fibers[18] and plays a primary role in regulating collagen fiber formation *in vivo*[15]. Fibromodulin, on the other hand, is present in sparse amounts in tendons[27]. The glycoprotein fibronectin binds collagen fibers and plays an important role in wound healing[17]

Tendons include two characteristic zones: the extension zone and the pressure zone. The extension zone of the tendon is around the myotendinous junction where the tendon connects the muscle[31,32]. The pressure zone, on the other hand, is where the tendon inserts into the bone through the osteotendinous junction or enthesis[31,32]. There is a difference in the

composition of the tendon between these two zones. The pressure zone includes up to 5% (DWT) GAGs while the tension zone includes only 0.2% (DWT) GAGs[33]. The major type of GAG in the pressure zone is chondroitin sulfate while in the tension zone it is dermatan sulfate. Heparin sulfate is mainly found at the myotendinous junction[31]. Microscopically, the osteotendinous junction is composed of four distinct regions: tendon, fibrocartilage, mineralized fibrocartilage, and bone[24,34,35]. The stellate cells of the tendon zone lose their characteristic ovoid shape and become rounded with shorter cell processes in the fibrocartilage zone where they stop expressing gap junction proteins[36]. This shows that cells communicate differently in the four distinct histological zones. In the fibrocartilage zone cell-cell interactions are overcome by cell/matrix and cell signaling interactions via growth factors and cytokines[36].

2.4. TENDON MECHANICAL PROPERTIES

Tendons have different anatomical locations in the body and thus different cross sectional areas relative to the muscles they are connected to[10]. Depending on the muscle they serve, tendons are subjected to different stress levels and therefore their tensile strength (σ), strain at maximum stress (ε), and modulus of elasticity (E) vary significantly (σ: 50-105 MPa, strain, ε: 8%-14%, and E: 1.2-1.8 GPa)[15,16,32]. However, these values are much lower for physiologic forces (σ: 15-30 MPa, ε: 1%-4%, and; E: 1.2GPa) [37,38]. Tendons are subjected to different loads during different sporting activities[39]. For instance, walking applies only 2600N of force on the Achilles tendon as opposed to an average force of 4200N due to running[40]. Moreover, blood flow in the peritendinous region increases due to excercise[7].

Tendons are characterized as being viscoelastic[24,41] due to the highly hydrated nature of the tissue and the sliding and slipping interactions between collagen and the rest of the ground substance[26]. Being viscoelastic, they form a hysteresis loop upon loading and unloading with the area under the hysteresis loop representing the energy released. Stress relaxation and creep are the two tests that demonstrate viscoelasticity[24,30]. During the stress relaxation test, the sample is subjected to a constant strain allowing the stress in the tissue to decrease with time. While in the creep test the tendon is stretched with a constant force while the tissue lengthens with time[41].

Figure 2.3 shows a typical stress strain curve of tendons[26]. Collagen fibers in tendons have a wavy morphology termed as "crimp"[12,42]. This crimp property enables the tendon to initially elongate, straightening the collagen fibers, at about 2% strain[43], without a significant increase in the stress experienced by the tissue[7], thus protecting the muscle during abrupt high loading events[12]. Due to the crimping of collagen fibers, tendons act as springs that store energy to be released upon exertion of force, thus transmitting the force from the muscle to the bone[12]. Crimp property of the tendon is responsible for the original nonlinear or "toe" region in the stress-strain curve, where collagen fibers stretch out and become straight loosing their crimp; then they reorient parallel to the direction of stretching[44]. Thus, the range of this region, typically around 2% strain[26], depends on the extent of waviness of the collagen fibers. Physiologic loads cause strain values of up to 4%[12,20,43] where the loading is totally reversible[12] and the crimp is reproducible[20].

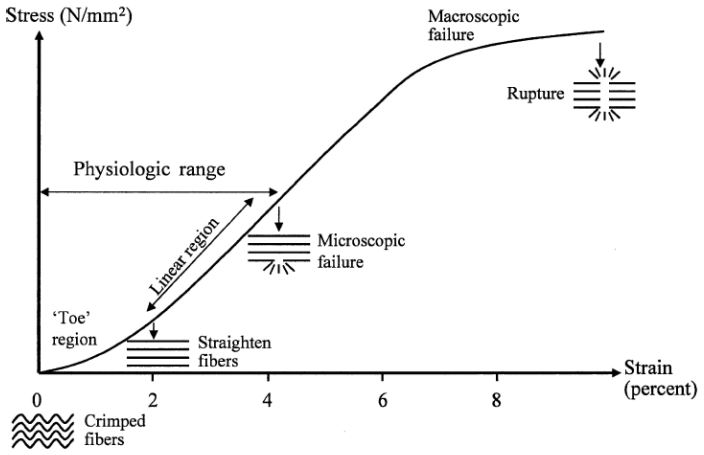

Figure 2.3: Typical stress strain curve for human tendons showing the four distinct regions: Toe region, linear region, microscopic failure region, and macroscopic failure region[26].

The region in the stress-strain curve that spans between 2% and 4% strain is termed the linear region where the stress increases proportionally to the strain and the constant of proportionality is known as the modulus of elasticity, E[12]. Region III is between 4% and 8% strain where the original wavy form of the fibers is not reproducible[20] since the strain was directly applied to the aligned and straightened collagen fibers causing them to either slide adjacent to other fibers or stretch further and deform[45]. In region III some of the collagen fibers rupture causing microscopic tears[43] decreasing the effective cross sectional area of the tendon[44] causing an increase in the stress value that the tendon is experiencing, and thus a decrease in the stiffness of the tissue with increased strain[26]. Strain values beyond 8% will cause macroscopic tears leading to tendon rupture at almost 12% strain[10,30,46,47].

Tissue mechanical adaptation is the process by which cells sense the external mechanical loading they are subjected to and respond by altering their structure, or secretion pattern[26] (Figure 2.4) leading to either tissue

regeneration or degeneration. However, the mechanotransduction mechanisms by which tenocytes convert mechanical signals into biochemical signals are still unclear to date[26]. Tenocytes communicate with one another via a three-dimensional network of cell processes and gap junctions which could be responsible for the ability of cells to detect external mechano-signals[36,48]. This initial detection leads eventually to the final gross response that affects the tendon tissue as a whole[43].

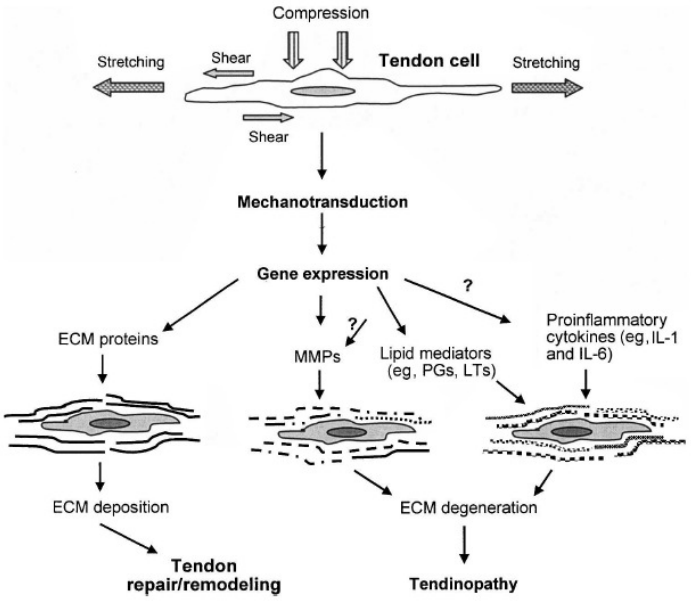

Figure 2.4: The biological responses of tenocytes due to mechanostimulation. Depending on the loading regime (duration, rate, magnitude) cells could either signal for tissue remodeling or degeneration[43].

Strain values that load the tendon ¼-⅓ its ultimate strength will potentially cause tendon rupture[49,50]. However, not only high strain and loading regimes cause tendon pathologies, including tendinitis and tendinoses or total rupture. Long term repetitive submaximal loading[43] will eventually lead to inflammation and might provoke matrix degradation[26,43], and cause fibrillar tears that would weaken the tissue[51,52]. Moderate exercise, on the other hand, signals ECM deposition[36,53,54], thus an increase in tendon cross

sectional area, which increases the stiffness of the tendon[55,56]. It also causes an increase in the expression of proteoglycans[36,54], matrix metalloproteinases (MMPs) for ECM remodeling[7], and blood flow through the outer layers of the tendon[7].

2.5. SYMPTOMS IN TENDON PATHOLOGIES

Healthy tendons have a white gleaming appearance that radiates under polarized light[8]. Microscopically, they are composed of parallel continuous bundles of collagen type I and spindle shaped cells longitudinally sandwiched between the collagen fascicles. Due to overuse or injury, tendons loose the glittering, become grayish or brownish in color[8], and get inflamed[43]. Collagen fibers undergo degeneration[16] and morphological alterations and cells proliferate causing hypercellularity in the affected area. Moreover, protein expression is altered causing a change in the properties and morphology of the tendon tissue. For example, tenocytes start depositing Type III collagen instead of Type I collagen which causes a decrease in the mechanical strength of the tendon[57-59].

In general, tendon pathologies could be classified into three main categories: tendinosis, tendinitis, and paratenonitis[8,10,16]. Tendinosis is a non-inflammatory degeneration of the ECM and fibers accompanied with a grayish appearance of the tissue[8-10,16,22,60]. A partial rupture is always surrounded by a non-inflammatory lesion suggesting that partial rupture is a complication of tendinosis[18]. Since tendinosis is a non-inflammatory pathology, steroid injections failed to alleviate the symptoms of this condition. A study was performed on 298 patients who suffered from chronic Achilles tendinopathies. Most patients complained of mornings stiffness, tenderness, and pain on

exertion[3]. In many cases steroid injections caused more advanced tendinosis and more frequent ruptures[61].

The pathology is termed as tendinitis when the tendon exhibits an inflammatory response[8,43,62-64]. It was shown that as soon as one day after tendon injury neutrophils and macrophages accumulate at the affected site and elicit an inflammatory response[65]. In this case non steroidal anti-inflammatory drugs (NSAIDS), corticosteroids, and steroid injections are successfully used to alleviate the pain and stop the inflammation. Paratenonitis is associated with the inflammation of the paratendon layer surrounding the tendon tissue[8,10,16].

In a review about tendon pathologies it was reported that abnormal tendons share some common features such as degeneration of collagen fibers, an increase in cellularity[66] leading to an increase in vasculature[67] and mucoid ground substance, and a reduction in strength[8,60,68,69]. Moreover, there seamed to be an increase in collagen type III production causing a decrease in the strength of the tissue[8,11,57-59]. Degradation of collagen fibers in injured tendons could be due to tenocyte upregulated expression of MMP1[70]. Tendons with changes in collagen morphology and ground substance were accompanied by changes in tenocyte morphology. The cytoplasmic area of tenocytes enlarged and their nuclei became rounded[32]. In all cases reviewed it was evident that there was a lack of inflammation suggesting that these pathologies were rather tendinosis[22,71].

To investigate the causes of hypercellularity a study was conducted on 11 patients having patellar tendinosis[66]. In all cases high cell proliferation rates were associated with an increase in the expression of platelet-derived

growth factor receptor beta (PDGFRβ) compared to the healthy controls. This suggests that hypercellularity is due to the upregulation in the expression of PDGFRβ [66] [72]. Furthermore, hypercellularity in tendinosis was verified by analyzing the expression of proliferation cell nuclear antigen (PCNA)[66]. This protein appears to be present only in proliferating cells[66].

2.6. CURRENT CLINICAL TREATMENTS

Common treatments to tendinosis and tendinitis include, but are not limited to, rest, strengthening, non-steroidal anti-inflammatory drugs, corticosteroids, braces, cryotherapy, and surgery[8]. Heat pads or cryotherapy could temporary alleviate pain associated with tendinitis. Bracing and immobilization relieves the stress from the tendon and helps it heal. However, prolonged immobilization causes a decrease in the strength and other mechanical properties of the tissue. As a result rehabilitation and therapy is required after a period of immobilization, which usually leads to an additional inflammatory response depending on the extent of therapy. After being stretched due to physiotherapy, tenocytes started secreting interleukin 6 (IL-6), which is partly responsible for the inflammatory response[73].

Even though NSAIDS and corticosteroids have been used to treat tendinitis, a non-inflammatory pathology, these therapies had minimal effects on the symptoms[8-11,18]. When preventive measurements fail, doctors attempt operative techniques such as excising the degenerated and abnormal parts of the tendon[61,74]. In case of total tendon rupture, and when the defect is less than 2 cm[75], suturing techniques provide adequate mechanical strength for the tissue and diminishes the gap between the tendon stumps. However, tendon replacement might be a necessity for defects larger than 2 cm, or in

case of peripheral nerve injury. Currently autografts, allografts, xenografts, and prosthetic devices are being used in tendon replacement surgeries[24,76]. The primary source of autografts is the hamstring[77,78]. Other options are the flexor digitorum longus[79], flexor hallucis longus[79] and semitendinous tendons[80]. Donor site morbidity and inflicted pain are the two major problems in autografts. On the other hand, most individuals using allografts and xenografts develop an immune response[81]. Synthetic grafts, such as carbon fibers[82-84], polyester fibers[84], polypropylene mesh[85], and dacron[86,87] result in decreased mechanical properties of the healing tissue[88] and moreover their integrity is compromised with increased usage[89], which leads in many cases to reruptures[90].

Due to the limitation in the current available treatments for tendon pathologies and injuries researchers started exploring other alternatives. Tissue engineering provides several choices for tendon replacements and thus a functional solution for the common and recurring problem of tendon pathologies.

2.7. CONCLUSIONS

Tendons are mainly composed of type I collagen bundles which are responsible for the tissue high tensile strength properties permitting it to act as a bridge transmitting the load exerted on muscles into bone. Most tendon injuries result in the degeneration and morphological alteration of collagen fibers. The exact causes of collagen degeneration are still not very well understood. In general, tendon pathologies are a result of overuse rather than trauma. Since tenocytes have low metabolic activity tendon healing, when possible, requires prolonged durations of rest and immobility. Current

surgical techniques to fix tendon ruptures have several limitations including decreased mechanical properties of the healed tissue, limited availability of autografts, high potential for inflammation and disease transmission from allografts and xenografts, and short functional lifetime of prosthetic devices.

Lacking a satisfactory clinical treatment for tendon pathologies research has been directed toward exploring alternative approaches. Tissue engineering provides several functional choices for tendon replacements. The different aspects of tendon tissue engineering are further discussed in Chapter 3.

CHAPTER 3
TENDON TISSUE ENGINEERING: LITERATURE REVIEW

3.1. INTRODUCTION

Tendons malfunction either due to a natural injury, trauma, or a disorder. In all cases natural regeneration needs to be enhanced by medication and, in many instances, by surgery. Surgical techniques are limited to suturing, autografts, allografts, xenografts, and prosthetics[24,76]. Tendon tissue engineering stems from the challenge presented by the limited resources for natural implants and the ineffectiveness of previous curing approaches. Since the native tendon tissue is subjected to stretching during physiological activities, and since Immobilization significantly lowers its ultimate strength[30,52,53,91], it is desirable to incorporate mechanical stimulation techniques in tissue engineered tendon models in an effort to mimic the *in vivo* environment. The challenge in tissue engineering resides in the design of a functional bioreactor that would: (1) house the engineered construct under sterile conditions; and (2) provide the appropriate stimuli that would result in a *neo tissue* with biochemical and biomechanical properties comparable to the *in situ* tissue. The various aspects of tendon tissue engineering and recent developments in that field are presented in this chapter.

3.2. FUNCTIONAL TISSUE ENGINEERING

Tissue engineering uses the principles of engineering, biology, and chemistry in designing a *neo tissue* that would augment a malfunctioning *in vivo* tissue[92]. Since the traditional methods of treating tendon injuries and

disorders are not completely effective and have several limitations, tissue engineering has gained remarkable support as an approach to treat tendon disorders circumventing the limitations of existing therapies[19,93].

The main requirements for a functional engineered tissue include reparative cellular components that proliferate on a biocompatible scaffold grown within a bioreactor which provides specific biochemical and biomechanical signals to regulate cell differentiation and tissue assembly[89,93-95]. Further explanation and elaboration on the different components of functional tissue engineering for tendon applications are included herein.

3.2.1. Cells

Cells are by far the most important component of an engineered tissue. They are the living component of the construct. Given the suitable environment cells would start secreting matrix that would eventually form the *neotissue*. The type and properties of secreted matrix depend on the different stimuli that cells are subjected to. For tendon tissue engineering fibroblasts and tenocytes have been commonly employed[96-98]. It is imperative that cells used in the tissue construct have the ability to proliferate and deposit matrix at a high rate in order to be able to implant the *neo tissue* in the patient soon after the injury. Primary tenocytes are almost mature and do not proliferate at a high rate[99]. Another type of cells that is abundant and has been widely exploited to treat tendon defects *in-vivo*[100-103] and in tendon tissue engineering *in-vitro* [102,104,105] is Mesenchymal Stem Cells (MSCs).

MSCs are undifferentiated pluripotent cells that have the potential to differentiate into a number of mature cells of different lineages, depending on

the biochemical and biophysical stimuli that they are subjected to[106-108]. These lineages include, but not limited to, osteoblasts (bone)[109-114], chrondocytes (cartilage)[111-114], hepatocytes (liver)[115], adipocytes (fat)[112,113,115], glial cells (neural tissue)[112,116,117], and fibroblasts (tendon and ligament)[94,114,118,119]. The most popular source of MSCs is the bone marrow, however, pluripotent stem cells have also been extracted from other anatomical locations such as the subcutaneous adipose tissue[120], and the Wharton's Jelly[105]. Although the number of MSCs decline dramatically with age, their ability to differentiate and repair tissue is retained[96]. Being intermediate between embryonic and adult tissue MSCs may provide an *in situ* source of healing cells throughout an adult's lifetime[121].

MSCs were found to undergo cell fusion in the case of tissue damage, rescuing dying cells by supplying extracellular matrix (ECM) and organellar components[115]. They provide a beneficial environment for damaged tissue by secreting cytokines and trophic factors[115]. However, fetal bovine serum (FBS) is a requirement for the culture of MSCs. As a result, MSCs cultured and expanded in FBS might elicit an immune response in some individuals. To evade the immune response MSCs could be cultured for two days in the serum of the host, prior to being injected.

3.2.2. Scaffolds

Cells are greatly affected by the surface to which they adhere. The type and properties of the scaffold used for seeding could alter the proliferation rate and ECM deposited by cells, and thus affect the final biomechanical and morphological properties of the engineered tissue[93]. The primary objective of using a scaffold is to provide mechanical stability and

integrity to the construct and to supply a template for three-dimensional organization of the developing tissue[93]. The final goal is to obtain *de novo* tissue with biomechanical properties comparable to the damaged tissue.

The scaffold used for tissue engineering must be non-toxic and biocompatible, i.e. evades the immune response. Biocompatible scaffolds could be either polymeric (non-biodegradable or biodegradable) or biological. However, a second surgery might be necessary to remove the implanted non-biodegradable scaffold after the tissue heals. If using a biodegradable polymer it is imperative that (1) the degradation products be biocompatible as well, and (2) the degradation rate of the scaffold be comparable to the tissue repair rate so that the implanted construct does not loose its mechanical integrity[76,89].

3.2.2.1. Polymeric Scaffolds

Non-biodegradable scaffolds include carbon fibers[82-84], polyester fibers[84], polypropylene mesh[85], and dacron[86,87]. As mentioned in chapter 2, these scaffolds result in decreased mechanical properties of the healing tissue[88] and they have a limited operative duration[89].

Biodegradable scaffolds include synthetic poly α-hydroxy ester (PHE) polymers such as polylactic acid (PLA)[122], polyglycolic acid (PGA) and its co-polymer with PLA (PLGA)[75,77], poly L-lactic acid (PLLA)[123], polycaprolactone (PCL)[122], poly N-acetyl-D-glucosamine (chitin)[122], polydioxanone[124], and composites like chitin/PCL[122,125]. Extensive research is being conducted on the regeneration of *in vivo* tissue using PHE. Since PLGA and its degradation products are non-toxic and biocompatible, and since its degradation rate can be tuned to follow the rate of formation of human tissue[125], this material has

gained the approval of the U.S. Food and Drug Administration for degradable sutures and it is currently investigated for a variety of human clinical applications[126].

Polymeric scaffolds have adequate initial tensile strength to act as tendon replacements; however they do not always evade the immune response, and once degraded the strength of the resulting construct decreases significantly. In general PLLA scaffolds have been shown to be a better scaffold for tendon and ligament tissue reconstruction than PGA[97,123].

Tenocytes were harvested from deep flexor tendons of hen feet and seeded ($20x10^6$ cells/ml) on PGA unwoven fibers[75]. The constructs were stretched continuously and were compared to the un-stretched controls. Six weeks post-seeding experimental samples showed parallel alignment of type I collagen with tensile strength values three folds higher than the controls. The authors extended their investigation to an *in-vivo* model in which they wrapped their PGA seeded constructs with intestinal submucosa and cultured them *in-vitro* for a week prior to transplanting them in hens flexor tendons defects [77]. Eight weeks post surgery the defect was bridged by a collagenous tube like structure with randomly shaped fibers and abundance of tenocytes. The PGA fibers in the defect area were not degraded and surrounded by inflammatory cells. Moreover, the tensile strength of the construct was similar to that of the biomaterial without cells reflecting that after 8 weeks of culturing *in-vivo* the remodeling action of cells did not account for any additional mechanical strength or tendon-like morphogenesis.

When implanted *in vivo* replacing Achilles tendon defects of Japanese white rabbits PLA and chitin/PCL scaffolds allowed deposition of collagen type

I and III, however, there was a significant decrease in the ultimate strength of the constructs 26 weeks after surgery for all tested materials[122].

Given the problems faced when using polymeric scaffolds, such as: the rate of degradation of the material, immune response development, and inferior mechanical properties; another source of scaffolding material was necessary. Biological scaffolds represent an alternative potential source for tissue engineering.

3.2.2.2. Biological Scaffolds

The use of natural acellular biomaterials as scaffolds for tissue engineering is very desirable since these materials, when processed properly, elude the immune response. Collagen gel is used extensively as scaffolding material for tendon and ligament applications[13,98,127,128]. However, constructs engineered with seeded collagen gels had inferior mechanical strength (<0.15 MPa after 2 weeks of seeding[13,128,129]) compared to human tendons (60-125 MPa[130]). Other recent options for biological scaffolds are small intestinal submucosa[131,132], collagen fibers[133], and Human Umbilical Veins (HUVs)[134]. The advantage of using these materials is that they have initial ultimate stress and stiffness values significantly higher than collagen gels.

3.2.2.3. The Human Umbilical Vein

The HUV is one of three vessels present in the human umbilical cord (Figure 3.1). It possesses longitudinal stiffness comparable to human tendons and ligaments (> 10 MPa[79]) and a tensile strength (1.56±1.04 MPa[79]) ten folds higher than seeded collagen gels. However, the non uniform thickness of the vein due to the manual dissection of the cord resulted in

significant variation in its mechanical properties[79,134]. A novel automated dissection technique has proven to render cords with more uniform thickness and surface morphology resulting in less variable mechanical properties[134].

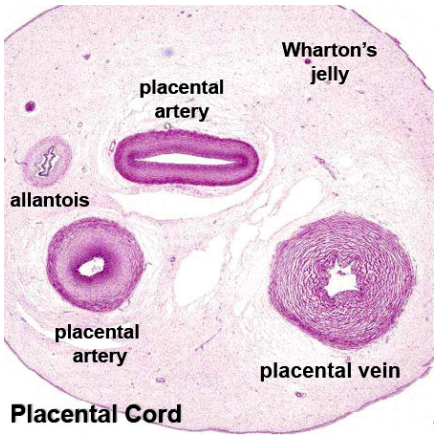

Figure 3.1: Histologic cross section of the umbilical cord[135].

The Wharton's jelly constitutes the embryonic connective tissue of the umbilical cord that surrounds the blood vessels[136] and protects them from external mechanical forces[137]. The HUV matrix is primarily composed of collagen and is rich in GAGs, mostly hyaluronic acid (70% of total GAG content)[138,139], and the proteoglycan decorin[138]. It is affluent with different growth factors including insulin-like growth factor[140], fibroblast growth factor[136], transforming growth factor beta[136,141], platelet-derived growth factor[136] and epidermal growth factor[136,141]. With such a composition abundant with growth factors, GAGs and proteoglycans, the HUV probably provides an environment that supports cell proliferation and ECM deposition.

3.2.3. Seeding Techniques

A large number of cells is required on the scaffold to achieve successful ECM deposition *in vitro*[142,143]. The final construct cellularity has been found to be relatively independent of the cell seeding number; however,

ECM components deposited were optimized with increased cell seeding density[144,145]. Moreover, uniform cell seeding is required to obtain homogeneous tissue formation throughout the scaffold especially in the central part[92]. Thus, optimizing seeding density and homogenizing seeding techniques are two critical components of functional tissue engineering.

3.2.4. Stimulation Techniques

Cells within a construct respond and adapt to the chemical and mechanical stimuli to which they are exposed *in vivo*[93]. To achieve efficient cell proliferation, proper differentiation and sufficient matrix deposition it is necessary to replicate the actual tissue environment. There are mainly two types of stimulation techniques: chemical and mechanical.

Chemical stimulation involves the addition of growth factors to the culture media. Growth factors are polypeptides that support various terminal phenotypes and stimulate cell proliferation[19,93]. Some of the most commonly used growth factors are transforming growth factors-β (TGF-β) which regulate stem cell recruitment and differentiation[146-148]; bone morphogenetic proteins (BMP) induce *in vivo* osteogenesis[146,149-151]; and fibroblast growth factors (FGF) are known to support angiogenesis especially in tendon and ligament tissue[104,147,152].

In vivo, cells and tissues are continuously subjected to mechanical stimuli that affect the tissue's developing morphology[153] and its biomechanical properties[154]. Thus it is important to replicate these loading regimes *in vitro* when attempting to develop a *neotissue*. As such, most of researchers incorporated stretching techniques in their bioreactor designs for tendon tissue engineering[94,98,129,155-158].

3.3. BIOREACTORS IN TISSUE ENGINEERING

A bioreactor is a device that provides a controlled sterile environment for the development of engineered tissue[92]. It confines the cultured cells within barriers that mimic the physiological conditions and provide mechanical stimulation to enhance mass transfer and nutrient transport within the seeded cells[89]. The dynamic environment within bioreactors has been shown to affect the phenotype of differentiated MSCs, the deposition of ECM components, and the growth and development of tissue[92].

There are several approaches for designing bioreactors for tendon tissue engineering. One possibility is to implant a conductive scaffold in the injury or diseased site that would give the tissue mechanical integrity prior to rejuvenation (*in vivo* bioreactor). Another approach is to seed the scaffold with autologous cells *in vitro* and then implant it into the defect site. A third approach is to engineer the whole tissue or organ *in vitro*, using a biocompatible scaffold, and only implant it in the patient when the morphological, biological and biomechanical properties of the engineered construct match those of the natural tissue (*in vitro* bioreactor).

Currently several designs of bioreactors are employed for different types of tissue culture. The different existing bioreactors for culturing tendon tissue are included henceforth.

3.3.1. Static Cultures

Static cell culture has been widely used in the past. The cells are deposited on a scaffold, supplied with the appropriate growth media, and cultured in an incubator. However, numerous studies have shown that static cultures result in a non-homogeneous cell distribution[159]. Moreover, transport

of nutrients into large scaffolds have been proven to be problematic[142] and consequently cells may grow preferentially at the periphery of the scaffold[160,161]. In this case ECM components would be deposited only on the external surface giving the engineered construct non-uniform morphological and biomechanical properties. The presence or absence of mechanical stimulation primarily affects the final ECM deposited in the engineered constructs[114,128,173].

Tendon tissue *in vivo* is subjected to mechanical stimulation, and thus static cultures cannot mimic the physiological environment and will not be capable of replicating the *in vivo* tissue. As such, it is imperative to apply a mechanical force during the culturing process to produce a phenotypically proper tissue[159,162,163]. Static cultures currently serve as controls to evaluate bioengineered tissue.

3.3.2. Autologous Cell Transplants

Autologous cell transplantation includes harvesting functional cells from the patient, proliferating them *in vitro*, and implanting the expanded cell culture in the defective or injured segment of the tissue. The transplanted cells secrete healthy natural ECM that would augment the deficiency in the tissue.

In a number of studies autologous MSCs were implanted in rabbit tendon defects[100,102,103]. In all cases engineered tendons demonstrated significantly higher mechanical properties than naturally healing tendons, but inadequate strength and stiffness compared to natural tendons. Moreover, ectopic bone formation was noted in one study[102]. In another study MSCs in the treated tendon remained round and collagen fibers did not align in a

parallel direction, possibly indicating that transplantation of MSCs without any chemical or mechanical stimulation did not affect the microstructure of the tendon[103].

3.3.3. *In Vivo* Bioreactors

The approach of *in vivo* bioreactors depends on the conductive properties of the implanted scaffold to recruit tenocytes and MSCs from the neighboring tissue. This approach takes advantage of the physiological environment to supply the necessary growth factors and nutrients to the construct. The main challenge is to find the appropriate scaffolding material that would induce the infiltration of cells and the differentiation of MSCs into an adequate lineage.

A polymeric fiber scaffold made of polylactide-co-glycolide was designed to serve as an *in vivo* bioreactor for tendon and ligament tissue regeneration[97]. The mechanical and morphometric properties of the scaffold were optimized *in vitro* to match those of the native tissue. However, no data was reported on the behavior of the scaffold once implanted *in vivo*.

Another example of a tendon *in vivo* bioreactor is a biological scaffold prepared by decellularizing the flexor digitorum profundus (FDP) tendon[164]. After decellularization and optimized modifications, the FDP had an increased porosity to allow cellular migration through the scaffold. It was reported that the novel design of the FDP scaffold proved to be cytocompatible *in vitro* and allowed tenocytes' infiltration *in vivo* without showing any significant immune rejection. Moreover, the scaffold retained almost 78% of the strength and stiffness of the native tissue prior to implantation.

3.3.4. *In-Vitro* Bioreactors

Several designs of bioreactors have been implemented to mechanically stimulate tissue constructs *in-vitro* [94,98,129,155-158]. All of the designed models use a motor to apply cyclic loading to the constructs under sterile conditions. The constructs are placed in a closed environment, fixed at one end and attached at the other end to an actuator that applies cyclic loading (Figure 3.2).

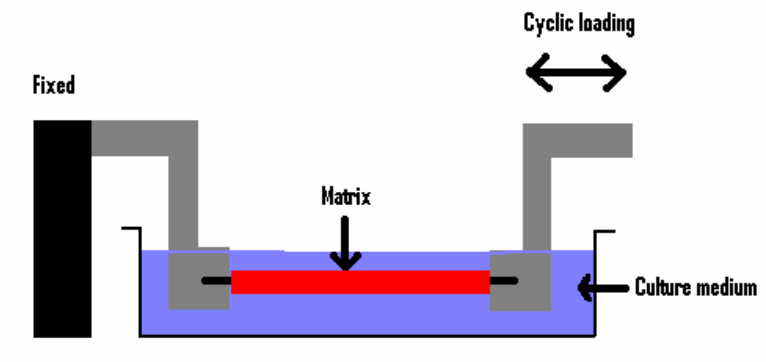

Figure 3.2: Simple design of a cyclic traction device[5].

The number of constructs that could be stimulated simultaneously using a single motor ranged from a single construct[5] to up to six constructs[157]. In some designs the actuator is controlled by a computer[129,157] for accurate application of loads, and the applied loading and resulting extension are monitored by a load cell and linear variable differential transformer (LVDT), respectively[156,157].

3.4. Chemical Stimulation in Tendon Tissue Engineering

Most of the growth factors studied in tendon tissue regeneration lead to an increase in matrix synthesis. For instance, platelet derived growth factor (PDGF)[165], insuline-like growth factor (IGF)[165,166], epidermal growth factor (EGF)[165], and fibroblast growth factor (FGF) [167] all increased cell proliferation

and matrix synthesis. Growth and differentiation factors 5 and 6 increased tensile strength of tendons[168], and induced *neotendon* formation[169].

Limited research has been conducted on the effect of growth factors on the differentiation of MSCs into a tendon lineage. The addition of fibroblast growth factor 2 in low doses (3 ng/ml) appears to increase the proliferation rate of MSCs and enhance the mRNA expression of some tendon markers (collagen types I and III and fibronectin)[104].

Most of the Bone Morphogenetic Protein (BMP) family directs MSCs into osteoblastic lineage, however, it has been reported that BMP12 rather directs these cells towards a tendon lineage[170]. In addition, this growth factor may play a role in early phases of tendon tissue regeneration[171]. Figure 3.3 shows the signaling pathway of BMP. BMPs are members of the transforming growth factor β (TGF-β) family which have a unique two-type serine/threonine kinase cell surface receptor. The initial binding of the BMP domains to the kinase receptors activates the signaling cascade[172]. Originally, type II receptor kinase phosphorylates the type I receptor, which in turn phosphorylates the signaling molecules Smads 1, 5, and 8. Upon phosphorylation, these cytoplasmic molecules bind to Smad4 and translocate into the cell nucleus activating the transcriptional factors for the early BMP response genes[172].

Bone Marrow MSCs transfected with BMP12 seem to differentiate into tenocytes[170,173]. The transfected cells became slimmer with thinner processes and more organelles than MSCs. Moreover, the transfected cells showed an increase in the production of type I collagen[173,174] and they were positive for CD44 and negative for HLA-DR suggesting that they are not fibroblastic.

Growth and differentiation factor 7 (GDF7), the homologous of human BMP-12 in mice, induced mice *neotendon* formation[174]. MSCs could be further directed toward a tendon lineage through the effect of the signaling molecule Smad8[118]. When MSCs were transfected with the active biological form of Smad8 (Smad8 L+MH2), the cells started to exhibit tenocyte morphological characteristics and gene expression[118].

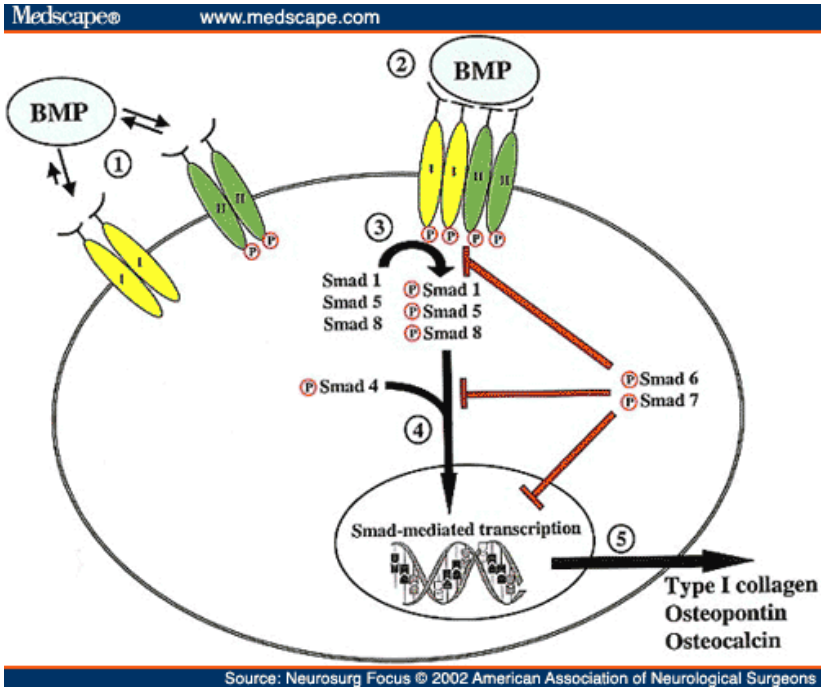

Figure 3.3: Signaling Mechanism for BMPs[175].

3.5. MECHANICAL STIMULATION IN TENDON TISSUE ENGINEERING

Tenocytes have been widely found to respond to mechanical stimuli[24,62]. This is only logical since tenocytes undergo mechanical stretching in their *in vivo* environment due to normal daily activities. Being in close proximity in the longitudinal direction, and connected by gap junction[176], these cells need to communicate to grow[48]. As a result, tendons need to protect their gap junctions when they undergo mechanical stretching[176]. It has been shown that tenocytes contained actin stress fibers that spread along their

longitudinal axes and intersect fibers from other tenocytes through adherens junctions[176]. It seams that when subjected to mechanical loading tenocytes protect their gap junctions by adhering more strongly together via their stress fibers. It is suggested that these contractile stress fibers may provide a dynamic stress recovering mechanism[176].

Immobilization lowers the ultimate strength of tendons eminently[30,52,53,91], whereas moderate exercise increases the stiffness and strength of the tendon[55,56]. Moreover, mechanostimulation increases the secretion pattern of important growth factors in tendons such as: TGF-β, basic FGF; and PDGF[147]. This reveals that stretching may have a positive influence on tendon healing[147]. As a result, tissue engineers incorporated cyclic and continuous stretching in their soft tissue replacement designs[13,94,98,155].

Mechanical stimulation of collagenous constructs seeded with MSCs increased the expression of ligament and tendon markers, namely collagens type I and type III[94], fibronectin[94], and tenascin-C[94,177]. These results indicate that MSCs could differentiate into tenocytes under the sole action of mechanical stimulation. However, poor mechanical properties of cultured collagen gel constructs prevent their use *in-vivo* for tendon replacement[178].

Upon the application of longitudinal force to tissue constructs, cells aligned in the direction of stretching[158,179,180] giving the construct a tendon-like appearance[13]. Two-dimensional tissue sheets deposited by human fibroblasts were subjected to static continuous mechanical loading[158]. Stretching induced cell and ECM alignment and increased the tensile strength and modulus of the tissue. Rat knee patellar tendons were transplanted into the subcutaneous tissue where they were cyclically stretched for 4 weeks.

Stimulated tendons were significantly stronger than non-stimulated constructs and possessed comparable strength to the natural tendon[181]. Human patellar tendon fibroblasts were cultured on silicone dishes and were cyclically stretched for different durations[98]. Stretching for 15 or 60 minutes/day resulted in an increase in DNA and collagen syntheses. Similar results were documented when embryonic tendons were subjected to cyclic loading[182].

It is important to mention that although mechanical stimulation affected the ultimate properties of the constructs, the form of load applied played an important factor. In a study comparing the effect of static[183] and cyclic stress[156] on the biomechanical properties of collagen fascicles it was reported that tensile strength and elastic modulus of cultured collagen fascicles strongly depended on the form and magnitude of stress applied. The study concluded that cyclic stresses work more effectively than static stresses in the biological system.

3.6. CONCLUSIONS

Tissue engineering provides a functional solution for the limited resources of natural implants and the ineffectiveness of present curing techniques for tendon diseases and injuries. The challenge of this approach resides in the design of a functional bioreactor that would provide the appropriate stimuli to the seeded biocompatible scaffold, under sterile conditions, resulting in a construct with biomechanical properties comparable to native tendons.

Several designs for bioreactors have been employed to engineer constructs capable of replacing the injured tendon, but the most effective ones incorporated mechanical stimulation in their designs. Using functional tissue

engineering concepts researchers were successful in engineering tissue with cellular density and morphology that closely resembled tendons. However, the mechanical properties of the *neotissue* were inferior to that of the *in vivo* tissue. As a result, there is a need to further explore the effects of biochemical and biomechanical stimulations on the microenvironment of cells and create innovative techniques to optimize the mechanical properties of engineered tissue.

A novel biological scaffold for musculoskeletal tissue engineering in general, and tendon tissue engineering in particular is introduced in Chapter 4.

CHAPTER 4

THE HUMAN UMBILICAL VEIN AS A POTENTIAL SCAFFOLD FOR MUSCULOSKELETAL SOFT TISSUE REGENERATION

The contents of this chapter were published in the Journal of Artificial Organs, volume **32**, issue 9, pp. 735-741, 2008.

4.1. INTRODUCTION

Musculoskeletal soft tissues that include tendons and ligaments, possess high tensile strength values compared to other tissues, but have poor intrinsic healing capabilities[8]. Current remedies to musculoskeletal pathologies and injuries include autografts, allografts, xenografts, and prosthetic implants[89,184]. Donor site morbidity and inflicted pain are the major two problems in autografts, whereas patients with allografts and xenografts often develop an immune response to the implanted tissue. Prosthetic devices are a short term solution as their performance declines with time[89]. Lacking a satisfactory clinical treatment for tendon and ligament pathologies research has been directed toward alternative approaches such as tissue engineering[24]. The first component of functional tissue engineering is the scaffold. Previous studies proposed using decellularized allogenic tissue as scaffolds for tissue engineered constructs[185-187]. When decellularized adequately biological tissues have several advantages over polymeric scaffolds, since they usually retain their biocompatibility, may evade the immune response, and once seeded with viable cells have the ability to self-repair and grow[187]. Several scaffolds were used in an attempt to engineer tendon and ligament models *in-vit*ro. The most common are collagen hydrogels[13,128,129]. However, such scaffolds resulted in constructs having

inferior mechanical strength (<0.15 MPa after 2 weeks of seeding[13,128,129]) compared to human tendons and ligaments (13-125 MPa[130,188]).

The human umbilical cord is a widely available tissue, easily procured directly after delivery. Even though cord blood cells and cord matrix (Wharton's jelly) cells were classified as stem cells with regenerative potential[105], the majority of umbilical cords are still discarded. The Wharton's jelly that surrounds the Human Umbilical Vein (HUV) is rich with growth factors , glycosaminoglycans , and proteoglycans[136,138]. With such a composition, the HUV provides a biocompatible environment that potentially supports cell proliferation and tissue regeneration.

Recent studies were targeted towards the use of the HUV as a vascular graft[134,189]. Hoenicka et al.[189] suggested cryopreserving the HUV for possible future vascular autograft. Daniel and McFetridge[134] decellularized the HUV suggesting its use as an allograft or as a tissue engineered blood vessel. In this study, the concept of using the HUV as a biological scaffold is expanded to include other tissues by taking advantage of the HUV's axial mechanical properties. The HUV possesses longitudinal stiffness comparable to human tendons and ligaments (>10 MPa)[79], and a tensile strength (1.56±1.04 MPa)[79], ten fold higher than seeded collagen gels[130,188]. The main goal of this study was to investigate the HUV seeded with bone marrow Mesenchymal Stem Cells (MSCs) as a scaffold for ligament and tendon tissue regeneration. To explore this possibility it is necessary that the HUV promotes cell integration and proliferation and provides initial mechanical stability to the engineered construct. Moreover, after 2 weeks of culture the

seeded construct should possess significantly higher mechanical properties than the initial scaffold.

4.2. MATERIALS AND METHODS

4.2.1. Procurement and Dissection of the Human Umbilical Vein

Fresh human umbilical cords from full term placentas were collected from the Women's Delivery Center at the Norman Regional Hospital, Norman, OK. Cords were stored at 4°C and processed for use no more than 72 hours after delivery. The HUV was automatically dissected as described by Daniel and McFetridge[134] . Briefly, the umbilical cord was thoroughly washed with distilled water (Figure 4.1) and cut into 8.5 cm long sections.

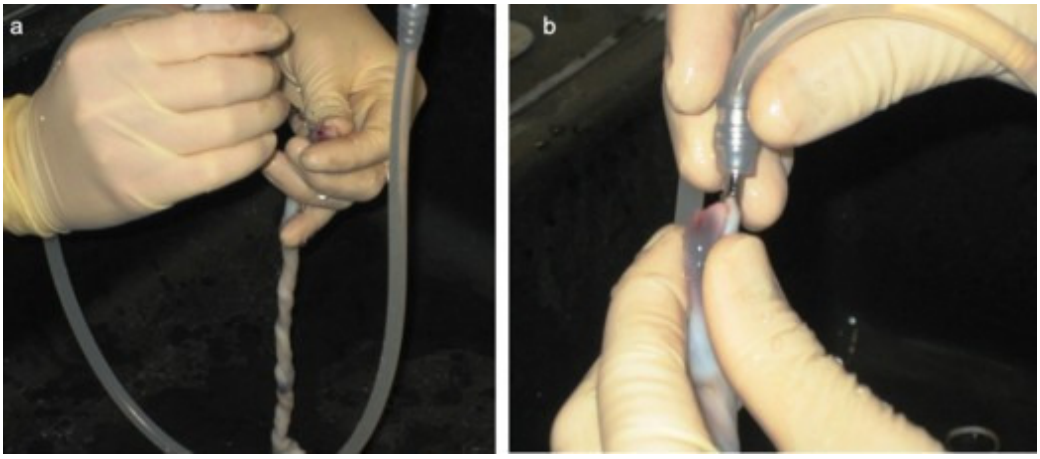

Figure 4.1: (a) Washing the human umbilical cord with distilled water. (b) A close up showing the insertion of a fine tip nozzle through the HUV.

Stainless steel mandrels (McMaster-Car, Altlanta, GA) were inserted into the umbilical vein of each section which was secured in place by zip ties on both ends (Figure 4.2-a). The sections were placed in a Styrofoam container, sealed, and gradually frozen to -80°C at the rate of 2.5°C/min[190,191]. A lathe (Central Machinery, Mod 33647, China) (Figure 4.2-b) was used to dissect the HUV from the umbilical cord resulting in an 8.5 cm long tubular

construct with a uniform wall thickness of 0.75 mm (Figure 4.2-c). The outer diameter of the HUV was measured, using digital calipers, to be 6.7 ± 0.3 mm.

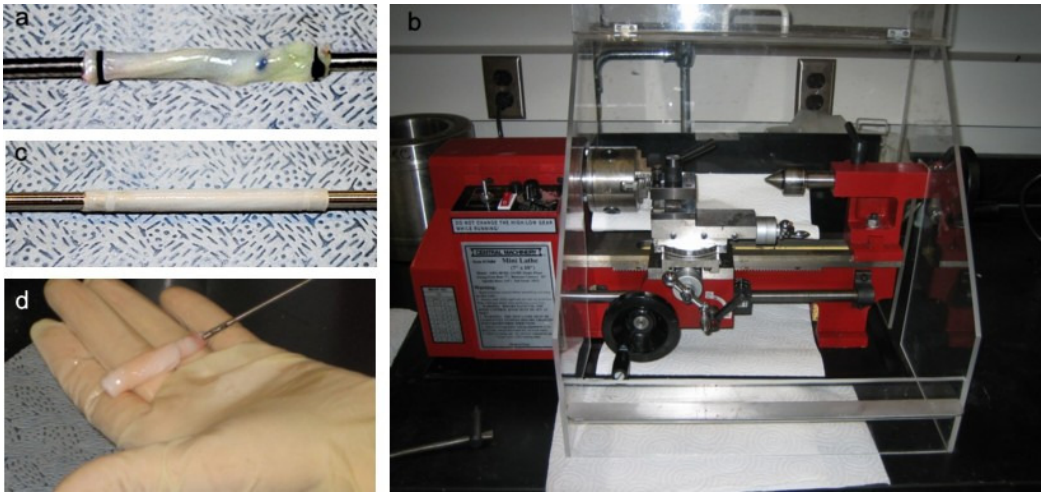

Figure 4.2: (a) 8.5 cm section of umbilical cord before processing. (b) Lathe used to dissect the HUV out of the umbilical cor. (c) HUV after automatic dissection. (d) invention of the HUV such that the Wharton's Jelly matrix is on the inside.

4.2.2. Decellularization and Storage of HUVs

HUV sections were thawed in phosphate buffered saline (Atlanta Biological, Lawrenceville, GA) at room temperature for 1 hour and then inverted such that the Wharton's jelly matrix was on the inside of the scaffold (Figure 4.2-d). One centimeter was discarded from each end of the HUV sections where the zip ties had compressed the walls of the matrix (Figure 4.2-c). Sections were decellularized in 1% weight/volume solution of Sodium Dodecyl Sulfate (Baker, Phillipsburg, NJ) on an orbital shaker at 100 rpm for 24 hours, then thoroughly rinsed in fresh batches of distilled water for 4 consecutive durations (10 minutes, 20 minutes, 30 minutes, and 24 hours) to extract the Sodium Dodecyl Sulfate (SDS) from the tissue. Cords were then immersed in 75% ethanol solution to remove residual surfactant[134], alleviate lipid eduction[185]. Three consecutive washes in water followed the ethanol treatment. Cords were then sterilized in a solution of 0.2% peracetic acid

(Sigma Aldrich, St. Louis, MO) for 2 hours, and washed four times in sterile distilled water. Sections were finally washed in sterile phosphate buffered saline for 24 hours to stabilize the pH of the HUVs at physiological levels (7.2-7.4). HUVs were stored for a maximum duration of one week at 4°C before use.

4.2.3. Extraction of MSCs

Bone marrow stromal cells were harvested from the femur and tibia of 6-8 week old male Wistar® rats weighing between 150 g and 200 g (Harlan, Indianapolis, IN) using standard procedures[192,193]. Briefly, bone marrow aspirates were suspended in alpha minimum essential medium (Invitrogen, Carlsbad, CA) supplemented with 10% fetal bovine serum (Atlanta Biologicals, Lawrenceville, GA), 1,000 Units/ml penicillin G (Invitrogen), 1 mg/ml streptomycin sulfate (Invitrogen), and 2.5 μg/ml amphotericin B (Invitrogen). Four sterile syringes were each filled with 5ml of standard media (alpha minimum essential medium supplemented with 10% fetal bovine serum, 100 Units /ml penicillin G, 100 μg/ml streptomycin sulfate, and 0.25 μg/ml amphotericin B). The bone marrow was flushed out of four bone aspirates into a 50ml falcon tube using the sterile syringes. Large conglomerates of bone marrow were separated and homogenized using a sterile pipette. The cells were plated on four 75cm^2 culture plates and incubated in a humidified environment at 37°C and 5% CO_2. Non-adherent cells were removed three days later after the first media change. Thereafter, the media was changed every 2 to 3 days. When the cells became 75% confluent they were split into 3 new flasks indicating a new passage. Cells used for seeding in the HUV were between passage 3 and 5.

4.2.4. Seeding of Constructs

Decellularized HUV sections were immersed in standard media at 37°C 24 hours prior to seeding MSCs were washed with 5ml of PBS and detached using 2 ml of 0.25% trypsin-EDTA (Invitrogen, Carlsbad, CA) for 5 minutes. The cell suspension was centrifuged at 2200 rpm for 5 minutes and the supernatant discarded. The cell pellet was dissolved in media and mixed with type I collagen (Angiotech Biomaterials, Vancouver BC, Canada) to yield a final cell density of 1 million cells/ml and collagen concentration of 2 mg/ml. Special end adapters were designed to hold the HUV in place during the seeding procedure (Figure 4.3-a). Using these adapters it was possible to insert the cellular collagen solutions into the HUV sections using a 1 ml pipette (loading volume 0.6 ml/HUV). The seeded constructs (Figure 4.3-b) were placed in 100-mm diameter tissue culture plates where the collagen hydrogel polymerized for 1 hour. Seeded HUV sections were then either immersed in 30 ml of standard media or mounted in a bioreactor and placed in an incubator at 37°C and 5% $C0_2$ for varying time durations of 1 and 2 weeks (Figure 4.3-c). A control group was included in which constructs were prepared as described above but without the use of cells. Thus HUV sections in the control group were filled with acellular collagen hydrogel.

Figure 4.3: (a) Novel design of an adapter to facilitate handling and seeding of HUV. (b) HUV seeded with collagen and MSCs and cultured for 1 week. (c) Cross section of seeded HUV 1 week post-culture. Arrow points to cellular collagen hydrogel that was injected in the center of the HUV.

4.2.5. Cell Density

The term “cellularity” is defined as the number of cells per construct. At least three constructs per culture duration were tested for cellularity, with triplicate sections tested from each construct. Sections were taken from the center and 1 cm away from the proximal and distal ends of the construct to avoid end effects. Each 5 mm long ringlet was dissected into sections≤ 0.25 mm^2 and incubated with 2 ml of collagenase type I (MP Biomedicals, Solon, OH) for 5 hours at 37°C. Following collagen digestion samples were sonicated for 1 minute and subjected to two cycles of freeze/thaw to ensure cells lyses and release of DNA into solution.

DNA quantification was conducted by measuring the fluorescence of the different samples using a PicoGreen DNA quantification kit (Invitrogen, Carlsbad, CA) and a Synergy HT plate reader (Bio-Tek, Winooski, VT). The kit included a buffer, a DNA standard, and a DNA dye. For each solution to be tested for DNA content, triplicate samples were assayed to account for sampling error. Five different DNA standard concentrations were employed (0, 0.1, 0.3, 1, and 3 μg/ml). In a white, opaque 96 well plate 107μl of buffer solution was added in each well to be used, supplemented with 43 μl of sample and/or standard, and then incubated in the dark for 5 minutes with 150 μl of dye solution. The fluorescence of different wells was measures using the Synergy HT plate reader at a wavelength of 550nm. The DNA concentration in μg/ml per cellular solution was computed through linear regression of the standard curve. Concentrations were then converted to cell densities using Equation 4.1 and knowing that the DNA content per MSC was 3 pg/cell. The PicoGreen DNA assay gives an indirect indication of cell viability by showing

an increase in DNA concentration, and thus an increase in cell number per construct, with time.

$$\#\ \text{of cells} = \frac{\text{DNA concentration } (\mu\text{g/ml}) \times \text{Volume (ml)} \times 10^6\ (\text{pg}/\mu\text{g})}{3(\text{pg/cell})}$$

Equation 4.1: Computing cell number using the DNA concentration of a cellular solution.

4.2.6. Light Microscopy

Supplies for conducting histology including neutral buffered formalin, paraffin, clear-Rite, Hematoxylin and Eosin (H&E), and mounting media were purchased from Richard-Allan Scientific (Kalamazoo, MI). Cords dedicated for histological evaluation were cut in two different directions: (1) cross sections corresponding to 5 mm thick ringlets, and (2) longitudinal sections corresponding to 5 mm thick portions cut parallel to the axial direction of the HUV. Tissue samples were fixed in 10% neutral buffered formalin overnight at room temperature and stored in 70% ethanol no more than 2 weeks prior to embedding. Fixed samples were dehydrated at 45°C in a series of increasing alcohol concentrations (70, 80, 95, and 100%), cleared with clear-Rite, infiltrated with melted paraffin at 60°C under vacuum, and embedded in paraffin blocks. 7-μm thick sections were sliced using a manual microtome, mounted on Histobond slides (VWR) and baked overnight at 45°C. Use of the Histobond slides minimized tissue loss during H&E staining. Tissue samples on slides were deparaffinized in clear-Rite, and then rehydrated in a series of decreasing alcohol concentrations. Slides for light microscopy were stained progressively in hematoxylin, cleared in acid alcohol, counterstained in eosin, and finally dehydrated and secured by cover slips.

All slides were studied under a Nikon E800 microscope (Nikon Instruments, Inc., Melville,NY,USA). Images were captured by a Nikon camera (Nikon Instruments, Inc.), and analyzed using the MetaMorph software V6.2 (Molecular Devices, Downingtown, PA, USA).

4.2.7. Mechanical Testing

Axial and radial mechanical testing was performed using a uniaxial tensile testing frame (United Testing Systems, model SSTM-2K, Flint, MI). Samples were preconditioned for 5 cycles to minimize hysteresis and then tested to failure at a strain rate of 1%/sec. For radial testing 5-mm thick ringlets were dissected out of the construct, clamped to the machine using hooks, and stretched radially to failure. For axial testing samples were hooked to the clamps using the steel adapters in order to avoid slippage. A 1-cm portion of the construct was attached to the adapter at each end with a gauge length of about 4 cm between clamps. The gauge length and cross sectional dimensions were measured for each sample using digital calipers. Force and extension data were collected only from samples that failed in the region away from the clamps (Figure 4.4).

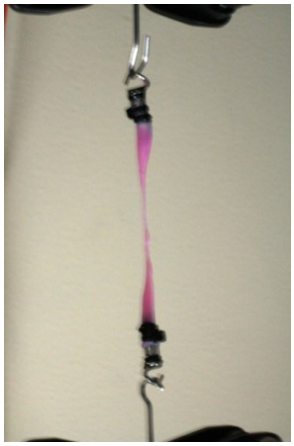

Figure 4.4: Stretching a construct to failure.

4.2.8. Statistical Analysis

For each culturing duration at least 3 samples were dedicated to cell density computations and histological evaluations (n≥3), and 6 samples for mechanical analysis (n≥6). All results were expressed as mean values ± standard deviation. Statistical analysis to compare results among groups was performed using the ANOVA method. A significant difference corresponds to $p<0.05$ (confidence level >95%).

4.3. RESULTS

4.3.1. Proliferation of Cells

Sections from three different locations on each of three seeded HUVs were tested for cellularity. The coefficient of variance of the measured cell densities for the 3 sections was less than 12% (Figure 4.5).

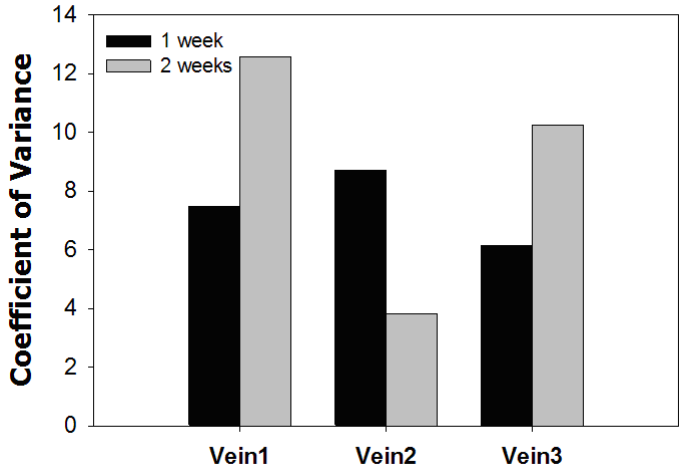

Figure 4.5: Coefficient of variance of cell density counts for three different constructs one and two weeks post culture. Three sections per HUV were tested for cellularity. Sections were taken from the center, and 1 cm away from the proximal and distal ends of the construct to avoid end effects. For both culture periods DNA quantification results for all three sections were similar with a coefficient of variance less than 12%.

A statistically significant increase in cell number was measured for the 1 and 2 weeks culture time points (Figure 4.6). The HUV was inoculated with 600,000 cells. After 1 week in culture the total cell number increased to more than 1 million cells, and at the end of the two week culture period the total number of MSCs in the HUV exceeded 1.5 million.

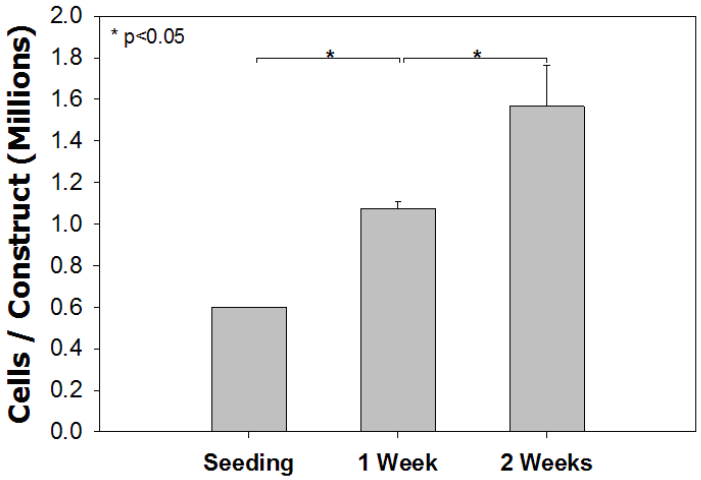

Figure 4.6: Cellularity of the HUVs cultured for different time points.

4.3.2. Histology

Decellularization was effective in removing cellular components. This is clearly demonstrated in the H&E stained longitudinal sections of the HUV scaffold before (Figure 4.7-a) and after (Figure 4.7-b) decellularization. Numerous intact cells can be seen on the HUV prior to treatment (Figure 4.7 3-a). Upon decellularization no intact cell bodies are visible (Figure 4.7-b); however, fibers within the scaffold seem to be partially disrupted.

Figure 4.7-c shows the morphology of acellular collagen gel in the central part of the control construct after 1 week of culture, while Figure 4.7-d shows the morphology of cellular collagen gel after 1 week of culture. Cells are visible in the center of the HUV surrounded by the collagen hydrogel as

seen in Figure 4.7-e, with cells after 2 weeks migrating into the construct, Figure 4.7-f. MSCs, denoted by circles, started integrating within the scaffold and migrating through the extracellular matrix (ECM) of the HUV.

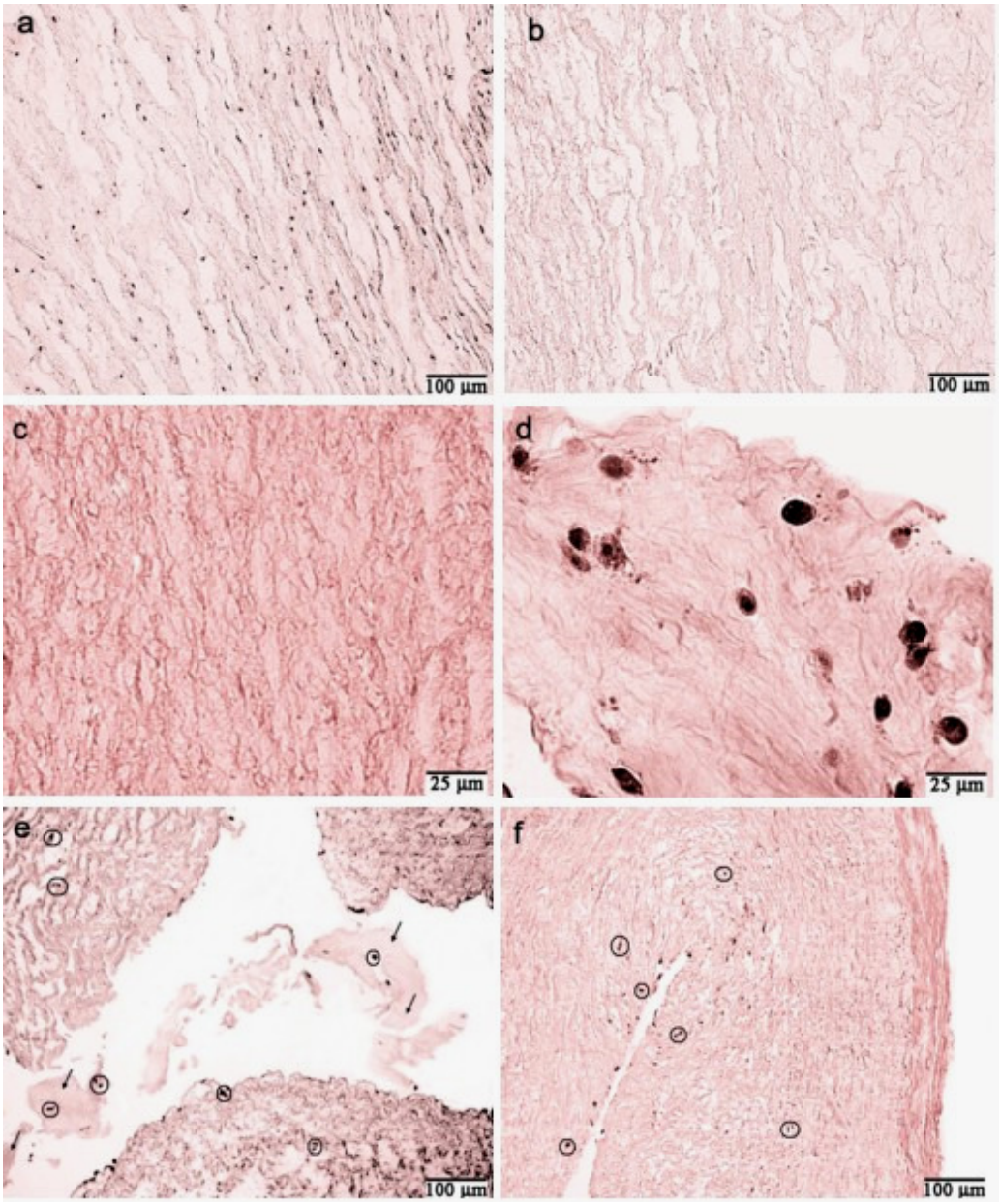

Figure 4.7: Histological images of HUV; Longitudinal Sections of (a) initial matrix of HUV before decellularization and (b) matrix after decellularization. The initial matrix is rich with cells, however, after decellularization no intact cells were obvious. Cross sections of (c) acellular collagen gel matrix 1 week after being injected into the HUV, (d) MSC seeded collagen gel matrix 1 week after being injected into the HUV, (e) HUV one week after culture showing the injected collagen gel (arrows) and cells (circles) starting to integrate within the scaffold, and (f) HUV 2 weeks after culture showing the cells migrating toward the exterior portion of the cylindrical scaffold.

4.3.3. Mechanical Analysis

Testing HUV constructs longitudinally and radially until failure resulted in a typical viscoelastic behavior due to the rearrangement of fibers upon stretching. Thus the constructs were preconditioned for 5 cycles prior to loading till failure (Figure 4.8). HUV sections were stronger in the longitudinal direction than in the radial direction. Figure 4.9 shows a typical stress strain plot for HUVs tested in both directions. While constructs are stronger and stiffer in the longitudinal direction, they stretch to a higher degree in the radial direction. This is reflected by the low slope and high strain values for the plot of the radial direction.

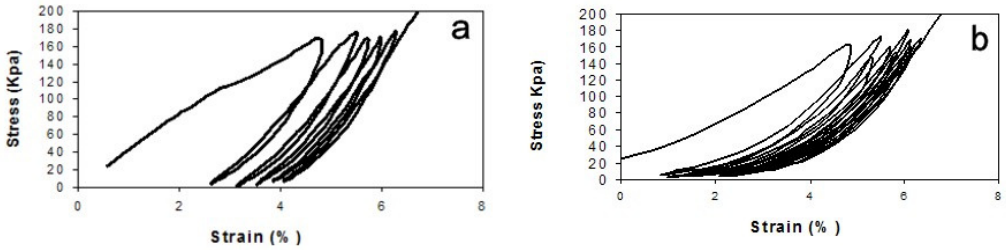

Figure 4.8: Toe region of stress-strain curves of HUVs preconditioned for (a) 5 and (b) 10 cycles. After 5 preconditioning cycles the load and unload paths became closer minimizing hysteresis.

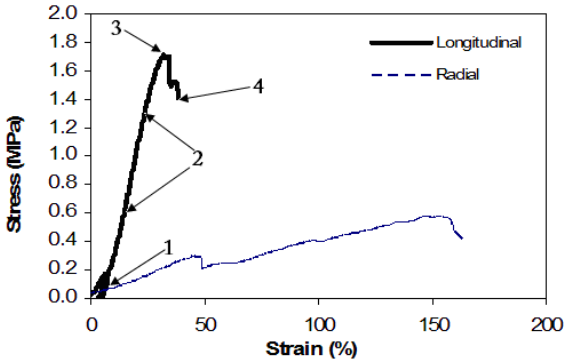

Figure 4.9: Typical stress stain curve of HUV. The curve has a bell shape with a "toe" region (1), a "linear" region (2), maxima at ultimate stress (3), and a final decrease in strength at the failure point (4). Both longitudinal and radial curves have similar trends; however, the longitudinal curve has a steeper slope (higher modulus), higher ultimate stress value, and lower strain value at failure.

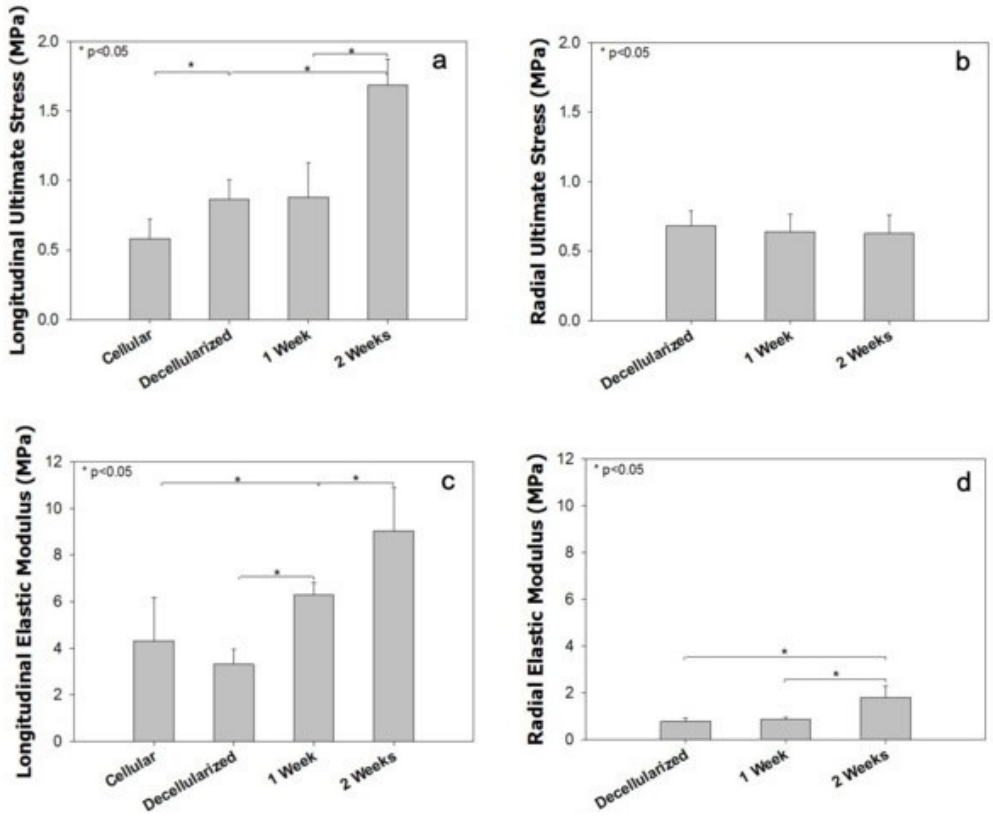

Figure 4.10: Mechanical properties of the seeded HUV for different culture periods including tensile strength in the (a) longitudinal and (b) radial directions, and modulus of elasticity in the (c) longitudinal and (d) radial directions. Tensile strength increased significantly in the longitudinal direction after 1 and 2 weeks of culture. However, no significant change was recorded in the radial direction. In both directions a significant increase in the modulus was measured after 2 weeks of culture indicating a stiffer material.

Decellularization significantly increased the longitudinal ultimate stress of the HUVs from 0.6±0.1 MPa to 0.9±0.1 MPa (Figure 4.10-a). Moreover, a statistically significant increase in the ultimate longitudinal stress values was observed 2 weeks post culture. HUVs cultured for 1 week had an average ultimate stress value of 0.9±0.2 MPa as compared to 1.7±0.2 MPa for 2 week cultures. This was not the case in the radial direction (Figure 4.10-b) where no change with culture time was observed. An increasing trend in the stiffness in both directions of the seeded HUVs was observed after 1 and 2 weeks of culture (Figure 4.10-c and Figure 4.10-d). The longitudinal modulus

of elasticity increased from 6.3±0.5 MPa 1 weeks after culture to 9.1±1.8 MPa after 2 weeks. Similarly, an increase in the radial direction was recorded from 0.8±0.1 MPa to 1.8±0.5 MPa.

4.3.4. Discussion

The goal of this study was to investigate the potential of the HUV as a biological scaffold for soft musculoskeletal tissues, particularly tendons and ligaments. The documented results show that it was possible to decellularize the HUV with minor disruptions to the ECM. Moreover, the HUV was shown to support cell integration and proliferation as histological analysis revealed cell migration from the center of the HUV into the scaffold, and a progressive increase in cell density over the 2 weeks culture period. Finally, culturing MSCs within the HUV scaffold for periods up to 2 weeks was shown to significantly increase the mechanical properties of engineered constructs.

Histological images showed adequate decellularization of tissue with minor disruption to ECM components. No intact cell bodies appeared post treatment with SDS (Figure 4.7-b). This is in agreement with previous studies reporting that the ionic surfactant SDS is efficient in removing and solubilizing cellular components including cytoplasmic proteins and nuclear debris from tissue[186,194]. Even though SDS was found to disrupt ECM proteins, decellularized tissues usually maintained their mechanical properties[194]. Decellularized HUV sections had similar stiffness but were 40% stronger than the cellular tissue. The increase in ultimate stress is possibly due to the dehydration of the tissue with ethanol[195].

The decellularized HUV has proven to support cell integration and proliferation since MSCs were able to populate the scaffold. After one week

of culture the cell density increased 1.8 fold and that increase became 2.5 fold after 2 weeks of culture (Figure 4.6). MSCs seem to be uniformly distributed along the longitudinal axis of the construct. Uniformity of cells through the construct was evaluated with DNA quantification tests in three different sections taken from the proximal, distal and mid-section of each construct. The three different sections yielded comparable cell densities, with a coefficient of variance less than 12% (Figure 4.5). The measured increase in the cellularity of the constructs 1 and 2 weeks post culture was also reflected in cross sectional histological images. H&E sections (Figure 4.7-e) revealed cells attached to the inner wall of the HUV and others populating and filling the central area of the scaffold. After two weeks of culture (Figure 4.7-f) MSCs migrated through the HUV matrix populating the scaffold and possibly remodeling the ECM. The characteristic random orientation of collagen fibers shown in Figure 4.7-c has significantly changed in the presence of cells (Figure 4.7-d) denoting ECM remodeling.

The increase in cellularity, ECM remodeling, and cell migration through the HUV were accompanied with an increase in the mechanical properties of the constructs. There was no significant increase in strength after one week of culture. This is likely due to cells adapting to the new environment. However, a 95% increase in the ultimate stress and 80% increase in the modulus were measured two weeks post culture. The increase in mechanical strength is not directly related to the increase in cell number. One week post culture the increase in cellularity was 79%; however there was no significant increase in ultimate stress. After 2 weeks of culture the cell number within the constructs almost doubled again. This time the cell number increase was

accompanied by a 92% increase in the ultimate stress. During both conditions there was a comparable increase in cell number however only in the second week did the ultimate stress increase. This suggests that the increase in mechanical strength is related to the activity of the cells within the construct. Potential ECM deposition and remodeling of existing ECM matrix by the second week of culture may be responsible for the enhancement of the mechanical properties of the construct.

The non-linear tensile behavior of the HUV is typical of soft biological tissues[41,79]. During load-unload cycles there is a dissipation of energy due to the rearrangement of the fibers within the scaffold, namely collagen. Constructs were preconditioned for 5 and 10 cycles. The energy dissipated was minimal after 5 preconditioning cycles where load-unload curves almost followed the same trajectory (Figure 4.8). Thus only 5 preconditioning cycles were applies prior to stretching the samples to failure. Mechanical testing yielded significantly higher modulus and ultimate stress values in the longitudinal direction than in the radial direction. Such differences were previously reported on manually dissected[79] as well as mechanically dissected HUVs[134]. Longitudinal ultimate stress values for decellularized HUVs were 26% higher than the radial direction (0.9±0.1 MPa compared to 0.7±0.2 MPa). Two weeks post culture the longitudinal ultimate stress became 167% higher than the radial strength. The elastic modulus for decellularized HUVs was 4 times higher in the longitudinal direction than in the radial direction (3.3±0.6 MPa compared to 0.8±0.2 MPa). Two weeks post culture the longitudinal elastic modulus became more than 5 folds stiffer than the radial modulus (9.0±1.9 MPa compared to 1.8±0.5 MPa). The ultimate

stress values reported in this study for the decellularized HUVs are in agreement with the results reported in a previous study that characterized the mechanical properties of manually dissected HUVs[79]. Pennati[79] reported longitudinal ultimate stress values of 1.6 ±1.1 MPa that were much higher than the radial ultimate stress values (0.5 ±0.1 MPa). In that study HUVs were manually dissected to a thickness of 4mm, 5 times thicker than our mechanically dissected cords (0.75mm thick). This explains the higher longitudinal ultimate stress value reported. However, it is interesting to note the variability in the ultimate stress values reported by Pennati[79] which had 67.3% coefficient of variance compared to 16.3% for our mechanical technique.

The fact that HUVs are stronger and stiffer in the longitudinal direction reflects the possibility of using them as a scaffold for engineering tissue that requires higher strength values in the longitudinal direction; such as tendons, and ligaments. It is possible to enhance the mechanical properties of the decellularized scaffold by increasing the thickness of the dissected HUV. This is simply accomplished by adjusting the thickness control on the automatic lathe.

4.4. CONCLUSIONS

The scaffold presented in this study supported cell integration, proliferation and migration. The seeded constructs possessed higher mechanical properties than the original decellularized HUV. These mechanical properties could be enhanced by increasing the initial thickness of the scaffold or increasing the seeding density. The use of MSCs in this study is due to their ability to differentiate into specific lineages, including soft

musculoskeletal tissue, depending on the mechanical and chemical stimuli that they are subjected to. Thus coupling the use of the decellularized HUV scaffold, with MSCs stimulated by the appropriate biochemical or biophysical factors opens up many opportunities for exploiting this readily available biological material.

In Chapter 5 the effects of cyclic mechanical stimulation on the seeded HUV are documented. Moreover, the potential of the resulting construct to act as a tissue engineered tendon is assessed.

CHAPTER 5

TENDON TISSUE ENGINEERING USING CELL SEEDED UMBILICAL VEINS CULTURED IN A MECHANICAL STIMULATOR

The contents of this chapter were published in Tissue Engineering, volume **15**, issue TBD, pp. TBD, 2009.

5.1. INTRODUCTION

Tendon injuries affect thousands of individuals annually. Athletes, in particular, are prone to Achilles tendon injuries[3], with more than 232,000 injuries documented in 2002[4]. One quarter of Achilles tendon injuries reported by athletes require surgery and almost one fourth of those who undergo surgery require further future operations[4]. Lacking an inclusive vascular network[67] and composed of cells with low metabolism[24], tendons have poor intrinsic healing capabilities[5,8], and when healing is possible, it requires prolonged durations of rest and immobility. The healing tendon develops scar tissue with reduced mechanical strength and is prone to further injury if used extensively or repetitively. When tendon replacement is inevitable there are four material options available: autografts, allografts, xenografts, and prosthetic devices. Autografts have limited availability, weaken the donor site, and result in a double incision that inflicts additional pain on the patient, while allografts and xenografts often result in an immune response. Prosthetic devices, on the other hand, are a temporary solution since their integrity is compromised with increased usage[89]. To augment the limitations in the current treatments of tendon defects and injuries, researchers have attempted to engineer tendon-like tissue *in-vitro* that

possesses comparable mechanical properties to the innate tissue and that would evade the immune response.

Since immobilization severely lowers the ultimate strength of tendons[91], current research has focused on the effect of stretching cell seeded constructs to enhance mechanical properties[13,98,155,196]. In a recent investigation two-dimensional tissue sheets secreted by human fibroblasts were subjected to continuous (non-cyclic) mechanical loading; results showed that cells and the extracellular matrix (ECM) became aligned and increased both the tensile strength and modulus of the tissue[158]. Mechanical stimulation of collagenous constructs seeded with Mesenchymal Stem Cells (MSCs) has also been shown to increase the expression of ligament and tendon markers[94,177], indicating the potential of MSCs to differentiate into tenocytes under the sole action of mechanical stimulation. However, poor mechanical properties of cultured collagen gel constructs prevent their use as tendon replacements[178].

Biological scaffolds, such as small intestinal submucosa[131,132], collagen fibers[133], and Human Umbilical Veins (HUVs)[134], have been targeted for tissue engineering applications since they are biocompatible, evade the immune response, and have initial ultimate stress and stiffness values significantly higher than collagen gels. It has been shown that HUV provides a suitable environment for musculoskeletal tissue engineering applications (CHAPTER 4). In this study we investigate the effect of cyclic mechanical stimulation on HUVs seeded with MSCs. To accomplish our goals a bioreactor was designed to cyclically tension the seeded scaffolds for periods of 1 and 2 weeks. We hypothesize that cyclic mechanical tensioning would increase

MSCs proliferation rates and enhance the mechanical and morphometric properties of seeded HUVs giving them the potential to act as tendon replacement models.

5.2. MATERIALS AND METHODS

5.2.1. Bioreactor Design

A Mechanical Stimulator for Tissue Engineering applications (MSTE) was designed specifically for this project. The main goals behind constructing the MSTE were; (1) to culture multiple tissue constructs under a sterile environment, and (2) to apply controlled mechanical stimuli at different frequencies, intensities, and waveforms to cell seeded scaffolds. The MSTE is capable of stimulating triplicate constructs simultaneously (Figure 5.1-a). Three samples cultured in separate vessels can be tensioned via a linear actuator controlled by a signal converter (Wavetec model 185, San Diego, CA). The applied signal is amplified before being transferred to the actuator (Figure 5.1-b). The specifications of the actuator are: linear travel zone = 5 in, peak force sustained for 10 seconds = 49 lb, and maximum force sustained continuously = 14 lb. Using the signal converter box (Figure 5.1-c) it is possible to apply several waveform signals with variable frequencies and amplitudes.

The cylindrical reactor vessels were made of glass (diameter = 2.5 cm, length = 10 cm) with an individual capacity of 49 ml. The total volume of media circulated through the system is 240ml. Media is flowed around the constructs continuously using a multi channel pump at the rate of 1 ml/min. Two media reservoirs are used to re-circulate the media around the MSTE

perfusion circuit. The use of the two-reservoir system facilitates the procedure of changing the media without having to move the system out of the incubator. Keeping the bioreactor in place in a closed environment minimizes contamination events. A filter on the media container and gas-permeable silicone tubing allow media oxygenation. The whole system is kept in a humidified incubator at 37ºC, 5% CO_2, and 95% air.

Figure 5.1: (a) Design of the Bioreactor, (b) Linear Motor, (c) Amplifier and signal converter, and (d) Close up to the reactor vessels.

The load is transferred from the actuator to the samples via a piston that connects to a triangular plate which in turn is hooked to the three constructs (Figure 5.1-d). The samples are attached to the triangular plexi-

glass plate via stainless steel adapters that can be screwed up or down to adjust the height of each sample separately accounting for individual plastic deformations upon stretching. To seal the top of each reactor vessel surgical gloves were used. The three middle finger portions of the surgical gloves were cut, and then attached to the top of the vessel from one side and to the stainless steel adaptors from the other side using zip-ties (Figure 1-d). All of the materials used to assemble the bioreactor can be sterilized either by ethylene oxide or steam (stainless steel adapters, glass bottles, plexi-glass bases, glass reactor vessels, zip ties, and surgical gloves).

5.2.2. Preparation of the Scaffold

Refer to sections 4.2.1 and 4.2.2

5.2.3. Extraction of MSCs

Refer to section 4.2.3

5.2.4. Seeding of Constructs

Refer to section 4.2.4.

Cell attachment and polymerization of collagen were allowed for a full hour after which the seeded constructs were divided into three groups as follows: (Group 1) Seeded HUVs were placed in 100-mm diameter well plates; (Group 2) Seeded HUVs were cultured in the MSTE without any mechanical stimulation; (Group 3) Seeded HUVs were cultured in the MSTE and subjected to mechanical stimulation of 2% strain for 1 hour per day at a frequency of 0.0167Hz. A fourth group (Group 4) consisted of acellular unseeded HUVs that were mechanically stimulated in the MSTE. Constructs

were cultured for durations of 1 and 2 weeks and then tested for (1) cell density, (2) gene expression, (3) morphology, and (4) mechanical properties.

5.2.5. Cell Density per Construct

Refer to section 4.2.5

5.2.6. Ribonucleic Acid Extraction and RT-PCR

Tissue samples (≤ 25 mg) dedicated for gene expression analysis were stored in 1.5 ml of RNAlater® (Ambion, Austin, TX) at -20°C to preserve Ribonucleic Acid (RNA) until further analysis. RNA was extracted from the tissue using an RNAqueous®-4PCR Kit (Ambion) following manufacturers directions. cDNA was synthesized from RNA using TaqMan® Reverse Transcription Reagents (Applied Biosystems, Austin, TX) in the presence of multiscribe reverse transcriptase (50 U/μl), RNase inhibitor (20U/L), deoxyNTPs mixture (2.5 mM), random hexamers (50μM), 10X buffer, and $MgCl_2$ solution (25 mM). Gene expression levels of collagens type I and type III, and glyceraldehyde 3-phosphate dehydrogenase (GAPDH) were quantified using a Power SYBR® Green PCR Master Mix kit (Applied Biosystems). Primers used were as follows:

Collagen type I: forward 5'-GGAGAGTACTGGATCGACCCTAAC-3''[197]

Collagen type I: backward 5'-CTGACCTGTCTCCATGTTGCA-3''[197];

Collagen type III: forward 5'-CAGCTGGCCTTCCTCAGACTT-3'[198],

Collagen type III: backward:5'-GCTGTTTTTGCAGTGGTATGTAATGT-3'[198]

GAPDH: forward 5'-AACTCCCTCAAGATTGTCAGCAA-3'[198]

GAPDH: backward 5'-GTGGTCATGAGCCCTTCCA-3'[198].

Quantitative real time polymerase chain reaction (qRT-PCR) was conducted according to the following steps: 95°C for 10 minutes, 45 cycles of 95°C for 15 minutes and 60°C for 1 minute. At the end of RT-PCR, melting curves were generated for each amplified product. The threshold cycle (C_T) for collagens type I and III was normalized to the housekeeping gene GAPDH and the relative expression was computed following the $\Delta\Delta C_T$ method[199] .

5.2.7. Light Microscopy

Refer to section 4.2.6

5.2.8. Fluorescent Microscopy

Tissue samples on slides dedicated to fluorescent microscopy were deparaffinized in clear-Rite, rehydrated in a series of decreasing alcohol concentrations, and then they were incubated for 30 minutes in the dark at 37°C with 100 µl of dye solution. The dye solution was composed of 5µl of lipophilic stain DID (Invitrogen) and 1 ml of media. Tissue samples were finally washed three times in media (10 minutes per wash).

All slides were studied under a Nikon E800 microscope and images were captured by a Nikon camera and analyzed using the MetaMorph software V6.2. An omega XF110 optical filter (Omega Optical, Brattleboro, VT) was employed to detect the fluorescence of the DID dye with an excitation wavelength of 644 nm and an emission wavelength of 665 nm. Using high excitation and emission wavelengths was necessary to avoid background autofluorescence from the tissue.

5.2.9. Analysis of Histological Slides

Three main criteria were followed to analyze histological slides. For each criterion the analysis was done on at least three slides and four different locations per slide were studied.

Unoccupied luminal space: The unoccupied luminal space in the central portion of the HUV was measured and reported as a percentage of the ratio of the central area that is devoid of cells and matrix to the total cross sectional area of the HUV. This parameter was monitored to evaluate the formation of new ECM in the central portion of the HUV beyond the collagen hydrogel that was originally inserted. For that reason, values of this parameter in decellularized HUV were compared with those of seeded HUV at different time points.

Fiber alignment: To analyze fiber alignment the axial direction of the HUV, which is parallel to the direction of mechanical stimulation, was considered the reference axis. The angular deviation of fibers from the axial direction was measured and the mean with the standard deviation were reported.

Shape of cells: Using the Metamorph program it was possible to count the cells that appear in a longitudinal slide and compute their dimensions (length, width and area). The shape factor is a measure of the ratio of the shorter dimension (width) to the longer dimension (length). This number is smaller than one. The closer it is to one the more round the shape of the cell is.

5.3. RESULTS

5.3.1. Cell Proliferation and RT-PCR

The culturing conditions of the four different groups are summarized in Table 5.1. For all seeded groups and all culturing durations a statistically significant increase in cell number was measured (Figure 5.2). After 1 week of culturing, group 1 (constructs cultured statically in a Petri dish) had the lowest cell density. The total cell number increased from 600,000 MSCs to 1.1±0.1 million cells for group 1, 2.1±0.4 million cells for group 2 (constructs cultured in the MSTE without tensioning), and 1.8±0.2 million cells for group 3 (constructs tensioned in the MSTE). However, after 2 weeks of culture, group 3 had more than 29 million cells compared to 1.6±0.2 million cells in group 1 and 3.6±2.0 million cells in group 2.

Table 5.1: Four different groups with varying culture conditions.

GROUP	CULTURE CONDITION
1	Seeded HUV's cultured in 100-mm diameter well plates
2	Seeded HUV's cultured in MSTE without any mechanical stimulation
3	Seeded HUV's mechanically stimulated in the MSTE
4	acellular unseeded HUV's mechanically stimulated in the MSTE

qRT-PCR conducted after 2 weeks of culture showed an upregulation in the expression of both collagen I (4 fold) and collagen III (3 fold) in stretched constructs of group 3 compared to groups 1 and 2.

5.3.2. Histology

Figure 5.3 shows cross sections of the HUV, before and after decellularization, fluorescently tagged by the DID dye. Numerous cells appear in Figure 5.3-a reflecting the Wharton's Jelly and HUV cells originally

present in the umbilical cord prior to decellularization. However, no intact cells were apparent in Figure 5.3-b after decellularizing the HUV.

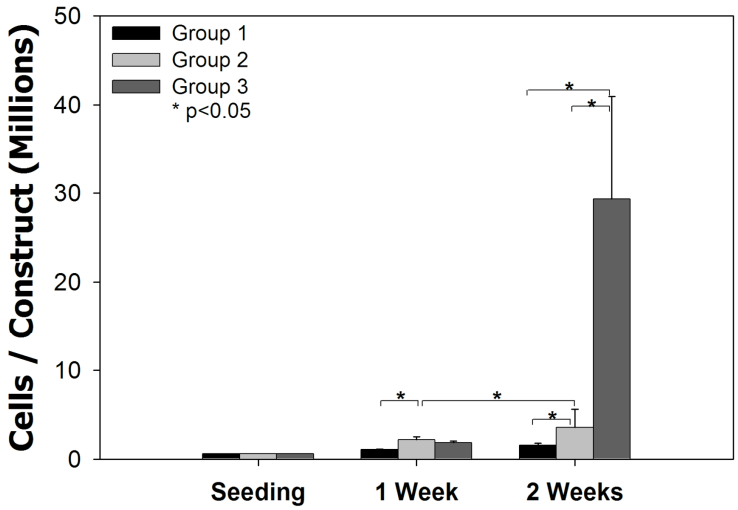

Figure 5.2: Proliferation of cells after 1 and 2 weeks of culture

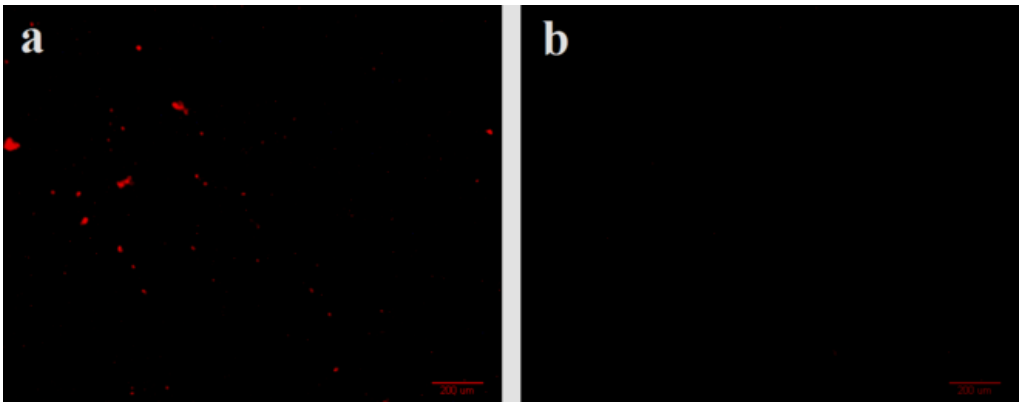

Figure 5.3: Cross sectional view of the HUV stained with DID lipophilic dye (a) cellular HUV, and (b) Decellularized HUV

Cross sectional histological images of constructs cultured statically in the MSTE (Figure 5.4-a) showed large unoccupied spaces in the central portion of the HUV compared to dynamically cultured samples (Figure 5.4-b) in which the central area was almost totally occupied with proliferating cells. The decellularized HUV had a cylindrical structure with a central unoccupied luminal space of 14 ± 4.0 %. After 2 weeks of culture the unoccupied luminal

space significantly decreased to 5.7±2.0% for group 3 (Figure 5.5). No statistically significant decrease was measured for group 2. For all cultures, cells were able to integrate with the HUV and migrate through the scaffold. For group 2 cells only reached the first quarter of the scaffold (Figure 5.6-a) whereas cells seeded in group 3 (constructs stimulated in the MSTE) migrated deep into the scaffold almost reaching the outer end of the HUV (Figure 5.6-b).

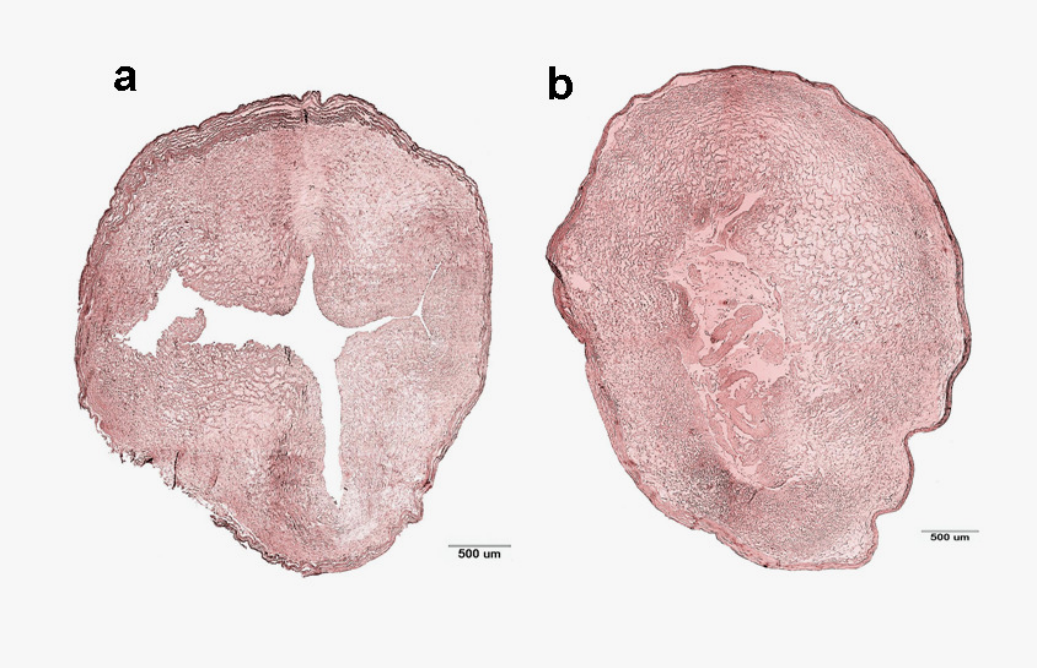

Figure 5.4: Cross section of constructs cultured for 2 weeks in the MSTE under (a) static conditions; (b) mechanical stimulation

Longitudinal histological sections show ECM fiber alignment for static and dynamic cultures (Figure 5.7). For static cultures, ECM fibers had random orientations 1 (Figure 5.7-a) and 2 weeks (Figure 5.7-b) post culture. Contrarily, mechanically stimulated constructs showed parallel alignment of fibers for both culture periods (Figure 5.7-c and Figure 5.7-d). After two weeks of culture, the average fiber deviation from the axial direction was measured to be 1.7°±1.8° for mechanically stimulated samples (Figure 5.8-b),

while this value was 34°±48° for static cultures (Figure 5.8-a). A closer view at the longitudinal sections showed rounded nuclei for cells in the static cultures (Figure 5.8-c) with a shape factor of 0.9 compared to spindle shaped nuclei for the dynamic cultures with a shape factor of 0.7 (Figure 5.8-d).

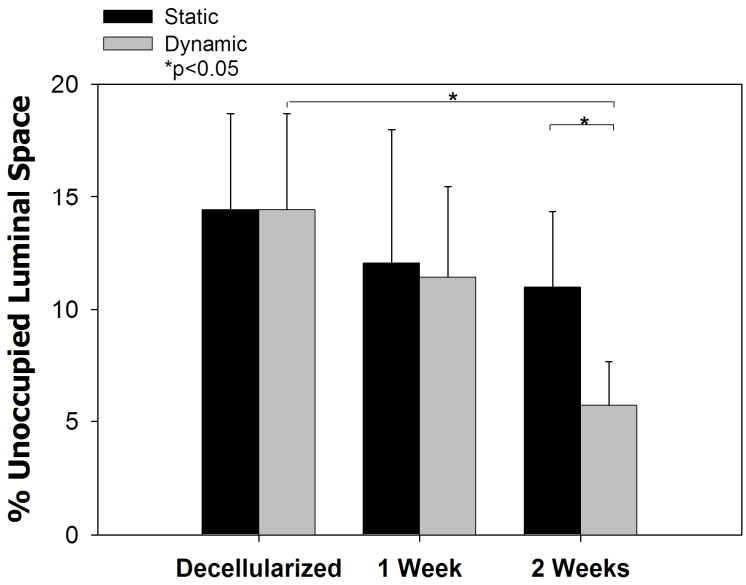

Figure 5.5: Percent of unoccupied luminal space in the seeded constructs cultured in the MSTE.

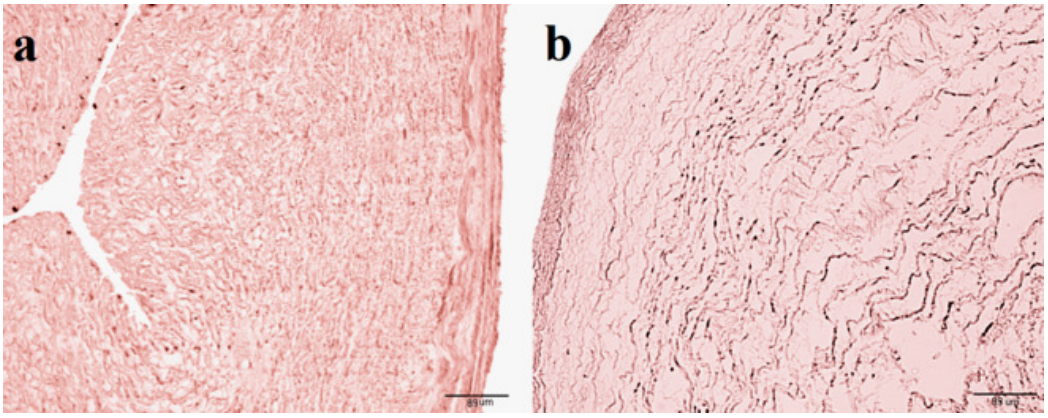

Figure 5.6: Histological cross sections of seeded HUV after 2 weeks of culture in the MSTE: (a) static, and (b) dynamic.

5.3.3. Mechanical Analysis

Mechanical properties were assessed by stretching HUV constructs to failure while recording deformation versus load data. After 1 week of culture a statistically significant increase in the ultimate tensile stress values was recorded for all cellular groups (Figure 5.9-a). Group 3 had the highest ultimate stress value 2 weeks post culture (2.6±0.7 MPa). No significant increase in ultimate tensile stress was measured for acellular dynamic samples (Figure 5.9-b).

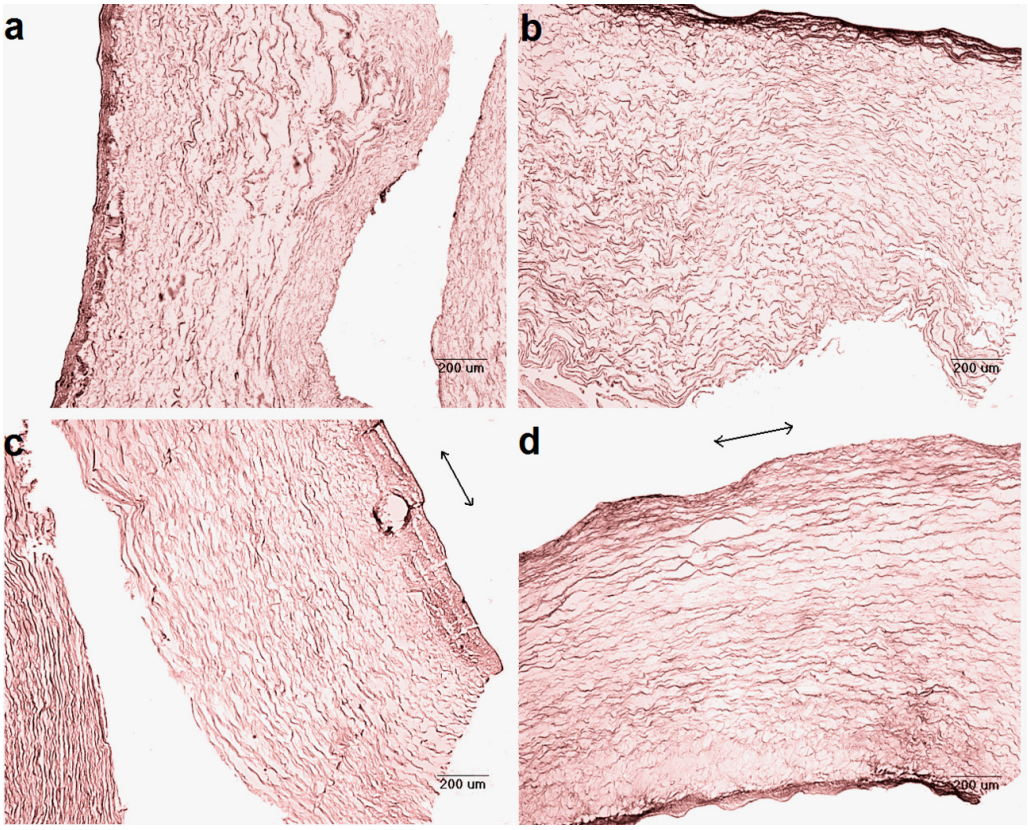

Figure 5.7: Longitudinal sections of HUVs cultured in the MSTE taken at 4X magnification. (a) 1 week static culture, (b) 2 weeks static culture, (c)1 week dynamic culture, (d) 2 weeks dynamic culture. Arrows indicate stretching.

A similar trend was observed for modulus of elasticity (E) values (Figure 5.10). Decellularized scaffolds had a modulus of elasticity E = 3.3±0.6 MPa. After 2 weeks of culture group 1 had E = 9.0±1.9 MPa, group 2 had E =

7.3±2.4 MPa, and group 3 had the highest modulus value of 9.9±2.2 MPa. Acellular samples of group 4 had inferior modulus of elasticity values (Figure 5.10-b) compared to other groups. One week after culture the modulus decreased from 3.3±0.6 MPa to 2.9±1.4 MPa. This value further decreased to 2.4±0.5 by the end of the second week of culture.

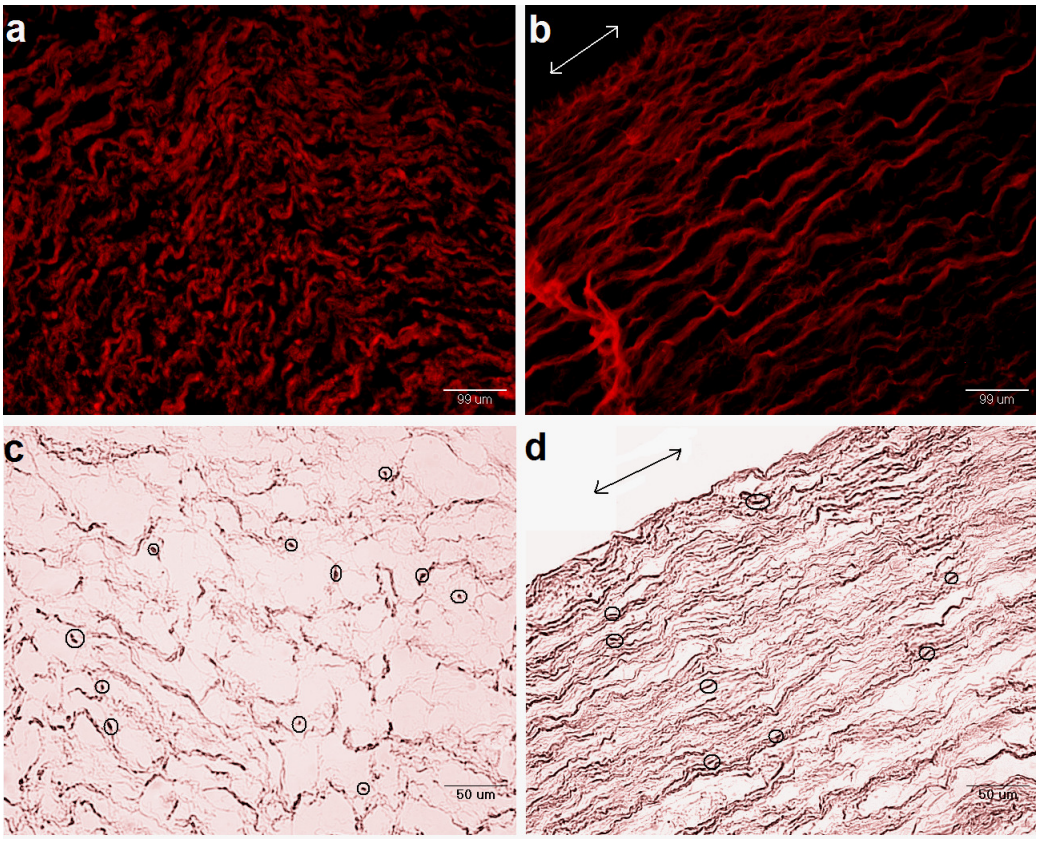

Figure 5.8: Longitudinal sections of HUVs cultured in the MSTE taken at higher magnifications. (a and b) 10X magnification of the HUVs revealing fiber alignment for 2 week static and dynamic cultures, respectively. (c and d) show shape of nuclei for static and dynamic cultures respectively, 2 weeks post culture at a 20X magnification. Arrows indicate stretching direction and circles indicate cell nuclei.

5.4. DISCUSSION

The goal of this study was to investigate the effect of cyclic mechanical stimulation on MSC seeded HUVs and to assess the construct's potential as an engineered tendon replacement. We hypothesized that cyclic mechanical tensioning would (1) increase MSCs' proliferation rates, (2) modify the

morphometric characteristics of seeded HUVs giving them a tendon-like appearance, and (3) enhance the mechanical properties of the construct.

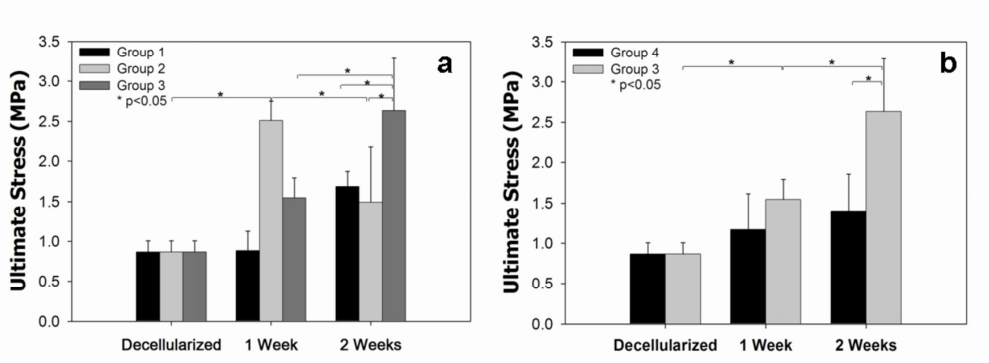

Figure 5.9: Ultimate tensile stress of (a) cellular groups (1-3), and (b) dynamically stimulated groups (3 and 4).

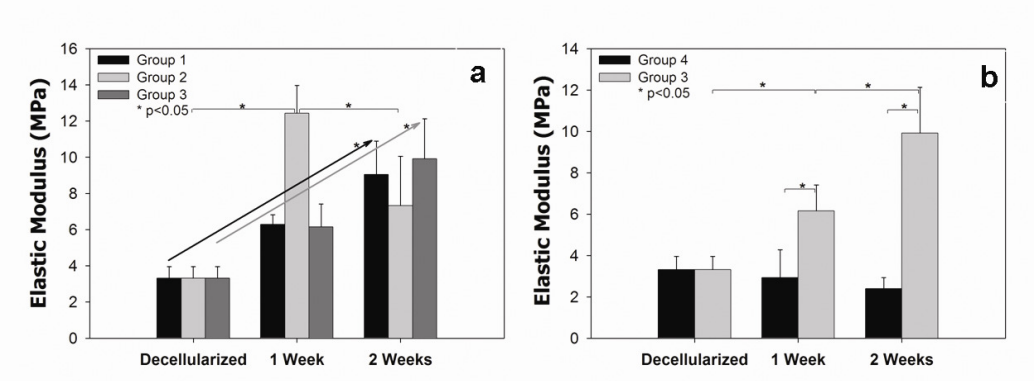

Figure 5.10: Elastic modulus of (a) cellular groups (1-3); and (b) dynamically stimulated groups (3 and 4)

For all cellular groups a statistically significant increase in the cell number was measured indicating that MSCs were able to proliferate within the scaffold (Figure 5.2). Mechanical stimulation significantly increased cell proliferation over the 2 week culture period by at least 8 fold. Under similar loading conditions, canine tendons deprived from stretching showed a decreased cell density compared to mechanically stimulated tendons[91]. In several other studies it was reported that mechanical stimulation increased proliferation rates of MSCs[94,98]. Stretching the constructs may have a direct or an indirect effect on the cells, where applying a shearing load may affect

surface receptors and/or stretch activated ion channels[16] leading to an increase in proliferation rates. Another explanation could be that cyclic loading enhances mass transport through the HUV thus mitigating potentially existing mass transport limitations of nutrients. Contrary to our findings, Androjna et.al reported no significant effect of mechanical stimulation on proliferation rates of primary tenocytes seeded on small intestinal submucosa[131]. The disagreement between the two studies could be due to differences in cell and scaffold type, and mechanical stimulation scenarios. Interestingly, after 1 week of culture group 2 (constructs cultured in MSTE without stimulation) had the highest cell number among all 3 groups. Initial stretching of the constructs after seeding may have caused some cells to detach from the matrix resulting in lower cell numbers in group 3 compared to group 2 after the first week of culture.

For all time points group 1 (constructs cultured in a Petri dish) had the lowest cell number compared to the other 2 groups that were cultured in the MSTE statically and dynamically. Constructs in group 1 were lying horizontal with their bottom part touching the Petri dish and stagnant media covering the rest of the constructs. Groups 2 and 3, on the contrary, were cultured in the MSTE with media continuously flowing around the samples on all sides. The lower cellularity in group 1 could imply the presence of external mass transport limitations to the HUV.

The significant increase in cell number after 2 weeks of culture for dynamic samples over static controls was also reflected in histological analysis. The unoccupied luminal space in the middle portion of the HUV remained almost unchanged for the static cultures of group 2 (Figure 5.5)

compared to a 50% decrease for mechanically stimulated constructs in which proliferating cells within collagen matrix filled up the central portion of the scaffold (Figure 5.4-b). The increase in ECM deposition was also reflected in RT-PCR results where collagen types I and III were upregulated 4 and 3 fold, respectively, in tensioned samples compared to the static cultures. Cells within mechanically stimulated constructs penetrated almost 75% of the thickness of the HUV unlike the static controls where this penetration was limited to the first quarter of the scaffold (Figure 5.6). Clearly mechanical stimulation enhanced the migratory capacity of MSCs into the tortuous porous network of the HUV extracellular matrix. Mechanical stimulation had also an effect on fiber alignment and cell shape within the scaffold (Figure 5.7 and Figure 5.8). Stretching the samples aligned collagen fibers parallel to each other and gave the cells a spindle shape (shape factor of 0.7) mimicking the morphology of native tendons[200] while fibers of static controls had a random orientation and the cells remained round typically like MSCs[201]. Stretching of the nuclei of the MSCs could be an indication of their differentiation in to a specific lineage, namely tenocytes[94]. Several cell types have been widely found to respond to mechanical stimuli[5,103]. It has been suggested that the shape of the cell and its nucleus are governed by cytoskeletal tension[16,202]. Nuclei of native tendons that were deprived for two weeks from stretching transformed from elongated to rounded[91]. Upon the application of longitudinal force to tissue constructs, cells aligned in the direction of stretching[158,179,180] giving the construct a tendon-like appearance[13]. Human fibroblasts plated on RGD coated silicone dishes were mechanically stimulated with varying loading values (0%, 4%, 8%, and 12% strain) at 1 Hz for 24 hours. Straining

substrates at a higher percent lengthened cells and resulted in an increase in their alignment[180].

All cellular groups had improved mechanical properties 1 and 2 weeks post culture, showing that the presence of cells in the scaffold contributed to the increase in the strength and stiffness of the seeded HUVs. *De-novo* secreted ECM and generated contractile forces through adhesion proteins are two ways in which cells could contribute to the increase in mechanical properties of the constructs[131]. Stretching significantly improved the mechanical properties of cellular constructs of group 3 compared to groups 1 and 2. The ultimate tensile stress and modulus of elasticity values for tensioned constructs were at least 1 fold higher than untensioned constructs after 2 weeks of culture (Figure 5.9-a and Figure 5.10-a). The significant increase in mechanical properties of the stimulated samples compared to all the controls was due to the combined effect of stretching and the presence of cells within the constructs. Stretching collagenous tissues or polymeric scaffolds has previously been found to align the *in-vitro* synthesized or already existing fibers in a parallel manner improving the mechanical properties of the biotissue[75,181,203]. Mechanically stimulating MSC seeded collagen gels for 2 weeks increased their linear modulus 4 folds compared to the untensioned controls[203]. Similar results were reported when rat knee patellar tendons, transplanted into the subcutaneous tissue, were cyclically tensioned for 4 weeks[181].

To determine whether the presence of cells played a role in improving mechanical properties of tensioned constructs group 4 was introduced. Acellular scaffolds were dynamically cultured in the MSTE in the same

manner and under the same conditions as group 3. If the increase in mechanical properties (ultimate tensile stress and modulus of elasticity) was solely due to stretching then group 4 should have similar mechanical properties as group 3. However, after 2 weeks of culture group 4 had an ultimate tensile stress of 1.4±0.5 MPa significantly lower than group 3 (2.6±0.7 MPa). Similarly, the modulus of elasticity for group 4 was 4 fold lower than that of group 3. Our results are in agreement with previous studies which reported that the presence of cells significantly increased the mechanical properties of collagen scaffolds[133].

After 2 weeks of stimulation, the resulting constructs in this study had ultimate tensile strength values only 1 order of magnitude lower than human tendons (50-125 MPa)[41,130] and within the range of ultimate strain of human tendons (9%-35%)[41] (Table 5.2). Moreover, the HUV scaffold had a characteristic toe region in the stress-strain curve reflecting crimp, which is an extremely important property of tendons and ligaments because it allows the soft tissue to briefly stretch before it acquires significant force, thus protecting the muscle and the joints[35]. The results obtained are promising and could lead to bio-artificial tendon tissue cultured *in-vitro* with the careful optimization of potentially critical culture parameters such as seeding density, loading regimes, and stretching durations.

Table 5.2: Strain at ultimate tensile stress for different groups.

	Strain at Ultimate Tensile Stress		
Culturing Duration	**Group 1**	**Group 2**	**Group 3**
1 week	27 ± 10	22 ± 3.0	21 ± 9.0
2 weeks	29 ± 9.0	20 ± 6.0	24 ± 2.0

A limitation of the current design is the lack of incorporating a transitional region that allows fixation of the construct to the bone. The major

function of tendons is to transmit loads from the soft tissue to the bone, thus failure to fix the engineered construct to the bone might render the bio-artificial tendon dysfunctional[35]. In an attempt to reproduce and better understand the bone to soft tissue attachment region, a number of studies were conducted in which osteoblasts, fibroblasts[204,205], and chondrocytes[206] were co-cultured. Several fixation methods of soft tissue to bone were investigated including staples, sutures, screws[207,208], and soft tissue plates[208]. Screws were reported to give superior results over the rest of the choices. After attaching soft tissue engineered constructs into bone via insertion through a drilled bone tunnel, bone growth into the construct was observed[209,210]. Therefore, it is possible that upon implanting the HUV tendon model *in-vivo*, the segment that is enveloped by the bone tunnel would calcify due to signaling effects from cells at the insertion point, giving the construct enough strength at the enthesis. Further research is required to fully understand these mechanisms.

5.5. CONCLUSIONS

Results have shown the ability of MSCs to proliferate and migrate deep into the HUV scaffold when subjected to stretching. After 2 weeks of culture an increase in cell number was measured for all groups, however the increase was at least 8 folds higher for tensioned constructs. Mechanically stimulating constructs with 2% strain for one hour per day increased the proliferation rate of MSCs and gave the construct a tendon like appearance. Histological images showed ECM fibers and cell nuclei aligned parallel to the direction of stretching mimicking the morphology of native tendons. Moreover, mechanostimulation resulted in significantly stronger and stiffer constructs compared to un-tensioned samples. It is recommended in future work to

investigate mass transport of nutrients through the HUV to better understand the relationship between mechanical stimulation and cell proliferation.

In Chapter 6 the diffusion of nutrients and biomolecules, having a wide range of molecular weights, through the different layers of the HUV is investigated.

CHAPTER 6

DIFFUSION OF NUTRIENTS AND BIOMOLECULES THROUGH THE HUMAN UMBILICAL VEIN

6.1. INTRODUCTION

The human umbilical cord has been recently documented as a source of stem cells and biological scaffolds for tissue engineering. Wharton's Jelly cells have been classified as stem cells that could differentiate into different lineages including adipose[105,211], bone[105,211,212], cartilage[105,211,212], cardiac[105,213] and neural[117,212,214] tissue. The Wharton's Jelly matrix is rich with collagen[137], proteoglycans[138,139], and growth factors[136,140,141] and could potentially evade the immune response[215,216], which makes the human umbilical vein an attractive biological scaffold for tissue engineering applications. The Human Umbilical Vein (HUV) has been used as a scaffold for nerve[217], cardiovascular[134,218-220], as well as, soft musculoskeletal[79] tissue engineering constructs. In most of *in vitro* tissue engineering applications the cells are seeded in the central portion of the HUV while nutrients are supplied at the external surface of the scaffold. As a result, the transport of nutrients and growth factors through the wall of the scaffold is critical for cell survival, proliferation and migration into the interior of the HUV, and for final construct biological and biomechanical properties.

In most tissue engineering applications the HUV is decellularized prior to being used as a biological scaffold[134,217]. Thus, to better simulate the diffusion of nutrients and biomolecules through this novel scaffold, the HUV was used in its decellularized form. Since the HUV is a multilayer biological tissue mainly composed of the WJ matrix and the wall of the vessel, glucose

permeability through the HUV wall was compared to that through the Wharton's Jelly matrix to determine which layer controls the rate of nutrients diffusion. Moreover, to better understand mass transport through this material, the permeability of the HUV to FITC-Dextran molecules spanning a wide range of molecular weights was measured. To our knowledge, this is the first published attempt to characterize the diffusion of nutrients through the different layers of the HUV, and measure the permeability of the HUV membrane to molecules of different molecular weights.

6.2. MATERIALS AND METHODS

6.2.1. Preparation of the HUV

Refer to sections 4.2.1 and 4.2.2.

Before being placed in the diffusion chamber the HUV was cut open along its longitudinal axis, and dissected into squares having a side length of approximately 1.5 cm.

6.2.2. Experimental Setup

A side-by side diffusion chamber was designed to allow the measurement of the effective diffusivity through the HUV. The setup was previously used to measure the permeability of small intestinal submucosa[221]. However, the apparatus had to be modified to fit the dimensions of the HUV. The set up consisted of two cylindrical chambers having a diameter of 9.5 mm, a length of 3.5 cm, and an individual volume of 2.5 ml (Figure 6.1). A 1.0±0.2 mm thick square section of HUV was placed between the two chambers. The molecule of interest was loaded in the first chamber, with a predetermined concentration, facing the luminal side of the HUV, and 2.5ml of

nano pure water were loaded in chamber 2 facing the ab-luminal side of the HUV. This layout for the HUV membrane was chosen because in musculoskeletal applications media was supplied to the construct at the luminal side of the HUV, and nutrients had to diffuse through the membrane thickness to the central portion where the cells were inoculated.

Two different solutions were used for the measurements of the apparent diffusion coefficient. The first solution was FITC-conjugated dextran molecules with three different molecular weights: (FITC-4) 4.4 KDa, (FITC-50) 50 KDa, and (FITC-580) 580 KDa. In experiments conducted with these molecules the biomolecule solutions were loaded at a concentration of 70μg/ml. Samples were taken out at 0, 6, 10, 20, 24, 31, and 45 hours. The second solution was glucose (0.18 KDa), which was chosen because it is a key component in cell culture media and necessary for cell nutrition and survival. Glucose was loaded into chamber 1 at a concentration of 100 mg/ml. Samples were taken at 0, 0.5, 1, 2, 4, 6, 8, 10, 12, 20, 22, 24 hours.

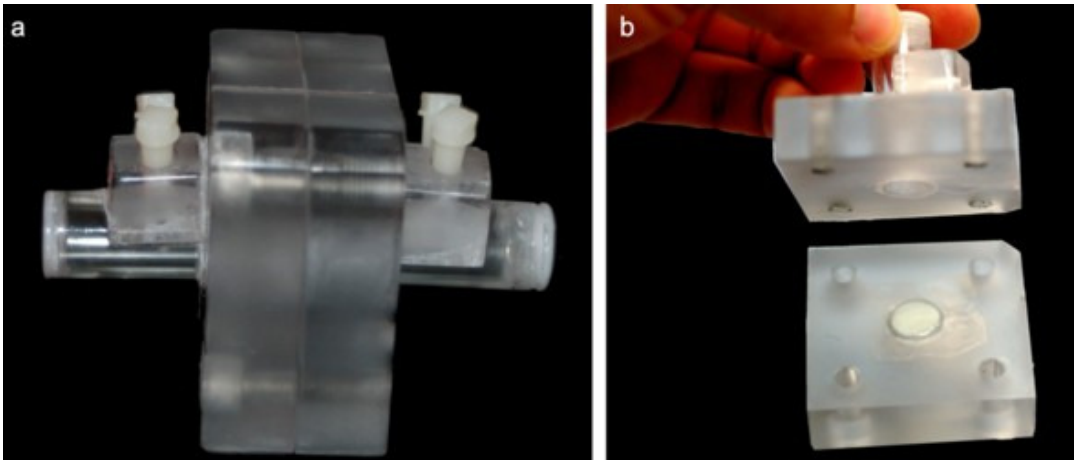

Figure 6.1: Experimental setup showing the side view (a) and cross sectional view (b) of the custom made diffusion chamber.

Being composed of different layers including the wall of the HUV, the loose irregular layer surrounding it, and a Wharton's Jelly (WJ) layer, the HUV

is considered anisotropic and non-homogeneous. Thus the diffusion of glucose was calculated through the HUV, as well as the WJ. Moreover, to determine the amount of time necessary for the HUV to become saturated with glucose, two different HUV sections were placed in the diffusion chamber with two different setups: the first HUV section was immersed in nano pure water (unsaturated HUV section), while, in the second setup, the HUV section was pre-saturated with 100mg/ml of glucose solution (saturated HUV section) for 48 hours on an orbital shaker.

For all experiments, several 10 µl samples were collected from both chambers at each time point, and were replaced by 10 µl of the original solution. Collected samples were diluted to 1 ml using nano pure water. The total volume of samples collected from the chamber was less than 5% of the total chamber capacity. The concentration of different molecules at each time point was calculated by measuring the fluorescence or absorbance of the sample as illustrated in the following sections. To calculate the coefficient of diffusion, The HUV was considered as a "thin membrane" and a quasi-steady state was assumed[222]. Equation 6.1 was used to calculate the apparent coefficient of diffusion[222]:

$$\ln\left(\frac{2C_1 - C_0}{C_0}\right) = -\frac{2A_m D_{eff}\phi}{VL_m}t$$

Equation 6.1: Quasi-steady transport across a thin membrane

Using the aforementioned expression it was possible to plot the value of $\ln\left(\frac{2C_1 - C_0}{C_0}\right)$ versus time (t), resulting in a linear fit with a slope of

$-\frac{2A_m D_{eff}\phi}{VL_m}$. Thus, the apparent diffusion coefficient was computed using Equation 6.2.

$$D_{apparent} = D_{eff}\phi = -\text{slope} * \frac{V * L_m}{2A_m}$$

Equation 6.2: Expression used to determine the apparent diffusion coefficient.

Where C_0 is the initial solute concentration in chamber 1

C_1 is the measured solute concentration in chamber 1 at time t

A_m is the cross sectional area of the HUV (0.713cm^2)

L_m is the thickness of the HUV (0.1 cm)

V is the volume of each chamber (2.50 ml)

The permeability of different molecules to the membrane was deduced from the apparent coefficient of diffusion using Equation 6.3[222].

$$P = \frac{D_{app}}{L_m}$$

Equation 6.3: Relationship between the coefficients of permeability and diffusion.

6.2.3. Glucose Assay

Glucose concentrations were computed using an enzymatic method that results in an increase in the absorbance of the samples which is proportional to the glucose content. Standards of known increasing glucose concentrations were prepared (0, 0.05, 0.1, 0.5, and 1 mg/ml). Samples and standards were assayed in triplicates to account for sampling error. 10 µl of sample or standard was added to each well. Each occupied well was then supplemented with 100 µl of glucose assay reagent (Sigma-Aldrich G3293, St. Louis, MO, USA). Blanks were prepared for each sample, in which 100 µl of nano pure water replaced the glucose assay reagent. The plate was

incubated on a shaker for 20 minutes allowing the glucose assay reagent to react with the samples. Finally, the absorbance was measured at 340 nm.

Using the data from the standards a linear relationship was developed between the absorbance and the glucose concentration. The glucose concentrations in the assayed samples were determined by linear regression analysis of the standard curve.

The enzymatic method used in this assay results in an increase in the final absorbance which is directly proportional to the glucose concentration in the sample. Upon the addition of the glucose assay reagent, glucose is phosphorylated by adenosine triphosphate (ATP), in the presence of hexokinase, into Glucose-6-Phosphate (G6P) (Equation 6.4). In a second reaction, catalyzed by glucose-6-phosphate dehydrogenase (G6PDH), G6P is oxidized to 6-phosphogluconate accompanied by the reduction of nicotinamide adenine dinucleotide (NAD) into NADH (Equation 6.5), which results in an increase in absorbance signal. All the components required for this reaction to occur are present in the glucose assay reagent, which is composed of: 1.5 mM nicotinamide adenine dinucleotide (NAD), 1.0 mM adenosine triphosphate (ATP), 1.0 unit/ml of hexokinase, and 1.0 unit/ml of glucose-6-phosphate dehydrogenase

$$\text{Glucose} + \text{ATP} \xrightarrow{\text{Hexokinase}} \text{G6P} + \text{ADP}$$

Equation 6.4: Phosphorylation of glucose followed by due to the addition of glucose assay reagent.

$$\text{G6P} + \text{NAD} \xrightarrow{\text{G6PDH}} 6\text{-phosphogluconate} + \text{NADH}$$

Equation 6.5: Reduction of NAD to NADH due to the addition of glucose assay reagent.

6.2.4. Measurement of Fluorescence of Dextran Molecules

For each collected sample triplicates of 100 µl were assayed. The fluorescence of assayed samples was read in a synergy plate reader (Bio-Tek, Winooski, VT) at an excitation wavelength of 480 nm and emission wavelength of 520 nm. The concentrations were deduced from the degree of fluorescence using a pre-generated standard curve.

6.2.5. Determination of the Partition Coefficient

The partition coefficient was determined using the same technique previously employed to measure glucose partition coefficient of the lower layers of the skin[223]. Briefly, a 0.75mm thick section of HUV was immersed in a solution containing 2mg/ml of glucose in nano pure water. After 24 hours, the glucose concentrations in the HUV and in the solution were measured. The partition coefficient was calculated as the ratio of the glucose concentration consumed by the HUV to the glucose concentration left in solution.

6.2.6. Statistical analysis

For each molecular weight 3 HUV sections were tested and results were expressed as mean values ± standard deviation. Statistical analysis to compare results among groups was performed using the multivariate analysis of variance (ANOVA) method. A significant difference corresponds to a confidence level >95%.

6.3. RESULTS

6.3.1. Apparent Coefficient of Diffusion of Glucose through the HUV

Figure 6.2 shows a plot of the increase in glucose concentration in chamber 2 versus time, for both glucose saturated and unsaturated HUV sections. There was an initial increase in the glucose concentration for the saturated HUV compared with a zero concentration for the unsaturated HUV at time zero. However, after 10 hours the two curves followed similar paths, indicating that the originally unsaturated decellularized HUV tissue became saturated with glucose. Thus, it is recommended to soak the scaffold with culturing medium overnight before using it for tissue engineering applications

Using the linear fit plots for the HUV sections (Figure 6.3-a) and the WJ sections (Figure 6.3-b), the average slopes were determined as -0.053 ± 0.013 for the HUV sections versus -0.063 ± 0.011 for the WJ sections. The resulting average apparent diffusion coefficients were $D_{app\ HUV}$ = 0.21 ± 0.04 cm^2/day versus $D_{app\ WJ}$= 0.26 ± 0.05 cm^2/day, respectively (Figure 6.4).

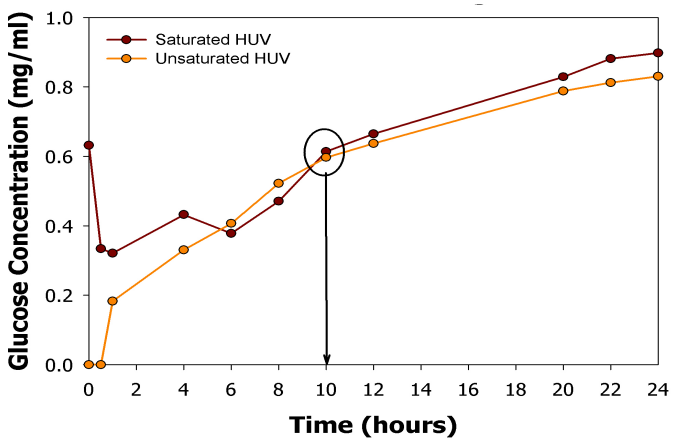

Figure 6.2: Increase in glucose concentration versus time for glucose saturated and un-saturated HUV sections.

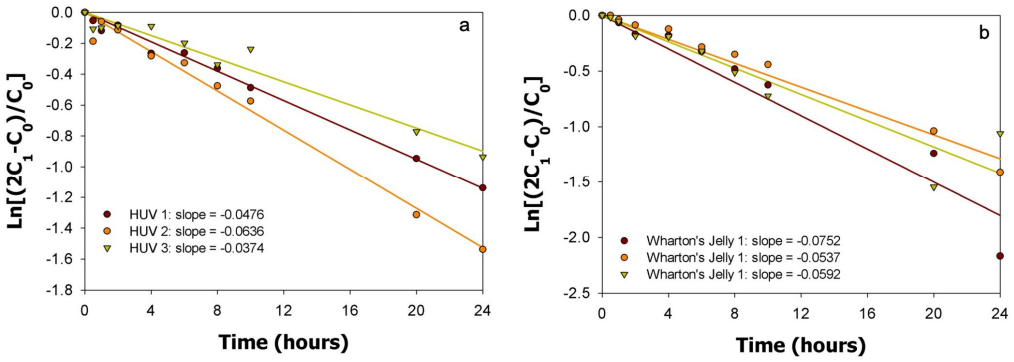

Figure 6.3: Linear fit plot used to determine the apparent diffusion coefficient of the (a) decellularized HUV and (b) Wharton's Jelly

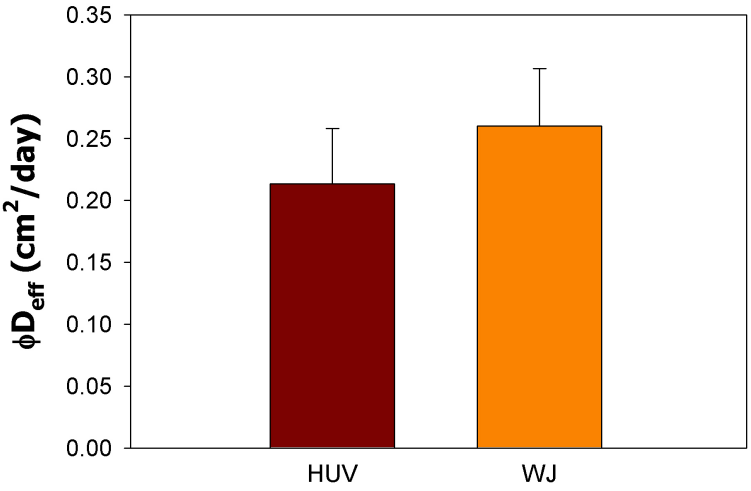

Figure 6.4: Glucose apparent diffusion coefficient of the HUV and the WJ.

6.3.2. Glucose Partition Coefficient of the HUV

Table 6.1 includes a list of the glucose partition coefficients for different sections of HUV and WJ having a thickness of 1.0 ± 0.2 mm. There was no significant variability in the glucose partition coefficients of either HUV or WJ sections obtained from different umbilical cords since their coefficients of variability were 12%, and 3%, respectively. However, the average glucose partition coefficient of the HUV (0.13 ± 0.02) was significantly lower than that of the WJ (0.21 ± 0.01).

Table 6.1: Glucose partition coefficients for HUV and WJ.

	Partition Coefficient (ϕ)	
	HUV	**WJ**
Section 1	0.13	0.21
Section 2	0.12	0.20
Section 3	0.15	0.20
Average	**0.13**	**0.20**
STDEV	**0.02**	**0.01**

6.3.3. Diffusion of Fluorescently Tagged Molecules through the HUV

Large molecules (50 KDa and 580 KDa) did not diffuse through the HUV during the time frame of 48 hours. Figure 6.5 shows the side-by-side diffusion chamber 48 hours after being loaded with the fluorescently tagged dextran molecules (70 μg/ml) having a molecular weight of 580KDa in chamber 1 and nano pure water in chamber 2. It is clear that none of the fluorescent molecules diffused to chamber 2 in which the solution showed no fluorescence. Moreover, there was no decrease in the fluorescence concentration with time during the experimental duration of 48 hours.

Figure 6.6 shows the linear fit plot of the logarithmic of concentrations versus time for the diffusion of different molecules through the HUV. The slope for the glucose molecule was -0.053±0.013 while that of the 4.4 KDa molecule was -0.013±0.002, resulting in apparent diffusion coefficients of $D_{app\ HUV}$ = 0.21 ± 0.04 cm^2/day versus $D_{app\ 4.4KDa}$= 0.05 ± 0.01 cm^2/day (Figure 6.7).

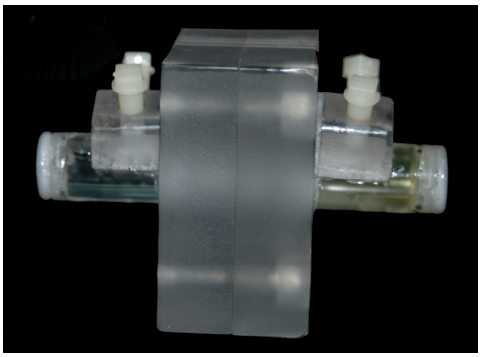

Figure 6.5: Diffusion chamber 48 hours after loading fluorescently tagged dextran molecules with a molecular weight of 580 KDa.

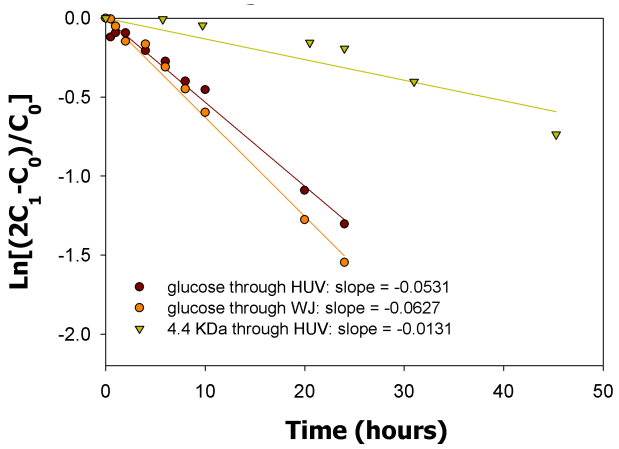

Figure 6.6: Linear fit plot used to determine the apparent diffusion coefficient of molecules with different molecular weights through the HUV.

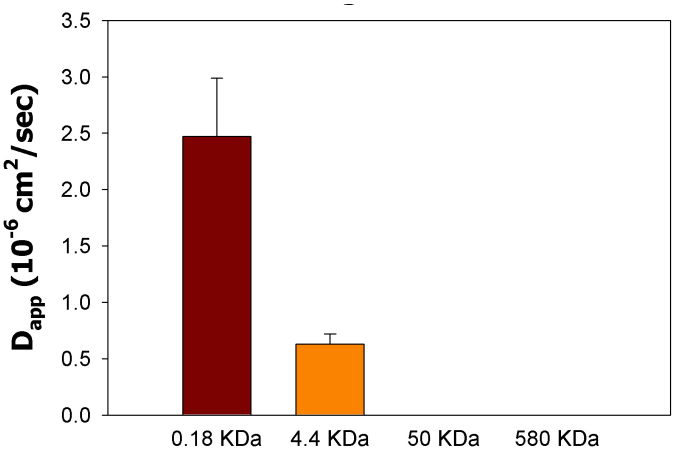

Figure 6.7: Apparent diffusion coefficient of molecules with different molecular weights through the HUV.

6.4. DISCUSSIONS

Although the average apparent diffusion coefficient of glucose through the WJ was slightly higher than that through the full HUV section, there was no statistical difference between the two values. The tested section of HUV had a total thickness of 1.0 ± 0.2 mm. Knowing that the wall of the HUV only composes 0.54 ± 0.02 mm[219] of the total thickness, we could deduce that the tested section of HUV had almost 45% of WJ matrix in it (Figure 6.8). The wall of the HUV, in turn, is composed of three sub-layers: intima (14%), media (59%) and adventitia (27%)[219]. Considering the variability in the thicknesses of the different layers composing the HUV, it would be more meaningful to compare the permeability of the membrane to glucose rather than the coefficient of diffusion through the HUV[224]. Since the flow of nutrients is passing through the two main stratified layers of the HUV, then the total coefficient of permeability (P_{HUV}) is limited by the individual coefficients of permeability of the WJ (P_{WJ}) and the HUV wall ($P_{HUV\ wall}$) layers.

$$\frac{1}{P_{HUV}} = \frac{1}{P_{WJ}} + \frac{1}{P_{\text{HUV wall}}}$$

Equation 6.6: The average permeability coefficient across the full HUV as a function of the permeability coefficients of individual layers.

Using the above relation, and normalizing the coefficients of permeability by the individual layer thickness, the resulting glucose coefficient of permeability through the WJ was $P_{WJ} = 3.0x10^{-5} \pm 5.4x10^{-6}$ cm/sec significantly larger than that of the HUV wall $P_{HUV\ wall} = 2.2x10^{-5} \pm 5.0x10^{-6}$ cm/sec (Figure 6.9). This was expected since the wall of the HUV includes the media layer that is composed of packed smooth muscle fibers and densely interwoven collagen fibers[219] compared to the loose architecture of

the fibers of the WJ (Figure 6.10). This observation was also reflected in the results of glucose partition coefficient that was significantly lower for the HUV (0.13 ± 0.02) than for the WJ (0.21 ± 0.01).

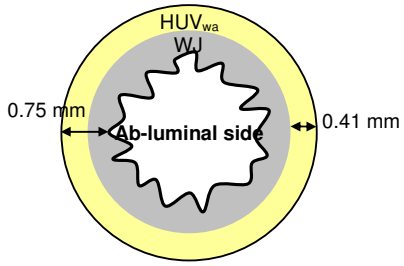

Figure 6.8: Schematic cross-section showing the main two layers composing the HUV.

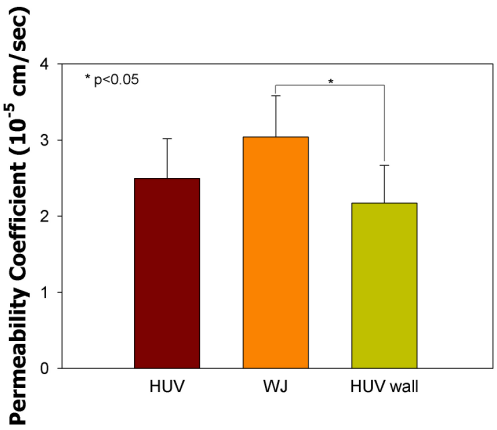

Figure 6.9: The permeability of different layers of the HUV to glucose.

The resulting permeability coefficients of the HUV to molecules with different molecular weights were documented in Table 6.2. Although large molecular weight dextrans (> 50 KDa) did not diffuse through the HUV, it could not be concluded that proteins having a molecular weight larger than 50 KDa would not permeate through the membrane. Two molecules having the same molecular weight might have significantly different geometries. For instance, bovine serum albumin has a molecular weight of 65 KDa but a molecular radius R = 3.5 nm[224] significantly lower than FITC-50 with an R = 4.9 nm Table 6.2. Thus, it was necessary to compare the permeability of the HUV using the molecular radius, or Stoke's radius, rather than the molecular

weight. Therefore, large proteins, such as immunoglobulin G antibodies (MW=140 KDa)[224], having a molecular radius of 5.0 nm[224] larger than 4.9 nm would not diffuse through the wall of the HUV.

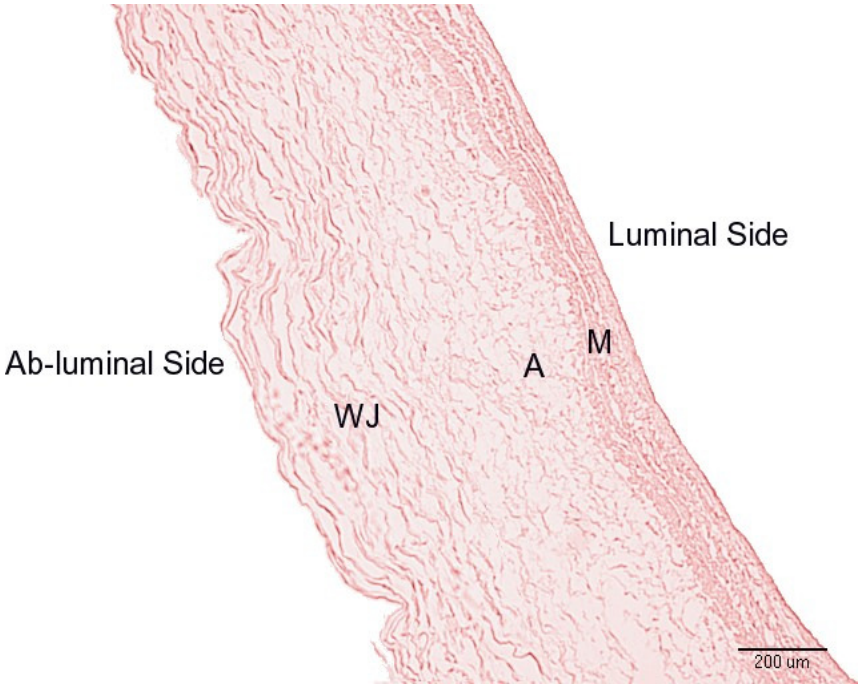

Figure 6.10: Longitudinal histological section of the decellularized inverted HUV showing fiber density in the different layers. Tunica Media (M), Tunica Adventitia (A), and Wharton's Jelly (WJ).

Table 6.2: Molecular weights (MW), Radii of gyration (Stokes radii, R) [225-227], and their coefficients of permeability (P) through the HUV.

Tracer	MW (KDa)	R (nm)	P (cm/sec)
Glucose	0.18	0.4	$2.5\text{x}10^{-5} \pm 5.0\text{x}10^{-6}$
FITC-4	4.4	1.3	$6.4\text{x}10^{-6} \pm 9.0\text{x}10^{-7}$
FITC-50	50	4.9	0
FITC-150	150	8.2	0
FITC-580	580	14.8	0

The apparent coefficient of diffusion through the HUV decreased exponentially with the increase in the molecular weight. However, an inversely proportional relationship was revealed when the coefficient of permeability was plotted against the molecular radius (Figure 6.11). Thus, using the resulting relation it is possible to predict the coefficient of

permeability of dextrans with different molecular weights through the HUV. However, dextran is known to be neutral. Thus, the proposed relation cannot be used to predict the diffusivity of proteins with different chemical properties, such as surface charge, that might demonstrate a strong affinity for the HUV.

One limitation of the current work is the dependency of all the documented results on the method employed to decellularize the HUV. Different decellularization techniques result in scaffolds with altered architectures, and thus the partition, diffusion, and permeability coefficient would vary significantly. For similar reasons, the presented values are not proper to analyze the cellular HUV.

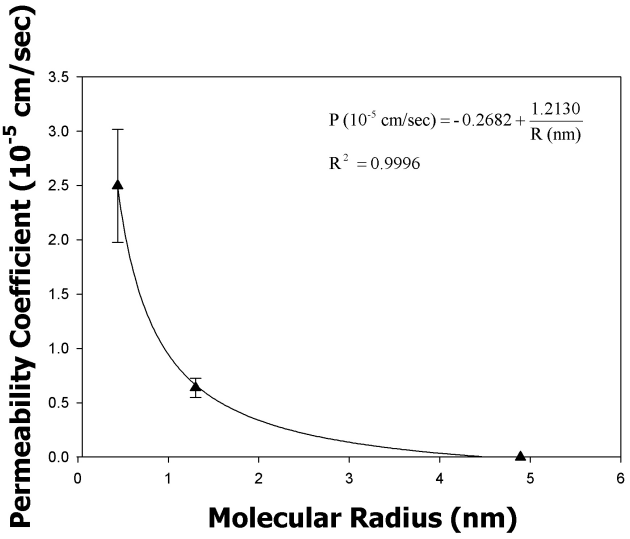

Figure 6.11: A plot showing the permeability coefficient of the HUV versus the molecular radius (Stoke's radius) of the diffusing molecule. The coefficient of permeability demonstrates an inversely proportional relation with the molecular radius.

6.5. CONCLUSIONS

It was determined that glucose permeability through the HUV wall was significantly lower than that through the WJ. It took the membrane almost 10 hours to get saturated with glucose. Thus to enhance glucose transport through the HUV on the onset of experimental setup, it is recommended to

soak the biological scaffold overnight with media before using it for tissue engineering applications which involve seeding cells at the interior void space of the HUV that lacks direct access to the cell culture media. Thus the cells initially seeded in the central cylindrical space of the HUV depend solely on diffusion to acquire glucose and other necessary metabolites for their survival and proliferation. If the cellular glucose consumption rate is known it would be possible to calculate the maximum number of cells that are able to reside in the central space of the HUV and still be sufficiently nourished.

The coefficient of permeability of glucose was almost an order of magnitude higher than that of FITC-Dextran 4.4 KDa. An inversely proportional relation was developed between the molecular radius and the permeability of dextran molecules through the HUV. However, this relation could be used to predict the coefficient of permeability of proteins that do not possess a strong net surface charge or a strong affinity for the HUV. High molecular weight FITC-Dextran molecules did not diffuse through the HUV, limiting the molecular radius of proteins that could permeate through the biological scaffold to less than 4.9 nm.

In Chapter 7 the cellular glucose consumption is computed and the maximum number of cells that could be efficiently seeded into the HUV is calculated.

CHAPTER 7

OPTIMIZING SEEDING DENSITY FOR A TISSUE ENGINEERED TENDONS USING THE HUMAN UMBILICAL VEIN

7.1. INTRODUCTION

The main three components of functional tissue engineering are cells, a biocompatible scaffold to house the cells and give the construct initial mechanical integrity, and a bioreactor which provides the appropriate biochemical and biomechanical signals to regulate cell differentiation and tissue assembly[89,93-95]. The initial seeding density is a critical variable in the attainment of a functional engineered tissue since cells are responsible for tissue deposition and extracellular matrix (ECM) remodeling. A large number of cells is required on the scaffold to achieve successful ECM deposition *in vitro*[142,143]. Moreover, uniform cell seeding throughout the scaffold is required to obtain homogeneous tissue formation throughout the scaffold, including the central part[92].

To our knowledge, only one study has been performed on the effect of seeding density on the morphometric properties of engineered tendons *in-vitro*. Collagen gels were seeded with rabbit MSCs at three different densities (1, 4, and 8 million cells/ml) and tensioned longitudinally[228]. Higher seeding densities resulted in more aligned and elongated cell nuclei 72 hours after seeding. No further investigation was conducted for cultures beyond 72 hours and no mechanical analysis was performed on the constructs. Extending the above study to include longer culture periods and mechanical analyses on constructs would provide valuable insight towards engineering a functional tendon model.

In a previous study the potential of the HUV, seeded with 1 million cells/ml and cyclically stretched for durations up to 2 weeks, to act as a tissue engineered tendon was assessed. There was a need to optimize potentially critical culture parameters such as seeding density, loading regimes, and stretching durations. Thus, in this study at attempt at optimizing seeding densities is made. Since a low seeding density of 1 million cells/ml was already considered, in the current study the effect of 2 additional seeding densities on the morphometric and mechanical properties of the tissue engineered tendon would be investigated: Medium Seeding Density (MSD = 5 million cells/ml) and High Seeding Density (HSD = 10 million cells/ml). Moreover, the cellular glucose consumption would be measured,. Knowing glucose diffusion coefficient through the HUV, the limiting seeding density inside the HUV would be computed.

7.2. MATERIALS AND METHODS

7.2.1. Preparation of the HUV

Refer to section 4.2.1 and 4.2.2.

7.2.2. Cell Source

Refer to section 4.2.3.

7.2.3. Experimental Setup

Refer to section 4.2.4 and 5.2.4.

Two groups were considered: Static samples were seeded controls cultured in the bioreactor without any mechanical stimulation; and dynamic cultures were seeded constructs cultured in the bioreactor and subjected to 1

hour of cyclic stretching per day at 2% strain and a frequency of 0.0167 Hz. Constructs were cultured for durations of 1 and 2 weeks. At the end of each culture duration, constructs were tested for glucose consumption, cell density by quantifying DNA content, morphology using histology, and mechanical properties by stretching to failure.

7.2.4. Calculation of Glucose Consumption

Two different methods were employed to calculate the glucose consumption per cell: 2-dimensional (2D) setup in 6-well plates, and a 3-dimentional (3D) setup using the HUV.

7.2.4.1. 2D Setups

For 2D setups cells were mixed with type I collagen gel and then suspended on plasma treated 6-well plates (BD Biosciences, San Jose, CA). The final concentration of collagen gel was 2 mg/ml. The collagen mix was allowed to polymerize at 37°C for 1 hour after which the cellular hydrogel was covered with 5 ml of standard media. The well plates were placed in an incubator at 37°C and 5% $C0_2$. Three different seeding densities were employed to investigate if the initial seeding density has an effect on the glucose consumption per cell: low seeding density of 5,000 cells/cm^2, medium seeding density of 20,000 cells/cm^2, and high seeding density of 50,000 cells/cm^2. Triplicate wells were prepared for each seeding density. After 24 hours of seeding the samples were nourished with fresh standard media. 0.5 ml samples were collected after 4 hours of incubation and tested for glucose content. Fresh media in a blank well plate was used as a control. The cell

number per well was quantified to permit evaluations of glucose consumption per cell.

7.2.4.2. 3D setups

In this setup glucose consumption was measured for seeded HUVs that were cultured for 1 week in the MSTE, as described previously. Constructs cultured in the MSTE were nourished with fresh media at day 6. A 1 ml centrifuge tube was filled with fresh media and placed in the incubator as a control sample. At day 7, 0.5 ml of media was collected from the MSTE and tested for glucose content. The constructs were also tested for DNA content. This allowed us to compute the glucose consumption per construct as well as the glucose consumption per cell.

7.2.4.3. Glucose Assay

Samples and controls stored in centrifuge tubes were tested for glucose content using an enzymatic method as follows. In a transparent 96-well plate, 10 μl of sample/control were pipetted into predetermined wells. Each occupied well was then supplemented with 100 μl of glucose assay reagent (Sigma-Aldrich G3293, St. Louis, MO, USA). Blanks were prepared for each sample/control, in which 100 μl of nano pure water replaced the glucose assay reagent. The addition of the glucose assay reagent results in a series of reactions which lead to the reduction of nicotinamide adenine dinucleotide (NAD) into NADH. This reduction, in turn, causes an increase in the absorbance signal, which is proportional to the sample glucose content. The plate was incubated on a shaker for 20 minutes allowing the glucose assay reagent to react with the glucose present in the samples, and the

absorbance was measured at 340 nm read using a Synergy HT plate reader (Bio-Tek, Winooski, VT). A plot was generated using the absorbance signals from standards with known glucose concentrations ranging between 0 and 1 mg/ml. The glucose concentrations in the assayed samples/controls were deducted from the linear regression analysis of the standard curve.

The glucose consumption was calculated as the difference between the glucose content of the control and that of the sample. Glucose consumption results were normalized by the number of cells in each sample.

7.2.5. Quantifying Cell Number

To quantify the cell number in each setup a PicoGreen DNA quantification kit (Invitrogen) was used. Cell number was quantified in two different setups: 2D-setups for cellular collagen hydrogels in 6-well plates, and 3D-setups for seeded HUV constructs. Different methods were used to prepare the two setups for the DNA assay.

7.2.5.1. 2D Setups

The media covering the well plates was discarded and cells were scraped with a cell scraper and dissolved in 1 ml of nano pure water. The cellular mix was sonicated in ice for 1 minute and then subjected to three freeze/thaw cycles to help cell lyses and release of the DNA into the solution.

7.2.5.2. 3D setups

To prepare the HUV for cell number analysis small 0.5 cm diameter ringlets were cut from three different locations (2 from each end and 1 from the middle section) to get an average representative number. Section were then dissected into smaller pieces $\leq 2mm^2$, and incubated with 1mm of

collagenase type I (MP Biomedicals, Solon, OH) for 5 hours at 37°C to help release the cells by digesting the extracellular matrix of the HUV. Then the solution was treated in a method similar to the 2D-setups, including sonication for 1 minute in ice followed by three freeze/thaw cycles.

7.2.5.3. DNA Assay

Refer to section 4.2.5.

7.2.6. Histology

Refer to section 4.2.6.

7.2.7. Mechanical Testing

Refer to section 4.3.3.

7.2.8. Statistical analysis

Refer to section 4.2.8.

7.3. RESULTS

7.3.1. Cell Proliferation

Table 7.1 includes cellularity of constructs and Figure 7.1 shows plots of cellular proliferation for the MSC and HSD 1 and 2 weeks post culture. A total volume of 0.6 ml of cellular collagen mix was originally inserted in the HUV. Thus, with a seeding density of 5 million cells/ml, the total number of cells originally inserted in the HUV was 3 million cells. Similarly, 6 million cells were inserted in the HUV for the high seeding density.

A significant increase in cell number was measured for the MSD (Figure 7.1-a) after 1 week of culture for both static and dynamic conditions,

however, there was no significant difference among the cellularity of the two culturing techniques (stretched versus unstretched). The cellularity of the HUV (Table 7.1) increased from 3 million to 7.8 ± 2.0 million cells for static controls and to 9.2 ± 1.4 million cells for stretched constructs. No additional increase in cell number was recorded for the construct 2 weeks post culture.

Contrarily to the above results, no significant increase in cell number was measured for the HSD for either culturing regimes at any time duration (Figure 7.1-b).

Table 7.1: Cellularity of constructs 1 and 2 weeks post culture.

	5 million cells/ml		10 million cells/ml	
	Static	**Dynamic**	**Static**	**Dynamic**
Original	3.00		6.00	
1 Week	7.8 ± 2.0	9.2 ± 1.4	5.9 ± 1.5	5.0 ± 0.7
2 Weeks	6.3 ± 0.8	1.1 ± 0.4	6.3 ± 0.8	5.5 ± 1.1

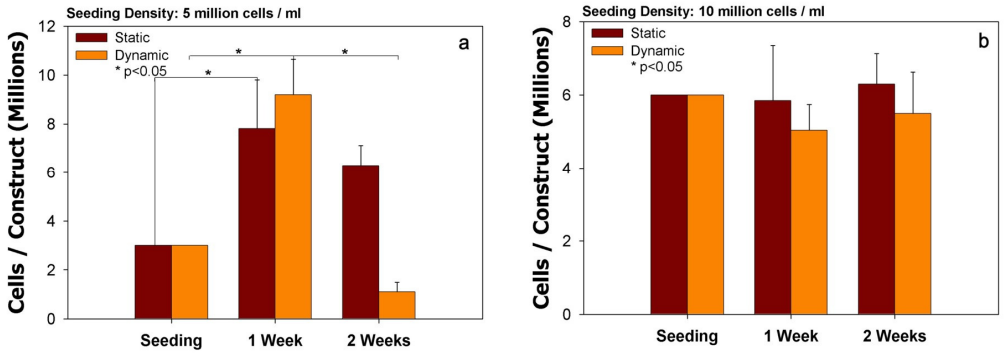

Figure 7.1: Plots of cell number (in million) per construct versus culturing duration for an initial seeding density of (a) 5 million cells/ml and (b) 10 million cells/ml.

7.3.2. Histology

Figure 7.2 shows the morphology of the HUV seeded with 5 million cells/ml after 1 week of culture. The HUV membrane seemed to preserve its original dissection thickness for both untensioned (Figure 7.2-a) and cyclically tensioned constructs (Figure 7.2-b).

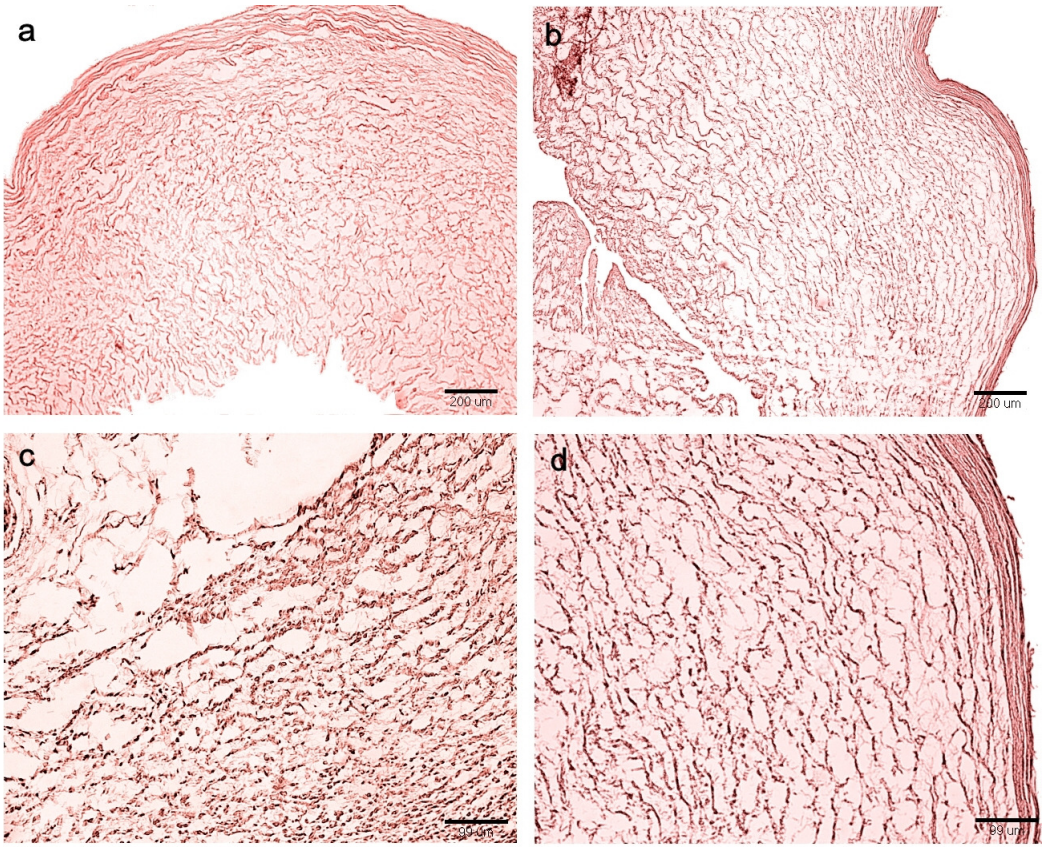

Figure 7.2: Histologic cross sections of the HUV seeded with 5 million cells/ml after 1 week of culture (a) static, (b) dynamic, (c) static at a high magnification of 10X, and (d) dynamic at a high magnification of 10X.

For both culturing conditions cells were able to proliferate and migrate into the wall of the HUV (Figure 7.2-c and Figure 7.2-d). It is clear that the scaffolds were occupied with numerous cells, some of which had reached the outer wall of the HUV in the case of stretched constructs. One significant observation is that the extracellular matrix of unstimulated constructs appeared to be degrading (Figure 7.2-c), since fewer fibers surround the cells compared to the extracellular matrix of the tensioned constructs (Figure 7.2-d). This observation was more obvious after two weeks of culture, where the wall of the HUV looked significantly thinner for both culturing conditions (Figure 7.3-a and Figure 7.3-b) compared to the scaffolds after 1 week of culture (Figure 7.2-a and in Figure 7.2-b). Fibers were clearly short and

disconnected (Figure 7.3-c) unlike the connected mesh-like morphology of the original decellularized HUV (Figure 7.3-f). Moreover, cells in the tensioned reactors had an irregular shape (Figure 7.3-d) which indicated to be lysed cell bodies at a magnification of 40X (Figure 7.3-e).

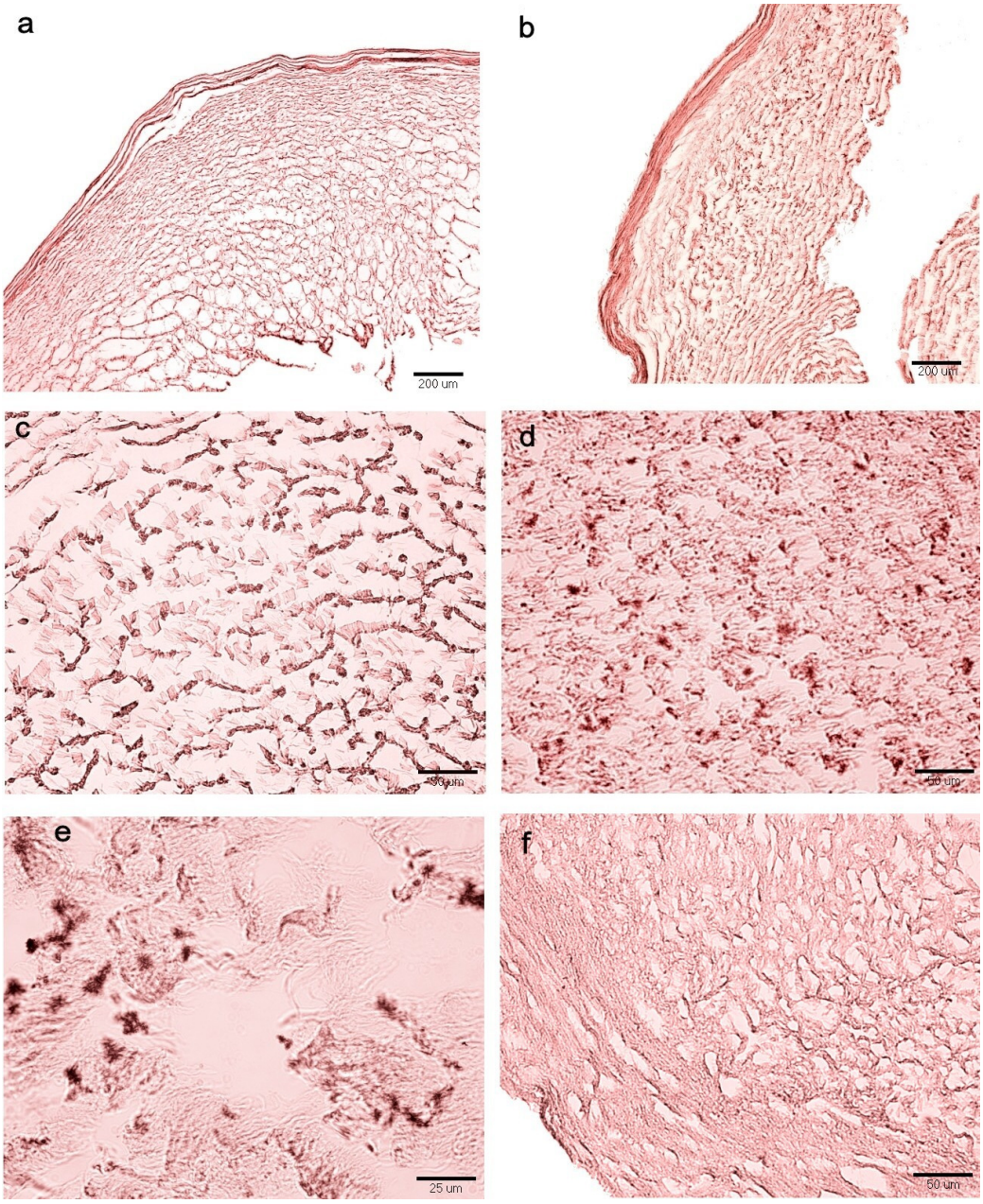

Figure 7.3: Histologic cross sections of the HUV seeded with 5 million cells/ml after 2 week of culture (a) static, (b) dynamic, (c) static with high magnification of 20X, (d) dynamic at a high magnification of 20X. (e) Close up at 40X showing lysed cell bodies after two weeks of stretching. (f) Decellularized HUV.

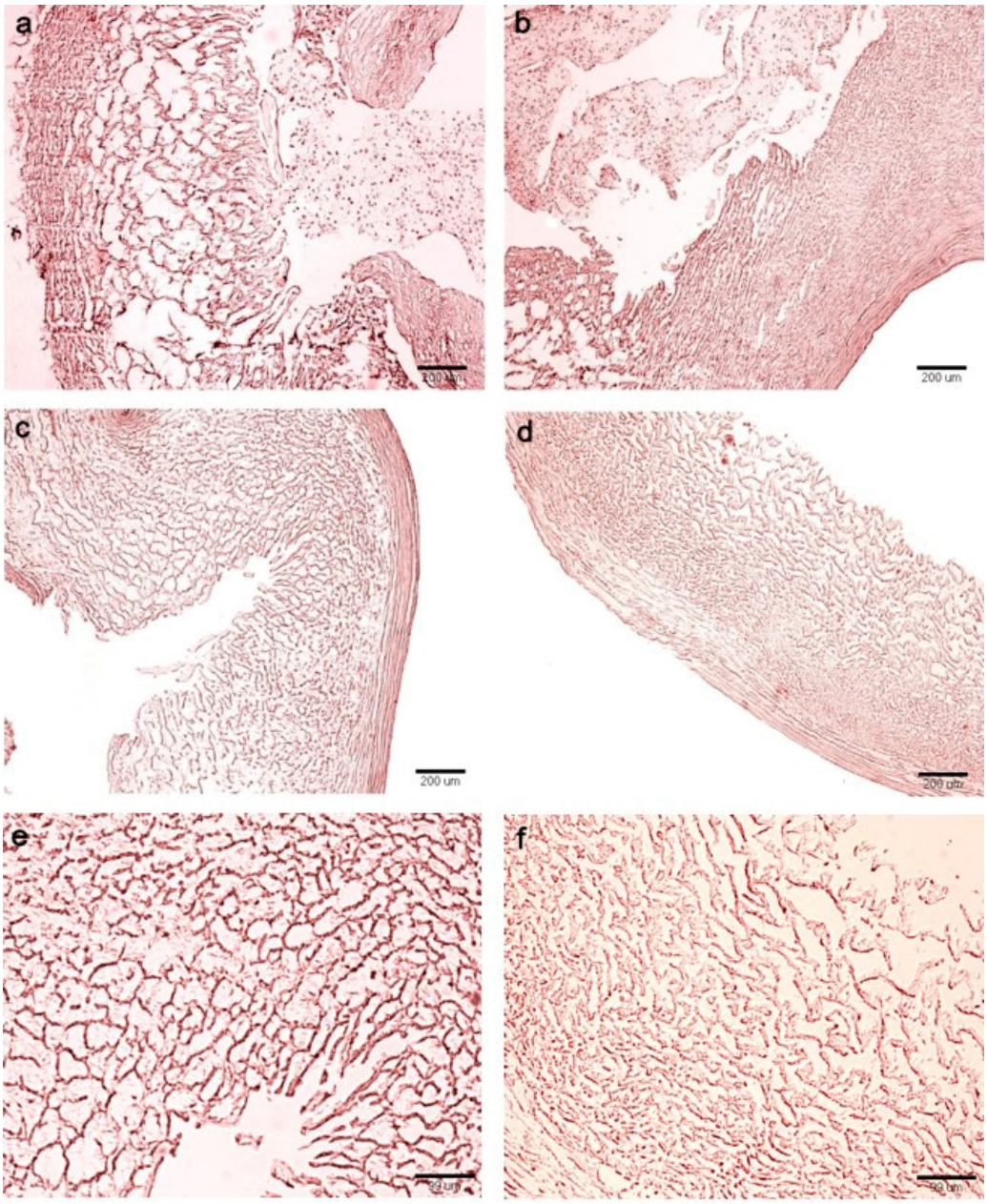

Figure 7.4: Histologic cross sections of the HUV seeded with 10 million cells/ml after 1 week of culture (a) static, (b) dynamic. HUV 2 weeks post culture (c) unstretched, and (d) stretched, (e) unstretched at a high magnification of 10X, and (f) stretched at a high magnification of 10X.

Similar results were observed for the HSD where the degradation of the matrix was more obvious at earlier culture durations. In Figure 7.4-a and Figure 7.4-b numerous cells appeared to be filling the central portion of the HUV for static and dynamic constructs, respectively. However, compared to the histological sections of MSD, the wall of the HUV looked thinner and the

matrix looked significantly degraded, especially for the unstretched samples. The thinning of the membrane persists after 2 weeks of culture (Figure 7.4-c and Figure 7.4-d). Fewer cells are visible in and around the HUV matrix (Figure 7.3-e and Figure 7.3-f).

7.3.3. Mechanical Properties

Figure 7.5 includes the results of assessed mechanical properties for both seeding densities. For the MSD, an improvement in mechanical properties was observed after the first week of culture. A statistically significant increase in the ultimate tensile stress values was recorded for tensioned samples (4100±500 KPa) compared to 1000±300 KPa for untensioned constructs and 900±100 KPa for decellularized HUVs. No additional increase in tensile strength was measured after 2 weeks of culture (Figure 7.5-a).

A similar trend was observed for the modulus of elasticity (E) values. Decellularized scaffolds had a modulus of elasticity E = 3.3±0.6 MPa. After 1 week of culture E almost doubled for static controls (E = 6.2±1.8 MPa) and quadrupled for cyclically stretched constructs (E = 12.6±4.4 MPa). No additional increase in the modulus was measured after 2 weeks of culture (Figure 7.5-b).

For the HSD, no significant increase in the ultimate tensile stress was observed for any culturing condition at either culturing points (Figure 7.5-c). However, a statistically increased trend was observed for the modulus of elasticity for both static and dynamic samples where E increased from 3.3±0.6 MPa to 10.4±1.1 MPa for unstretched constructs and to 12.2±3.1 MPa for

stretched construct 2 weeks post culture (Figure 7.5-d). No significant difference was observed among the 2 groups at any culturing duration.

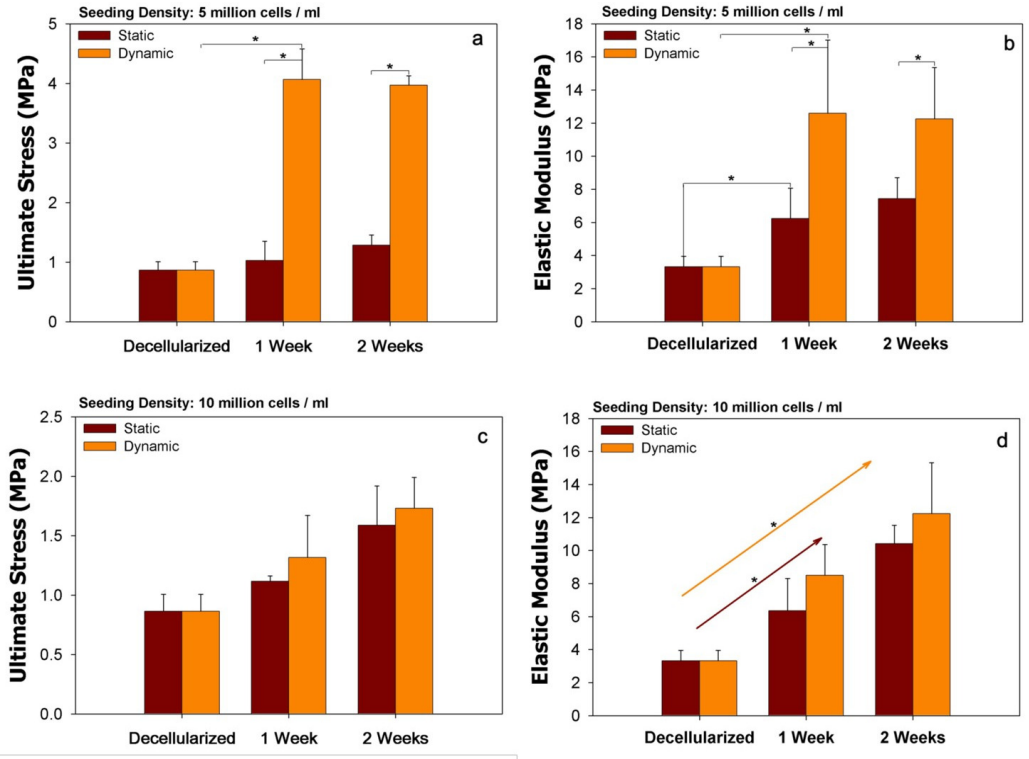

Figure 7.5: Mechanical properties of the seeded HUV for different culture periods including tensile strength (a) and modulus of elasticity (b) for the medium seeding density, and tensile strength (c) and modulus of elasticity (d) for the high seeding density.

7.3.4. Glucose Consumption

For 2-D setups, the glucose consumption significantly depended on the cell number where an inversely proportional relationship was observed among the two variables (Figure 7.6). The glucose consumption varied between 0.6 ng/cell for high seeding densities of 50,000 cells/cm^2 and 7.0 ng/cell for low seeding densities of 5,000 cells/cm^2. When the glucose consumption was plotted against the inverse of the cell number, a linear regression plot was generated (Figure 7.8) with an R^2 value of 0.97.

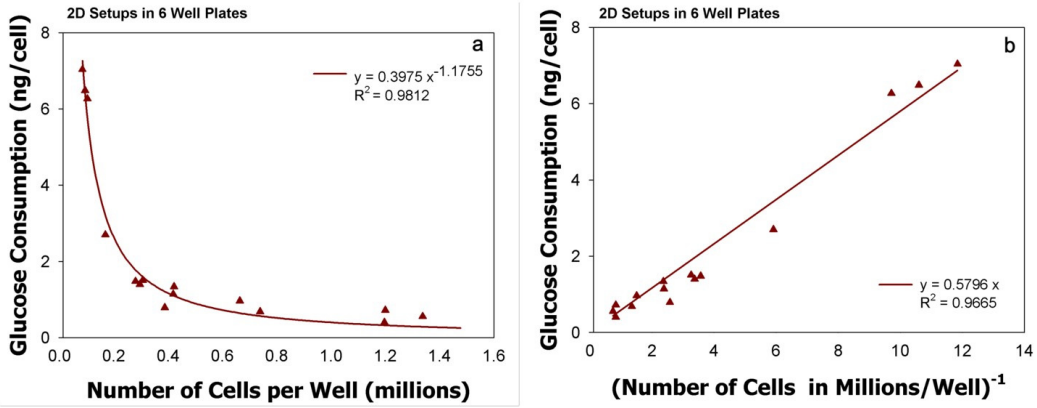

Figure 7.6: (a) inversely proportional relationship between glucose consumption and cell number and (b) linear regression between cellular glucose consumption and the inverse of the number of cells.

Similar trends were obtained for 3D setups of HUVs cultured in the bioreactor (Figure 7.7). Even through both cultures resulted in a decreasing trend, however, glucose consumption per cell decreased linearly with the increase in cell number for 3D setups compared to an inversely proportional relationship for 2D setups

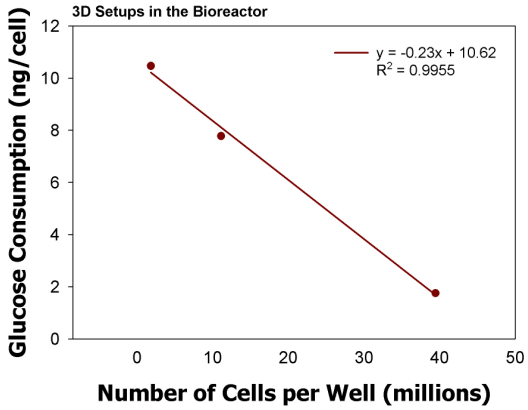

Figure 7.7: Linear relationship between glucose consumption per cell and cell number for 3D setups in the bioreactor.

7.4. DISCUSSIONS

The decellularized HUV has been previously seeded with 1 million cells/ml (Low Seeding Density: LSD) and mechanically stimulated for 1 hour/day at a frequency of 0.0167 Hz and 2% strain. After 2 weeks of culture,

the constructs had a 20 fold increase in cell number and a 3 fold increase in ultimate tensile strength values. Histologically, fibers aligned parallel to the direction of stretching and cells populated the scaffold almost migrating 75% into the thickness of the HUV. In an attempt to better understand the effect of the original seeding density on the final morphologic and material properties of the tissue engineered constructs, two additional seeding densities were further investigated: Medium Seeding Density (MSD = 5 million cells/ml) and high seeding density (HSD = 10 million cells/ml).

For MSD constructs, a statistically significant increase in cell number was measured after 1 week of culture for both, tensioned and untensioned constructs. However, no additional increase in cell number was recorded 2 weeks post culture. Moreover, HSD constructs did not show any significant increase in cell number during the 2 weeks of culture. There results were in agreement with histologic slides. Cross sections for the MSD 1 week post culture revealed numerous cells invading the ECM of the scaffold reaching the outer wall of the HUV for both, stimulated and unstimulated constructs (Figure 7.2). However, after the end of the second week of culture the wall of the HUV became thinner, the ECM fibers appeared to be degraded, and lysed cell bodies were present in significant numbers for both culturing conditions (Figure 7.3). Similar observations were noted for the high seeding density after only 1 week of culture.

Numerous lysed cell bodies are noted in Figure 7.2-d for stretched constructs after 2 weeks of culture. Moreover, the ECM appeared to be significantly different from the original matrix of the decellularized HUV (Figure 7.2-f) denoting extensive ECM remodeling by proliferating cells.

Mechanical testing revealed an increase in the mechanical properties (ultimate tensile strength and modulus of elasticity) for stretched MSD constructs only 1 week post culture. No further increase in the mechanical properties was measure after 2 weeks of culture. For HSD constructs the lack of cell proliferation, thinning of the HUV wall, and evident degradation of the ECM all contributed to the lack of improvement in the mechanical properties of the constructs.

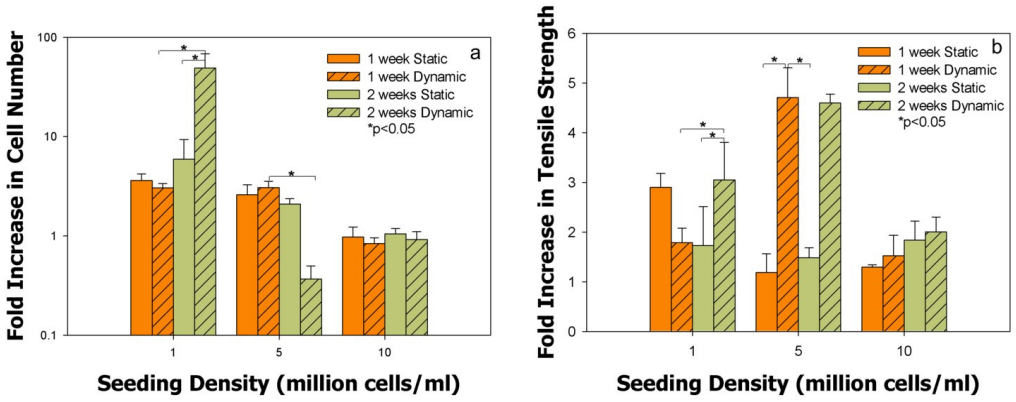

Figure 7.8: (a) Comparison, among three different seeding densities, of (a) Proliferation rates, and (b) Tensile strength.

Figure 7.8-a shows the fold increase in cell number within the HUV for all three seeding densities: Low Seeding Density (LSD = 1 million cells/ml), Medium Seeding Density (MSD = 5 million cells/ml), and High Seeding Density (HSD = 10 million cells/ml). Figure 7.8-b includes the corresponding increase in ultimate tensile stress values. For the MSD, the cellularity within the constructs increased more than 2 fold 1 week post culture (Figure 7.8-a). These results were consistent with proliferation rates within HUVs seeded with the LSD. With similar proliferation rates, MSD stimulated HUVs had an ultimate stress value of 4.1 ±0.5 MPa, almost 4 fold higher than LSD stretched constructs (Figure 7.8-b). However, proliferation ceased after 2 weeks of

culture, and no increase in the ultimate tensile strength was measured for MSD constructs. LSD stimulated construct, on the other hand, showed an additional 20 fold increase in proliferation rates, accompanied by a 1 fold increase in the ultimate tensile stress value after 2 weeks of culture (Figure 7.8). This is in agreement with other studies in which lower seeding densities using MSCs resulted higher proliferation rates[229]

It is possible that not enough nutrients were available for the cells to proliferate and survive at the MSD and HSD. Moreover, cells could have been attempting to remodel the ECM by secreting metalloproteinases (MMPs). However, the rate of ECM deposition was not balanced by the rate of MMP secretion. When cells remodel the ECM, they also deposit new matrix that could potentially decrease the effective porosity of the scaffold, and in turn decrease the flow of nutrients through the membrane. These facts would result in an increase in mass transport limitations which could be causing the cells to lyse.

Another possible explanation for the lack of proliferation is due to the entrapment of the cell lysates in the scaffold rather than being washed out of the matrix. Since cells are originally seeded in the central portion of the HUV and the media is being supplied around the outer wall of the scaffold that has a poor porous network, it is possible that cell lysates concentrated with time in the scaffold which could affect the condition of the healthy cells. Moreover, at MSD and HSD cells become metabolically more active which leads to an increase in metabolic byproducts such as production of lactic acid. The accumulation of lactic acid in the HUV causes a PH drop accompanied by an acidic environment that would become toxic to the remaining viable cells and

might be the cause of ECM degradation. This could explain why the media in the system was turning orange almost 1 week after culture for MSD and HSD.

The documented results indicate that cells were not able to survive at an original seeding concentration equal to or higher than 5 million cells/ml. As a result, it is recommended to optimize the original seeding density to a value between 1 and 5 million cells/ml or modify the HUV to improve the transport of nutrients.

Cellular glucose consumption significantly depended on the cell number. For both 2D and 3D setups; the higher the cell number the lower the glucose cellular consumption. MSCs are affected by the availability of glucose in cell culture, where high glucose concentrations induced replicative senescence and apoptosis[230]. Cells cultured in the 3D matrix of the HUV consumed almost 20 fold the amount of glucose as opposed to cells cultured in 2D well plates. For example, 1.8 million cells cultured in the HUV consumed 10.5 ng/cell/day of glucose, while, 1.4 million cells cultured in the 2D well plate consumed only 0.6 ng/cell/day of glucose. The differences in the results between the two setups were expected since 2D cultures result in significantly different cell phenotype compared to 3D cultures[231]. Cells in a 3D environment develop different morphologies, cellular adhesions, and signaling pathways compared to cells in conventional 2D tissue cultures[232-234]. Cellular biological activities are significantly enhanced[232,235], and cell migratory velocities[234] and proliferation rates[235] increase in 3D cultures compared to 2D cultures. Since the metabolic activity of cells is influenced by cell-cell interactions, and since the 2D well plate has a significantly smaller space for cells to grow than the HUV, it is more relevant to compare the cellular glucose

consumption per cellular space available. Thus, the cellular glucose consumption for MSCs seeded in the 2D setup is comparable to that seeded in the HUV at low seeding densities (7.0 ng/cell/day compared to 10.5 ng/cell/day, respectively).

In order to compute a limiting initial seeding density in the HUV above which no glucose would be available to cellular nutrition Fick's first law of diffusion (Equation 7.1) could be applied. Using Equation 7.1 it is possible to compute the flux of glucose, by diffusion, from the media surrounding the outer wall of the HUV into the full thickness of the decellularized scaffold.

$$J = -D_{app}\frac{dC_m}{dx} = \frac{D_{app}}{L_m}(C_o - C_i)$$

Equation 7.1: Fick's first law of diffusion.

Where: J is the flux (mg/cm^2/day).

D_{app} is the apparent glucose diffusion coefficient across the membrane. D_{app} was previously measured to be 0.21 ± 0.04 cm^2/day.

dC_m is the change in the glucose concentration across the HUV membrane.

C_o is the concentration of glucose outside the HUV that is available in the culture media = 1mg/ml.

C_i is the concentration of glucose on the internal surface of the HUV.

L_m is the thickness of the HUV = 0.1 cm.

Assuming that all the available glucose that diffuses across the HUV membrane gets consumed by cells (C_i = 0 mg/ml), the resulting flux would be: J = 2.16 mg/cm^2/day. Knowing the circumferential area of the HUV = 8.5 cm^2,

the available glucose for cellular consumption inside the wall of the HUV was 18 mg/day. The resulting cellular glucose consumption inside the HUV was dependent on the cellularity of the construct, as stated earlier. Table 7.2 shows the resulting limiting seeding densities using the cellular glucose consumptions for HUVs with different cellularities.

Table 7.2: Limiting number of cells inside the HUV.

HUV Cellularity (millions)	Glucose consumption (ng/cell/day)	Calculated Limiting Cell Number (millions)
39.5	1.8	10.4
11.1	7.8	2.4
1.8	10.5	1.8

It is important to note that the method employed to calculate the number of cells was PicoGreen DNA assay. This method measures the DNA concentration in the tissue, which is converted to cell number knowing the cellular DNA concentration. Thus, not all the reported cellularities represent viable cells. Therefore, the glucose consumption rate might be underestimated. One more limitation is that glucose consumption and DNA assay were performed on the HUVs after 6 days in culture. As a result, not all the cells are present in the central portion of the HUV, some cells had already migrated and populated the scaffold. Since we are attempting to calculate a limiting seeding density, then the cellular glucose consumption that results in a limiting cell number comparable to the cellularity of the HUV would be considered. According to the values in Table 7.2 the limiting number of cells in the HUV is 1.8 million cells which corresponds to a seeding density of 3 million cells/ml. This value is in agreement with the above results that indicated that the optimal seeding density is between 1 and 5 million cells/ml. It is important to note that when the HUVs are mechanically stimulated, nutrients do not only diffuse through the scaffold, but there is also a

convective flow due to the effect of stretching. This convective force potentially enhances the transport of nutrients through the wall of the HUV. Thus, the limiting seeding density of 3 million cells/ml corresponds to non-stimulated controls. Coupling the constructs with stretching would increase the allowable seeding density, with 3 million cells/ml being a minimum number.

7.5. CONCLUSIONS

Higher seeding densities resulted in an initial increase in proliferation rates and a modest improvement in mechanical properties. However, proliferation ceased after the second week of culture, and constructs had poorer mechanical properties with seemingly thinner HUV walls and degraded ECM. Histologic images revealed lysed cell bodies 2 weeks post culture. It appears that at high seeding densities not enough glucose diffused through the HUV to support cell survival and proliferation. The optimal seeding density was found to be less than 5 million cells/ml. A decreasing linear relationship was recorded between the number of cells in the HUV and the cellular glucose consumption with values ranging between 1.8 ng/cell/day and 10.5 ng/cell/day. The limiting seeding density was calculated based on glucose consumption rates to be 3 million cells/ml for unstretched samples. This number increases for mechanically stimulated sample due to the effect of convective flow. Finally, the numbers reported in this study are highly dependent on the current design and experimental procedures employed. Thus, varying any factors, such as the decellularization procedure, thickness of the HUV, stimulation scenarios, or seeding protocol, would significantly affect the documented results.

7.6. CONCLUSIONS

The Human Umbilical Vein (HUV) was presented in this research study as a potential biological scaffold for musculoskeletal tissue engineering in general, and tendon tissue engineering in particular. The HUV, seeded with Mesenchymal Stem Cells (MSCs), supported cell integration, proliferation and migration to the existing 3 dimensional matrix of the scaffold. The seeded constructs possessed higher mechanical properties than the original decellularized HUV. Mechanically stimulating constructs with 2% strain for one hour per day increased the proliferation rate of MSCs and gave the construct a tendon like appearance. Histological images showed extracellular matrix fibers and cell nuclei aligned parallel to the direction of stretching mimicking the morphology of native tendons. Moreover, mechanostimulation resulted in significantly stronger and stiffer constructs compared to un-tensioned samples.

To characterize the HUV as a biological scaffold for tissue engineering, mass transport of nutrients through the HUV was investigated. It was determined that glucose permeability through the HUV wall was significantly lower than that through the Wharton's Jelly. It took the membrane almost 10 hours to get saturated with glucose. Thus to enhance glucose transport through the HUV on the onset of experimental setup, it is recommended to soak the biological scaffold overnight with media before using it for tissue engineering applications which involve seeding cells at the interior void space of the HUV that lacks direct access to the cell culture media. Cells initially seeded in the central cylindrical space of the HUV depend solely on diffusion

rates to acquire glucose and other necessary metabolites for their survival and proliferation.

The coefficient of permeability of glucose was almost an order of magnitude higher than that of FITC-Dextran 4.4 KDa. An inversely proportional relation was developed between the molecular radius and the permeability of dextran molecules through the HUV. However, this relation could be used to predict the coefficient of permeability of proteins that do not possess a strong net surface charge or a strong affinity for the HUV. High molecular weight FITC-Dextran molecules did not diffuse through the HUV, limiting the molecular radius of proteins that could permeate through the biological scaffold to less than 4.9 nm.

When higher seeding densities, of 5 million cells/ml, and 10 million cells/ml, were attempted, the ECM of the HUV significantly degraded, mechanical properties of the constructs did not show any improvement, and cell bodies lysed after 2 weeks of culture, for both tensioned and un-tensioned constructs. These results indicated that cells were not able to survive at original seeding concentration higher than 5 million cells/ml. A decreasing linear relationship was recorded between the number of cells in the HUV and the cellular glucose consumption with values ranging between 1.8 ng/cell/day and 10.5 ng/cell/day. The limiting seeding density for unstimulated samples was calculated based on glucose consumption rates to be 3 million cells/ml. This value increases for mechanically stimulated constructs due to the effect of convective flow associated with stretching.

7.7. RECOMMENDATIONS

7.7.1. Investigating the Effect of Alternative Stretching Regimes on the Seeded HUVs

In the current study the seeded HUVs were only stretched for 1 hour/day in the MSTE at 2% strain and a frequency of 0.0167Hz. In other studies constructs were stretched up to 8 hours[203] and 24 hours[180] per day at strains ranging between 2.4% and 12%[129,131,180,203]. It has been previously reported that mechanical properties of collagenous substrates strongly depended on the form, magnitude, and duration of stress applied, and that cyclic stresses work more effectively than static stresses in the biological system[156,183]. Thus it is recommended to investigate the effect of different stretching durations, intensities, and frequencies on the morphometric and mechanical properties of the tissue engineered tendon in order to optimize mechanical stimulation variables.

7.7.2. Investigating the Potential of Facilitating Mass Transport through the HUV

The current HUV has a very tortuous network of pores that limits the molecular radius of proteins that could permeate through the biological scaffold to less than 4.9 nm. This limitation will increase as cells migrate into the HUV to remodel the existing matrix and deposit new ECM. Thus, it is recommended to investigate techniques that would facilitate mass transport of nutrients and biomolecules through the scaffold. One option would be to poke micro-holes into the HUV after seeding it with MSCs. Another possibility would be to perfuse media through the central portion of the HUV by

incorporating small channels in the steel adapters that hold the ends of the scaffold.

7.7.3. Investigating other Decellularization Options

The material properties of the HUV depend strongly on the decellularization technique used. In the current study the surfactant SDS was the primary decellularization product. It is recommended to investigate the effect of other decellularizing agents, such as ethanol, Triton-X, or tributyl phosphate, on glucose and metabolite coefficients of diffusivity through the HUV.

7.7.4. Developing a Finite Element Model

A finite element model of the HUV would be very beneficial as a critical tool to help simulate and understand the effects of nutrients' diffusion through the scaffold on cell migration, proliferation and new extracellular matrix deposition.

LITERATURE CITED

1. US Department of Labor. Bureau of Labor Statistics. 1999.
2. Griffin Global Systems. Everything About Achilles Tendons. AchillesTendon.com Division; 2003.
3. Astrèom M. Partial rupture in chronic achilles tendinopathy. A retrospective analysis of 342 cases. Acta orthopaedica Scandinavica. 1998;69(4):404-7.
4. Systems GG. Everything About Achilles Tendons. 2003.
5. Ouyang HW, Goh JC, Thambyah A, Teoh SH, Lee EH. Knitted poly-lactide-co-glycolide scaffold loaded with bone marrow stromal cells in repair and regeneration of rabbit Achilles tendon. Tissue Eng 2003;9(3):431-9.
6. Hauser R. Chronic Foot Problems and the Achilles Tendon. 1999.
7. Kjaer M, Langberg H, Miller BF, Boushel R, Crameri R, Koskinen S, Heinemeier K, Olesen JL, Dossing S, Hansen M and others. Metabolic activity and collagen turnover in human tendon in response to physical activity. J Musculoskelet Neuronal Interact 2005;5(1):41-52.
8. Khan KM, Cook JL, Bonar F, Harcourt P, Astrom M. Histopathology of common tendinopathies. Update and implications for clinical management. Sports Med 1999;27(6):393-408.
9. Renstrèom P, Johnson RJ. Overuse injuries in sports. A review. Sports Med 1985;2(5):316-33.
10. Jozsa LG, Kannus P. Overuse Injuries of Tendons. Human tendons : anatomy, physiology, and pathology. Champaign, IL: Human Kinetics; 1997. p 164-253.
11. Jèarvinen M, Jâozsa L, Kannus P, Jèarvinen TL, Kvist M, Leadbetter W. Histopathological findings in chronic tendon disorders. Scandinavian journal of medicine & science in sports. 1997;7(2):86-95.
12. Jâozsa LG, Kannus P. Human tendons : anatomy, physiology, and pathology. Champaign, IL: Human Kinetics; 1997. 574 p.
13. Garvin J, Qi J, Maloney M, Banes AJ. Novel system for engineering bioartificial tendons and application of mechanical load. Tissue Eng 2003;9(5):967-79.
14. Ker RF. The design of soft collagenous load-bearing tissues. J Exp Biol 1999;202(Pt):3315-24.
15. Woo SL-Y, An K-N, Frank CB, Livesay GA, Ma CB, Zeminski J, Wayne JS, Myers BS. Anatomy, Biology, and Biomechanics of Tendon and Ligament. In: Buckwalter JA, Einhorn TA, Simon SR, American Academy of Orthopaedic Surgeons., editors. Orthopaedic basic science : biology and biomechanics of the musculoskeletal system. Rosemont, IL: American Academy of Orthopaedic Surgeons; 2000. p 582-616.
16. Butler DL, Juncosa N, Dressler MR. Functional efficacy of tendon repair processes. Annu Rev Biomed Eng 2004;6:303-29.
17. Jozsa LG, Kannus P. Structure and Metabolism of Normal Tendons. Human tendons : anatomy, physiology, and pathology. Champaign, IL: Human Kinetics; 1997. p 46-96.
18. Astrèom M, Rausing A. Chronic Achilles tendinopathy. A survey of surgical and histopathologic findings. Clinical orthopaedics and related research. 1995(316):151-64.
19. Lodish HF. Molecular cell biology. New York: W.H. Freeman and Company; 2004.

20. Screen HRC, Bader DL, Lee DA, Shelton JC. Local Strain Measurement within Tendon. Strain 2004;40(4):157-163.
21. Ross MH, Kaye GI, Pawlina W. Connective Tissue. Histology : a text and atlas. Philadelphia, Pa.: Lippincott Williams & Wilkins; 2002. p 126-155.
22. Khan KM, Bonar F, Desmond PM, Cook JL, Young DA, Visentini PJ, Fehrmann MW, Kiss ZS, O'Brien PA, Harcourt PR and others. Patellar tendinosis (jumper's knee): findings at histopathologic examination, US, and MR imaging. Victorian Institute of Sport Tendon Study Group. Radiology. 1996;200(3):821-7.
23. Alfredson H, Ohberg L. Neovascularisation in chronic painful patellar tendinosis-promising results after sclerosing neovessels outside the tendon challenge the need for surgery. Knee surgery, sports traumatology, arthroscopy 2005;13(2):74-80.
24. Goh JC, Ouyang HW, Teoh SH, Chan CK, Lee EH. Tissue-engineering approach to the repair and regeneration of tendons and ligaments. Tissue Eng 2003;9 Suppl 1:S31-44.
25. Beredjiklian PK, Favata M, Cartmell JS, Flanagan CL, Crombleholme TM, Soslowsky LJ. Regenerative versus reparative healing in tendon: a study of biomechanical and histological properties in fetal sheep. Annals of biomedical engineering. 2003;31(10):1143-52.
26. Wang JHC. Mechanobiology of tendon. Journal of Biomechanics 2006;39(9):1563-1582.
27. Vogel KG, Meyers AB. Proteins in the tensile region of adult bovine deep flexor tendon. Clin Orthop Relat Res 1999(367 Suppl):S344-55.
28. Duance VC, Restall DJ, Beard H, Bourne FJ, Bailey AJ. The location of three collagen types in skeletal muscle. FEBS Lett 1977;79(2):248-52.
29. Birk DE, Mayne R. Localization of collagen types I, III and V during tendon development. Changes in collagen types I and III are correlated with changes in fibril diameter. European journal of cell biology. 1997;72(4):352-61.
30. Butler DL, Grood ES, Noyes FR, Zernicke RF. Biomechanics of ligaments and tendons. Exercise and sport sciences reviews. 1978;6:125-81.
31. Jarvinen M, Kannus P, Kvist M, Isola J, Lehto M, Jozsa L. Macromolecular composition of the myotendinous junction. Exp Mol Pathol 1991;55(3):230-7.
32. Jozsa LG, Kannus P. Functional and Mechanical Behavior of Tendons. Human tendons : anatomy, physiology, and pathology. Champaign, IL: Human Kinetics; 1997. p 98-113.
33. Merrilees MJ, Flint MH. Ultrastructural study of tension and pressure zones in a rabbit flexor tendon. Am J Anat 1980;157(1):87-106.
34. Cooper RR, Misol S, Stimmel P. Tendon and Ligament Insertion: A Light and Electron Microscopic Study. The Journal of Bone and Joint Surgery 1970;52(1):1.
35. Gentleman E, Livesay GA, Dee KC, Nauman EA. Tissue Engineering of Ligament. In: Wnek GLBG, editor. Encyclopedia of Biomaterials and Biomedical Engineering. New York, NY: Informa Healthcare; 2004. p 1559 - 1569.
36. Ralphs JR, Benjamin M, Waggett AD, Russell DC, Messner K, Gao J. Regional differences in cell shape and gap junction expression in rat Achilles tendon: relation to fibrocartilage differentiation. J Anat 1998;193 (Pt 2):215-22.

37. Ker RF, Alexander RM, Bennett MB. Why are mammalian tendons so thick. J Zool Lond 1988;216:309-324.
38. Zajac FE. Muscle and tendon: properties, models, scaling, and application to biomechanics and motor control. Crit Rev Biomed Eng 1989;17(4):359-411.
39. Fukashiro S, Komi PV, Jarvinen M, Miyashita M. In vivo Achilles tendon loading during jumping in humans. Eur J Appl Physiol Occup Physiol 1995;71(5):453-8.
40. Giddings VL, Beaupre GS, Whalen RT, Carter DR. Calcaneal loading during walking and running. Med Sci Sports Exerc 2000;32(3):627-34.
41. Woo SL, Debski RE, Zeminski J, Abramowitch SD, Saw SS, Fenwick JA. Injury and repair of ligaments and tendons. Annu Rev Biomed Eng 2000;2:83-118.
42. Kastelic J, Palley I, Baer E. A structural mechanical model for tendon crimping. J Biomech 1980;13(10):887-93.
43. Wang JH, Iosifidis MI, Fu FH. Biomechanical basis for tendinopathy. Clinical orthopaedics and related research. 2006;443:320-32.
44. Atkinson TS, Ewers BJ, Haut RC. The tensile and stress relaxation responses of human patellar tendon varies with specimen cross-sectional area. J Biomech 1999;32(9):907-14.
45. Purslow PP, Wess TJ, Hukins DW. Collagen orientation and molecular spacing during creep and stress-relaxation in soft connective tissues. J Exp Biol 1998;201(Pt 1):135-42.
46. Bennett MB, Ker RF, Dimery NJ, Alexander RMN. Mechanical properties of various mammalian tendons. Journal of zoology. Series A 1986;209(4):537-548.
47. Abrahams M. Mechanical behaviour of tendon in vitro. A preliminary report. Med Biol Eng 1967;5(5):433-43.
48. Banes AJ, Weinhold P, Yang X, Tsuzaki M, Bynum D, Bottlang M, Brown T. Gap junctions regulate responses of tendon cells ex vivo to mechanical loading. Clin Orthop Relat Res 1999(367 Suppl):S356-70.
49. Malaviya P, Butler DL, Korvick DL, Proch FS. In vivo tendon forces correlate with activity level and remain bounded: evidence in a rabbit flexor tendon model. J Biomech 1998;31(11):1043-9.
50. Korvick DL, Cummings JF, Grood ES, Holden JP, Feder SM, Butler DL. The use of an implantable force transducer to measure patellar tendon forces in goats. J Biomech 1996;29(4):557-61.
51. Moore JS. Function, structure, and responses of components of the muscle-tendon unit. Occup Med 1992;7(4):713-40.
52. Kirkendall DT, Garrett WE. Function and biomechanics of tendons. Scand J Med Sci Sports 1997;7(2):62-6.
53. Savolainen J, Vaananen K, Puranen J, Takala TE, Komulainen J, Vihko V. Collagen synthesis and proteolytic activities in rat skeletal muscles: effect of cast-immobilization in the lengthened and shortened positions. Arch Phys Med Rehabil 1988;69(11):964-9.
54. Robbins JR, Evanko SP, Vogel KG. Mechanical loading and TGF-beta regulate proteoglycan synthesis in tendon. Arch Biochem Biophys 1997;342(2):203-11.
55. Langberg H, Olesen JL, Gemmer C, Kjaer M. Substantial elevation of interleukin-6 concentration in peritendinous tissue, in contrast to muscle, following prolonged exercise in humans. J Physiol 2002;542(Pt 3):985-90.

56. Michna H, Hartmann G. Adaptation of tendon collagen to exercise. Int Orthop 1989;13(3):161-5.
57. Holz U. Achilles tendon rupture and achillodynia. The importance of tissue regeneration. Fortschr Med 1980;98(39):1517-20.
58. Riley GP, Harrall RL, Constant CR, Chard MD, Cawston TE, Hazleman BL. Tendon degeneration and chronic shoulder pain: changes in the collagen composition of the human rotator cuff tendons in rotator cuff tendinitis. Ann Rheum Dis 1994;53(6):359-66.
59. Liu SH, Yang RS, al-Shaikh R, Lane JM. Collagen in tendon, ligament, and bone healing. A current review. Clin Orthop Relat Res 1995(318):265-78.
60. Cook JL, Feller JA, Bonar SF, Khan KM. Abnormal tenocyte morphology is more prevalent than collagen disruption in asymptomatic athletes' patellar tendons. Journal of orthopaedic research : official publication of the Orthopaedic Research Society. 2004;22(2):334-8.
61. Williams JG. Achilles tendon lesions in sport. Sports medicine (Auckland, N.Z.) 1986;3(2):114-35.
62. Almekinders LC, Banes AJ, Ballenger CA. Effects of repetitive motion on human fibroblasts. Medicine and science in sports and exercise. 1993;25(5):603-7.
63. Stanish WD, Curwin S, Rubinovich M. Tendinitis: the analysis and treatment for running. Clinics in sports medicine. 1985;4(4):593-609.
64. Stanish WD, Rubinovich RM, Curwin S. Eccentric exercise in chronic tendinitis. Clinical orthopaedics and related research. 1986(208):65-8.
65. Marsolais D, Cote CH, Frenette J. Neutrophils and macrophages accumulate sequentially following Achilles tendon injury. J Orthop Res 2001;19(6):1203-9.
66. Rolf CG, Fu BS, Pau A, Wang W, Chan B. Increased cell proliferation and associated expression of PDGFRbeta causing hypercellularity in patellar tendinosis. Rheumatology (Oxford, England) 2001;40(3):256-61.
67. Alfredson H, Ohberg L. Neovascularisation in chronic painful patellar tendinosis--promising results after sclerosing neovessels outside the tendon challenge the need for surgery. Knee surgery, sports traumatology, arthroscopy : official journal of the ESSKA. 2005;13(2):74-80.
68. Cook JL, Feller JA, Bonar SF, Khan KM. Abnormal tenocyte morphology is more prevalent than collagen disruption in asymptomatic athletes' patellar tendons. Journal of orthopaedic research 2004;22(2):334-8.
69. Fu SC, Wang W, Pau HM, Wong YP, Chan KM, Rolf CG. Increased expression of transforming growth factor-beta1 in patellar tendinosis. Clinical orthopaedics and related research. 2002(400):174-83.
70. Fu SC, Chan BP, Wang W, Pau HM, Chan KM, Rolf CG. Increased expression of matrix metalloproteinase 1 (MMP1) in 11 patients with patellar tendinosis. Acta orthopaedica Scandinavica. 2002;73(6):658-62.
71. Yu JS, Popp JE, Kaeding CC, Lucas J. Correlation of MR imaging and pathologic findings in athletes undergoing surgery for chronic patellar tendinitis. AJR. American journal of roentgenology. 1995;165(1):115-8.
72. Smits A, Funa K, Vassbotn FS, Beausang-Linder M, af Ekenstam F, Heldin CH, Westermark B, Nistâer M. Expression of platelet-derived growth factor and its receptors in proliferative disorders of fibroblastic origin. The American journal of pathology. 1992;140(3):639-48.

73. Skutek M, van Griensven M, Zeichen J, Brauer N, Bosch U. Cyclic mechanical stretching enhances secretion of Interleukin 6 in human tendon fibroblasts. Knee Surg Sports Traumatol Arthrosc 2001;9(5):322-6.
74. Leadbetter WB, Mooar PA, Lane GJ, Lee SJ. The surgical treatment of tendinitis. Clinical rationale and biologic basis. Clin Sports Med 1992;11(4):679-712.
75. Cao DJ, Zhai HL, Liu W, Cui L, Zhong B, Cao YL. Preliminary study on in vitro tendon engineering using tenocytes and polyglycolic acids. Zhonghua Wai Ke Za Zhi 2004;42(2):110-3.
76. Laurencin CT, Ambrosio AM, Borden MD, Cooper JAJ. Tissue engineering: orthopedic applications. Annu Rev Biomed Eng 1999;1:19-46.
77. Cao Y, Liu Y, Liu W, Shan Q, Buonocore SD, Cui L. Bridging tendon defects using autologous tenocyte engineered tendon in a hen model. Plast Reconstr Surg 2002;110(5):1280-9.
78. Hallam P, Bain GI. Repair of chronic distal biceps tendon ruptures using autologous hamstring graft and the Endobutton. J Shoulder Elbow Surg 2004;13(6):648-51.
79. Pennati G. Biomechanical properties of the human umbilical cord. Biorheology 2001;38(5-6):355-66.
80. Park HG, Lee BK, Sim JA. Autogenous graft repair using semitendinous tendon for a chronic multifocal rupture of the extensor hallucis longus tendon: a case report. Foot Ankle Int 2003;24(6):506-8.
81. Pinkowski JL, Rodrigo JJ, Sharkey NA, Vasseur PB. Immune response to nonspecific and altered tissue antigens in soft tissue allografts. Clin Orthop Relat Res 1996(326):80-5.
82. Howard CB, Winston I, Bell W, Mackie I, Jenkins DH. Late repair of the calcaneal tendon with carbon fibre. J Bone Joint Surg Br 1984;66(2):206-8.
83. Parsons JR, Weiss AB, Schenk RS, Alexander H, Pavlisko F. Long-term follow-up of achilles tendon repair with an absorbable polymer carbon fiber composite. Foot Ankle 1989;9(4):179-84.
84. Amis AA, Campbell JR, Kempson SA, Miller JH. Comparison of the structure of neotendons induced by implantation of carbon or polyester fibres. J Bone Joint Surg Br 1984;66(1):131-9.
85. Ozaki J, Fujiki J, Sugimoto K, Tamai S, Masuhara K. Reconstruction of neglected Achilles tendon rupture with Marlex mesh. Clin Orthop Relat Res 1989(238):204-8.
86. Audenaert E, Van Nuffel J, Schepens A, Verhelst M, Verdonk R. Reconstruction of massive rotator cuff lesions with a synthetic interposition graft: a prospective study of 41 patients. Knee Surg Sports Traumatol Arthrosc 2006;14(4):360-4.
87. Ketchum LD. Twenty-five-year follow-up evaluation of an active silicone/Dacron tendon interposition prosthesis: A case report. J Hand Surg [Am] 2000;25(4):731-3.
88. Bagnaninchi PO, Yang Y, El Haj AJ, Maffulli N. Tissue engineering for tendon repair. Br J Sports Med 2006.
89. Vunjak-Novakovic G, Altman G, Horan R, Kaplan DL. Tissue engineering of ligaments. Annu Rev Biomed Eng 2004;6:131-56.
90. Kashuk KB, Haber E. Tendon and ligament prostheses. Clin Podiatry 1984;1(1):131-43.

91. Hannafin JA, Arnoczky SP, Hoonjan A, Torzilli PA. Effect of stress deprivation and cyclic tensile loading on the material and morphologic properties of canine flexor digitorum profundus tendon: an in vitro study. J Orthop Res 1995;13(6):907-14.
92. Martin I, Wendt D, Heberer M. The role of bioreactors in tissue engineering. Trends Biotechnol 2004;22(2):80-6.
93. Bonassar LJ, Vacanti CA. Tissue engineering: the first decade and beyond. J Cell Biochem Suppl 1998;30-31:297-303.
94. Altman GH, Horan RL, Martin I, Farhadi J, Stark PR, Volloch V, Richmond JC, Vunjak-Novakovic G, Kaplan DL. Cell differentiation by mechanical stress. FASEB J 2002;16(2):270-2.
95. Butler DL, Goldstein SA, Guilak F. Functional tissue engineering: the role of biomechanics. J Biomech Eng 2000;122(6):570-5.
96. Dressler MR, Butler DL, Boivin GP. Effects of age on the repair ability of mesenchymal stem cells in rabbit tendon. J Orthop Res 2005;23(2):287-93.
97. Cooper JA, Lu HH, Ko FK, Freeman JW, Laurencin CT. Fiber-based tissue-engineered scaffold for ligament replacement: design considerations and in vitro evaluation. Biomaterials 2005;26(13):1523-32.
98. Zeichen J, van Griensven M, Bosch U. The proliferative response of isolated human tendon fibroblasts to cyclic biaxial mechanical strain. Am J Sports Med 2000;28(6):888-92.
99. Hu JB, Zhou Y, Jiang DD, Tan WS. Proliferation and differentiation characteristics of human bone marrow mesenchymal stem cells during ex-vivo expansion. Xi bao yu fen zi mian yi xue za zhi = Chinese journal of cellular and molecular immunology. 2006;22(1):7-10.
100. Butler DL, Awad HA. Perspectives on cell and collagen composites for tendon repair. Clin Orthop Relat Res 1999(367 Suppl):S324-32.
101. Young RG, Butler DL, Weber W, Caplan AI, Gordon SL, Fink DJ. Use of mesenchymal stem cells in a collagen matrix for Achilles tendon repair. J Orthop Res 1998;16(4):406-13.
102. Awad HA, Boivin GP, Dressler MR, Smith FN, Young RG, Butler DL. Repair of patellar tendon injuries using a cell-collagen composite. Journal of orthopaedic research : official publication of the Orthopaedic Research Society. 2003;21(3):420-31.
103. Awad HA, Butler DL, Boivin GP, Smith FN, Malaviya P, Huibregtse B, Caplan AI. Autologous mesenchymal stem cell-mediated repair of tendon. Tissue engineering. 1999;5(3):267-77.
104. Hankemeier S, Keus M, Zeichen J, Jagodzinski M, Barkhausen T, Bosch U, Krettek C, Van Griensven M. Modulation of proliferation and differentiation of human bone marrow stromal cells by fibroblast growth factor 2: potential implications for tissue engineering of tendons and ligaments. Tissue Eng 2005;11(1-2):41-9.
105. Wang HS, Hung SC, Peng ST, Huang CC, Wei HM, Guo YJ, Fu YS, Lai MC, Chen CC. Mesenchymal stem cells in the Wharton's jelly of the human umbilical cord. Stem Cells 2004;22(7):1330-7.
106. Enderle JD, Blanchard SM, Bronzino JD. Introduction to biomedical engineering. San Diego: Academic Press; 2000. 1062 p.
107. Bruder SP, Kurth AA, Shea M, Hayes WC, Jaiswal N, Kadiyala S. Bone regeneration by implantation of purified, culture-expanded human mesenchymal stem cells. J Orthop Res 1998;16(2):155-62.

108. Bruder SP, Kraus KH, Goldberg VM, Kadiyala S. The effect of implants loaded with autologous mesenchymal stem cells on the healing of canine segmental bone defects. J Bone Joint Surg Am 1998;80(7):985-96.
109. Sikavitsas VI, Bancroft GN, Holtorf HL, Jansen JA, Mikos AG. Mineralized matrix deposition by marrow stromal osteoblasts in 3D perfusion culture increases with increasing fluid shear forces. Proc Natl Acad Sci U S A 2003;100(25):14683-8.
110. Sikavitsas VI, Bancroft GN, Mikos AG. Formation of three-dimensional cell/polymer constructs for bone tissue engineering in a spinner flask and a rotating wall vessel bioreactor. J Biomed Mater Res 2002;62(1):136-48.
111. Solchaga LA, Gao J, Dennis JE, Awadallah A, Lundberg M, Caplan AI, Goldberg VM. Treatment of osteochondral defects with autologous bone marrow in a hyaluronan-based delivery vehicle. Tissue Eng 2002;8(2):333-47.
112. Tondreau T, Lagneaux L, Dejeneffe M, Massy M, Mortier C, Delforge A, Bron D. Bone marrow-derived mesenchymal stem cells already express specific neural proteins before any differentiation. Differentiation; research in biological diversity. 2004;72(7):319-26.
113. Barry FP. Biology and clinical applications of mesenchymal stem cells. Birth defects research. Part C, Embryo today : reviews. 2003;69(3):250-6.
114. Ringe J, Kaps C, Burmester GR, Sittinger M. Stem cells for regenerative medicine: advances in the engineering of tissues and organs. Naturwissenschaften 2002;89(8):338-51.
115. Gregory CA, Gunn WG, Reyes E, Smolarz AJ, Munoz J, Spees JL, Prockop DJ. How wnt signaling affects bone repair by mesenchymal stem cells from the bone marrow. Annals of the New York Academy of Sciences. 2005;1049:97-106.
116. Bossolasco P, Cova L, Calzarossa C, Rimoldi SG, Borsotti C, Deliliers GL, Silani V, Soligo D, Polli E. Neuro-glial differentiation of human bone marrow stem cells in vitro. Experimental neurology. 2005;193(2):312-25.
117. Ortiz-Gonzalez XR, Keene CD, Verfaillie CM, Low WC. Neural induction of adult bone marrow and umbilical cord stem cells. Current neurovascular research. 2004;1(3):207-13.
118. Hoffmann A, Pelled G, Turgeman G, Eberle P, Zilberman Y, Shinar H, Keinan-Adamsky K, Winkel A, Shahab S, Navon G and others. Neotendon formation induced by manipulation of the Smad8 signalling pathway in mesenchymal stem cells. The Journal of clinical investigation. 2006;116(4):940-52.
119. Nèoth U, Schupp K, Heymer A, Kall S, Jakob F, Schèutze N, Baumann B, Barthel T, Eulert J, Hendrich C. Anterior cruciate ligament constructs fabricated from human mesenchymal stem cells in a collagen type I hydrogel. Cytotherapy. 2005;7(5):447-55.
120. Erickson GR, Gimble JM, Franklin DM, Rice HE, Awad H, Guilak F. Chondrogenic potential of adipose tissue-derived stromal cells in vitro and in vivo. Biochem Biophys Res Commun 2002;290(2):763-9.
121. Bruder SP, Jaiswal N, Haynesworth SE. Growth kinetics, self-renewal, and the osteogenic potential of purified human mesenchymal stem cells during extensive subcultivation and following cryopreservation. J Cell Biochem 1997;64(2):278-94.

122. Sato M, Maeda M, Kurosawa H, Inoue Y, Yamauchi Y, Iwase H. Reconstruction of rabbit Achilles tendon with three bioabsorbable materials: histological and biomechanical studies. J Orthop Sci 2000;5(3):256-67.
123. Lu HH, Cooper JA, Jr., Manuel S, Freeman JW, Attawia MA, Ko FK, Laurencin CT. Anterior cruciate ligament regeneration using braided biodegradable scaffolds: in vitro optimization studies. Biomaterials 2005;26(23):4805-16.
124. Curtis AS, Wilkinson CD, Crossan J, Broadley C, Darmani H, Johal KK, Jorgensen H, Monaghan W. An in vivo microfabricated scaffold for tendon repair. Eur Cell Mater 2005;9:50-7; discussion 57.
125. Saad B, Suter UW. Biodegradable polymeric materials. In: Buschow KHJ, Cahn RW, Flemings MC, Ilschner B, Kramer EJ, Mahajan S, editors. Encyclopedia of materials science and technology. Oxford, UK: Elsevier; 2001. p 551-555.
126. Yaszemski MJ, Payne RG, Hayes WC, Langer R, Mikos AG. Evolution of bone transplantation: molecular, cellular and tissue strategies to engineer human bone. Biomaterials 1996;17(2):175.
127. Dunn MG, Liesch JB, Tiku ML, Zawadsky JP. Development of fibroblast-seeded ligament analogs for ACL reconstruction. J Biomed Mater Res 1995;29(11):1363-71.
128. Feng Z, Yamato M, Akutsu T, Nakamura T, Okano T, Umezu M. Investigation on the mechanical properties of contracted collagen gels as a scaffold for tissue engineering. Artif Organs 2003;27(1):84-91.
129. Cacou C, Palmer D, Lee DA, Bader DL, Shelton JC. A system for monitoring the response of uniaxial strain on cell seeded collagen gels. Med Eng Phys 2000;22(5):327-33.
130. Cronkite A. Tensile strength of human tendons. The Anatomical Record 1936;64:173-186.
131. Androjna C, Spragg RK, Derwin KA. Mechanical Conditioning of Cell-Seeded Small Intestine Submucosa: A Potential Tissue-Engineering Strategy for Tendon Repair. Tissue Eng 2007;13(2):233-243.
132. Karaoglu S, M BF, Woo SL, Fu YC, Liang R, Abramowitch SD. Use of a bioscaffold to improve healing of a patellar tendon defect after graft harvest for ACL reconstruction: A study in rabbits. J Orthop Res 2007.
133. Gentleman E, Lay AN, Dickerson DA, Nauman EA, Livesay GA, Dee KC. Mechanical characterization of collagen fibers and scaffolds for tissue engineering. Biomaterials 2003;24(21):3805-13.
134. Daniel J, Abe K, McFetridge PS. Development of the human umbilical vein scaffold for cardiovascular tissue engineering applications. ASAIO J 2005;51(3):252-61.
135. Hill M. Placenta Histology. The University of New South Wales: http://embryology.med.unsw.edu.au; 2008.
136. Sobolewski K, Malkowski A, Bankowski E, Jaworski S. Wharton's jelly as a reservoir of peptide growth factors. Placenta 2005;26(10):747-52.
137. Nanaev AK, Kohnen G, Milovanov AP, Domogatsky SP, Kaufmann P. Stromal differentiation and architecture of the human umbilical cord. Placenta 1997;18(1):53-64.
138. Gogiel T, Bankowski E, Jaworski S. Proteoglycans of Wharton's jelly. Int J Biochem Cell Biol 2003;35(10):1461-9.

139. Valiyaveettil M, Achur RN, Muthusamy A, Gowda DC. Characterization of chondroitin sulfate and dermatan sulfate proteoglycans of extracellular matrices of human umbilical cord blood vessels and Wharton's jelly. Glycoconj J 2004;21(6):361-75.
140. Palka J, Banikowski E, Jaworski S. An accumulation of IGF-I and IGF-binding proteins in human umbilical cord. Mol Cell Biochem 2000;206(1-2):133-9.
141. Rao CV, Li X, Toth P, Lei ZM. Expression of epidermal growth factor, transforming growth factor-alpha, and their common receptor genes in human umbilical cords. J Clin Endocrinol Metab 1995;80(3):1012-20.
142. Freed LE, Vunjak-Novakovic G, Langer R. Cultivation of cell-polymer cartilage implants in bioreactors. J Cell Biochem 1993;51(3):257-64.
143. Freed LE, Marquis JC, Nohria A, Emmanual J, Mikos AG, Langer R. Neocartilage formation in vitro and in vivo using cells cultured on synthetic biodegradable polymers. J Biomed Mater Res 1993;27(1):11-23.
144. Vunjak-Novakovic G, Obradovic B, Martin I, Bursac PM, Langer R, Freed LE. Dynamic cell seeding of polymer scaffolds for cartilage tissue engineering. Biotechnol Prog 1998;14(2):193-202.
145. Saini S, Wick TM. Concentric cylinder bioreactor for production of tissue engineered cartilage: effect of seeding density and hydrodynamic loading on construct development. Biotechnol Prog 2003;19(2):510-21.
146. Day SM, Ostrum RF, Chao EYS, Rubin CT, Aro HT, Einhorn TA. Bone Injury, Regeneration, and Repair. In: Buckwalter JA, Einhorn TA, Simon SR, American Academy of Orthopaedic Surgeons., editors. Orthopaedic basic science : biology and biomechanics of the musculoskeletal system. Rosemont, IL: American Academy of Orthopaedic Surgeons; 2000. p 372-399.
147. Skutek M, van Griensven M, Zeichen J, Brauer N, Bosch U. Cyclic mechanical stretching modulates secretion pattern of growth factors in human tendon fibroblasts. Eur J Appl Physiol 2001;86(1):48-52.
148. Yaeger PC, Masi TL, de Ortiz JL, Binette F, Tubo R, McPherson JM. Synergistic action of transforming growth factor-beta and insulin-like growth factor-I induces expression of type II collagen and aggrecan genes in adult human articular chondrocytes. Exp Cell Res 1997;237(2):318-25.
149. Holt GE, Halpern JL, Dovan TT, Hamming D, Schwartz HS. Evolution of an in vivo bioreactor. J Orthop Res 2005;23(4):916-23.
150. Jagodzinski M, Drescher M, Zeichen J, Hankemeier S, Krettek C, Bosch U, van Griensven M. Effects of cyclic longitudinal mechanical strain and dexamethasone on osteogenic differentiation of human bone marrow stromal cells. Eur Cell Mater 2004;7:35-41; discussion 41.
151. Zegzula HD, Buck DC, Brekke J, Wozney JM, Hollinger JO. Bone formation with use of rhBMP-2 (recombinant human bone morphogenetic protein-2). J Bone Joint Surg Am 1997;79(12):1778-90.
152. Sellke FW, Laham RJ, Edelman ER, Pearlman JD, Simons M. Therapeutic angiogenesis with basic fibroblast growth factor: technique and early results. Ann Thorac Surg 1998;65(6):1540-4.
153. Cowin SC. Tissue growth and remodeling. Annu Rev Biomed Eng 2004;6:77-107.
154. Grodzinsky AJ, Levenston ME, Jin M, Frank EH. Cartilage tissue remodeling in response to mechanical forces. Annu Rev Biomed Eng 2000;2:691-713.

155. Langelier E, Rancourt D, Bouchard S, Lord C, Stevens PP, Germain L, Auger FA. Cyclic traction machine for long-term culture of fibroblast-populated collagen gels. Ann Biomed Eng 1999;27(1):67-72.
156. Yamamoto E, Tokura S, Hayashi K. Effects of cyclic stress on the mechanical properties of cultured collagen fascicles from the rabbit patellar tendon. J Biomech Eng 2003;125(6):893-901.
157. Altman GH, Lu HH, Horan RL, Calabro T, Ryder D, Kaplan DL, Stark P, Martin I, Richmond JC, Vunjak-Novakovic G. Advanced bioreactor with controlled application of multi-dimensional strain for tissue engineering. Journal of biomechanical engineering. 2002;124(6):742-9.
158. Grenier G, Râemy-Zolghadri M, Larouche D, Gauvin R, Baker K, Bergeron F, Dupuis D, Langelier E, Rancourt D, Auger FA and others. Tissue reorganization in response to mechanical load increases functionality. Tissue Eng 2005;11(1-2):90-100.
159. Vunjak-Novakovic G, Martin I, Obradovic B, Treppo S, Grodzinsky AJ, Langer R, Freed LE. Bioreactor cultivation conditions modulate the composition and mechanical properties of tissue-engineered cartilage. J Orthop Res 1999;17(1):130-8.
160. Goldstein AS, Juarez TM, Helmke CD, Gustin MC, Mikos AG. Effect of convection on osteoblastic cell growth and function in biodegradable polymer foam scaffolds. Biomaterials 2001;22(11):1279-88.
161. Wendt D, Marsano A, Jakob M, Heberer M, Martin I. Oscillating perfusion of cell suspensions through three-dimensional scaffolds enhances cell seeding efficiency and uniformity. Biotechnol Bioeng 2003;84(2):205-14.
162. Darling EM, Athanasiou KA. Articular cartilage bioreactors and bioprocesses. Tissue Eng 2003;9(1):9-26.
163. Gooch KJ, Kwon JH, Blunk T, Langer R, Freed LE, Vunjak-Novakovic G. Effects of mixing intensity on tissue-engineered cartilage. Biotechnol Bioeng 2001;72(4):402-7.
164. Whitlock PW, Smith TL, Poehling GG, Shilt JS, Van Dyke M. A naturally derived, cytocompatible, and architecturally optimized scaffold for tendon and ligament regeneration. Biomaterials 2007;28(29):4321-9.
165. Kang HJ, Kang ES. Ideal concentration of growth factors in rabbit's flexor tendon culture. Yonsei Med J 1999;40(1):26-9.
166. Abrahamsson SO, Lohmander S. Differential effects of insulin-like growth factor-I on matrix and DNA synthesis in various regions and types of rabbit tendons. J Orthop Res 1996;14(3):370-6.
167. Chan BP, Fu S, Qin L, Lee K, Rolf CG, Chan K. Effects of basic fibroblast growth factor (bFGF) on early stages of tendon healing: a rat patellar tendon model. Acta Orthop Scand 2000;71(5):513-8.
168. Aspenberg P, Forslund C. Enhanced tendon healing with GDF 5 and 6. Acta orthopaedica Scandinavica. 1999;70(1):51-4.
169. Wolfman NM, Hattersley G, Cox K, Celeste AJ, Nelson R, Yamaji N, Dube JL, DiBlasio-Smith E, Nove J, Song JJ and others. Ectopic induction of tendon and ligament in rats by growth and differentiation factors 5, 6, and 7, members of the TGF-beta gene family. The Journal of clinical investigation. 1997;100(2):321-30.
170. Lou J, Tu Y, Ludwig FJ, Zhang J, Manske PR. Effect of bone morphogenetic protein-12 gene transfer on mesenchymal progenitor cells. Clinical orthopaedics and related research. 1999(369):333-9.

171. Fu SC, Wong YP, Chan BP, Pau HM, Cheuk YC, Lee KM, Chan KM. The roles of bone morphogenetic protein (BMP) 12 in stimulating the proliferation and matrix production of human patellar tendon fibroblasts. Life sciences. 2003;72(26):2965-74.
172. Rengachary SS. Bone morphogenetic proteins: basic concepts. Neurosurg Focus 2002;13(6):e2.
173. Wang QW, Chen ZL, Piao YJ. Mesenchymal stem cells differentiate into tenocytes by bone morphogenetic protein (BMP) 12 gene transfer. Journal of bioscience and bioengineering. 2005;100(4):418-22.
174. Lou J, Tu Y, Burns M, Silva MJ, Manske P. BMP-12 gene transfer augmentation of lacerated tendon repair. Journal of orthopaedic research : official publication of the Orthopaedic Research Society. 2001;19(6):1199-202.
175. Walker DH, Wright NM. Bone morphogenetic proteins and spinal fusion. Neurosurg Focus 2002;13(6):e3.
176. Ralphs JR, Waggett AD, Benjamin M. Actin stress fibres and cell-cell adhesion molecules in tendons: organisation in vivo and response to mechanical loading of tendon cells in vitro. Matrix Biol 2002;21(1):67-74.
177. Chiquet-Ehrismann R, Tannheimer M, Koch M, Brunner A, Spring J, Martin D, Baumgartner S, Chiquet M. Tenascin-C expression by fibroblasts is elevated in stressed collagen gels. J Cell Biol 1994;127(6):2093-101.
178. Chen J, Horan RL, Bramono D, Moreau JE, Wang Y, Geuss LR, Collette AL, Volloch V, Altman GH. Monitoring Mesenchymal Stromal Cell Developmental Stage to Apply On-Time Mechanical Stimulation for Ligament Tissue Engineering. Tissue Eng 2006.
179. Neidlinger-Wilke C, Grood E, Claes L, Brand R. Fibroblast orientation to stretch begins within three hours. J Orthop Res 2002;20(5):953-6.
180. Neidlinger-Wilke C, Grood ES, Wang J-C, Brand RA, Claes L. Cell alignment is induced by cyclic changes in cell length: studies of cells grown in cyclically stretched substrates. J Orthop Res 2001;19(2):286-93.
181. Takakuda K, Koyama Y, Matsumoto HN, Katakura H, Muneta T. Effects of Cyclic Tensile Forces on the Strength of Fibrous Tissue Examined in an in vivo Model. JSME International Journal. C Series, Mechanical systems, machine elements and manufacturing 2004;47(4).
182. Slack C, Flint MH, Thompson BM. The effect of tensional load on isolated embryonic chick tendons in organ culture. Connect Tissue Res 1984;12(3-4):229-47.
183. Yamamoto E, Iwanaga W, Miyazaki H, Hayashi K. Effects of static stress on the mechanical properties of cultured collagen fascicles from the rabbit patellar tendon. J Biomech Eng 2002;124(1):85-93.
184. Milthorpe BK. Xenografts for tendon and ligament repair. Biomaterials 1994;15(10):745-52.
185. McFetridge PS, Daniel JW, Bodamyali T, Horrocks M, Chaudhuri JB. Preparation of porcine carotid arteries for vascular tissue engineering applications. J Biomed Mater Res A 2004;70(2):224-34.
186. Gilbert TW, Sellaro TL, Badylak SF. Decellularization of tissues and organs. Biomaterials. 2006;27(19):3675-83.
187. Ketchedjian A, Jones AL, Krueger P, Robinson E, Crouch K, Wolfinbarger L, Jr., Hopkins R. Recellularization of decellularized allograft scaffolds in ovine

great vessel reconstructions. The Annals of thoracic surgery. 2005;79(3):888-96; discussion 896.
188. Noyes FR, Grood ES. The strength of the anterior cruciate ligament in humans and rhesus monkeys. Journal of Bone and Joint Surgery 1976;58(8):1074-82.
189. Hoenicka M, Lehle K, Jacobs VR, Schmid FX, Birnbaum DE. Properties of the Human Umbilical Vein As a Living Scaffold for a Tissue-Engineered Vessel Graft. Tissue Eng 2007;13(1):220-9.
190. Oegema TR, Jr., Deloria LB, Fedewa MM, Bischof JC, Lewis JL. A simple cryopreservation method for the maintenance of cell viability and mechanical integrity of a cultured cartilage analog. Cryobiology 2000;40(4):370-5.
191. Pena AI, Johannisson A, Linde-Forsberg C. Validation of flow cytometry for assessment of viability and acrosomal integrity of dog spermatozoa and for evaluation of different methods of cryopreservation. J Reprod Fertil Suppl 2001;57:371-6.
192. Alvarez-Barreto JF, Sikavitsas VI. Improved mesenchymal stem cell seeding on RGD-modified poly(L-lactic acid) scaffolds using flow perfusion. Macromol Biosci 2007;7(5):579-88.
193. Sikavitsas VI, Bancroft GN, Lemoine JJ, Liebschner MA, Dauner M, Mikos AG. Flow perfusion enhances the calcified matrix deposition of marrow stromal cells in biodegradable nonwoven fiber mesh scaffolds. Ann Biomed Eng 2005;33(1):63-70.
194. Cartmell JS, Dunn MG. Effect of chemical treatments on tendon cellularity and mechanical properties. Journal of biomedical materials research. 2000;49(1):134-40.
195. Maciel KT, Carvalho RM, Ringle RD, Preston CD, Russell CM, Pashley DH. The effects of acetone, ethanol, HEMA, and air on the stiffness of human decalcified dentin matrix. J Dent Res 1996;75(11):1851-8.
196. Shimko DA, White KK, Nauman EA, Dee KC. A device for long term, in vitro loading of three-dimensional natural and engineered tissues. Ann Biomed Eng 2003;31(11):1347-56.
197. Tai JT, Brooks EE, Liang S, Somogyi R, Rosete JD, Lawn RM, Shiffman D. Determination of temporal expression patterns for multiple genes in the rat carotid artery injury model. Arterioscler Thromb Vasc Biol 2000;20(10):2184-91.
198. Maekawa Y, Anzai T, Yoshikawa T, Sugano Y, Mahara K, Kohno T, Takahashi T, Ogawa S. Effect of granulocyte-macrophage colony-stimulating factor inducer on left ventricular remodeling after acute myocardial infarction. J Am Coll Cardiol 2004;44(7):1510-20.
199. Livak KJ, Schmittgen TD. Analysis of Relative Gene Expression Data Using Real-Time Quantitative PCR and the 2- ??CT Method. Methods 2001;25(4):402-408.
200. Doroski DM, Brink KS, Temenoff JS. Techniques for biological characterization of tissue-engineered tendon and ligament. Biomaterials 2007;28(2):187-202.
201. Kraitchman DL, Heldman AW, Atalar E, Amado LC, Martin BJ, Pittenger MF, Hare JM, Bulte JW. In vivo magnetic resonance imaging of mesenchymal stem cells in myocardial infarction. Circulation 2003;107(18):2290-3.
202. Ingber DE. Cellular mechanotransduction: putting all the pieces together again. Faseb J 2006;20(7):811-27.

203. Juncosa-Melvin N, Matlin KS, Holdcraft RW, Nirmalanandhan VS, Butler DL. Mechanical stimulation increases collagen type I and collagen type III gene expression of stem cell-collagen sponge constructs for patellar tendon repair. Tissue Eng 2007;13(6):1219-26.
204. Wang IN, Shan J, Choi R, Oh S, Kepler CK, Chen FH, Lu HH. Role of osteoblast-fibroblast interactions in the formation of the ligament-to-bone interface. J Orthop Res 2007;25(12):1609-20.
205. Mikos AG, Herring SW, Ochareon P, Elisseeff J, Lu HH, Kandel R, Schoen FJ, Toner M, Mooney D, Atala A and others. Engineering complex tissues. Tissue Eng 2006;12(12):3307-39.
206. Spalazzi JP, Dagher E, Doty SB, Guo XE, Rodeo SA, Lu HH. In vivo evaluation of a multiphased scaffold designed for orthopaedic interface tissue engineering and soft tissue-to-bone integration. J Biomed Mater Res A 2008;86(1):1-12.
207. Kurosaka M, Yoshiya S, Andrish JT. A biomechanical comparison of different surgical techniques of graft fixation in anterior cruciate ligament reconstruction. Am J Sports Med 1987;15(3):225-9.
208. Robertson DB, Daniel DM, Biden E. Soft tissue fixation to bone. Am J Sports Med 1986;14(5):398-403.
209. Zelle BA, Lattermann C, Chhabra A, Fu FH, Huard J. Biological considerations of tendon graft incorporation within the bone tunnel. Operative Techniques in Orthopaedics 2005;15(1):36-42.
210. Dunn MG, Maxian SH, Zawadsky JP. Intraosseous incorporation of composite collagen prostheses designed for ligament reconstruction. J Orthop Res 1994;12(1):128-37.
211. Baksh D, Yao R, Tuan RS. Comparison of proliferative and multilineage differentiation potential of human mesenchymal stem cells derived from umbilical cord and bone marrow. Stem Cells 2007.
212. Karahuseyinoglu S, Cinar O, Kilic E, Kara F, Akay GG, Demiralp DO, Tukun A, Uckan D, Can A. Biology of stem cells in human umbilical cord stroma: in situ and in vitro surveys. Stem Cells 2007;25(2):319-31.
213. Wu KH, Zhou B, Yu CT, Cui B, Lu SH, Han ZC, Liu YL. Therapeutic potential of human umbilical cord derived stem cells in a rat myocardial infarction model. Ann Thorac Surg 2007;83(4):1491-8.
214. Cho SR, Yang MS, Yim SH, Park JH, Lee JE, Eom YW, Jang IK, Kim HE, Park JS, Kim HO and others. Neurally induced umbilical cord blood cells modestly repair injured spinal cords. Neuroreport 2008;19(13):1259-63.
215. Weiss ML, Medicetty S, Bledsoe AR, Rachakatla RS, Choi M, Merchav S, Luo Y, Rao MS, Velagaleti G, Troyer D. Human umbilical cord matrix stem cells: preliminary characterization and effect of transplantation in a rodent model of Parkinson's disease. Stem Cells 2006;24(3):781-92.
216. Weiss ML, Anderson C, Medicetty S, Seshareddy KB, Weiss RJ, Vanderwerff I, Troyer D, McIntosh KR. Immune Properties of Human Umbilical Cord Wharton's Jelly-Derived Cells. Stem Cells 2008.
217. Crouzier T, McClendon T, Tosun Z, McFetridge PS. Inverted human umbilical arteries with tunable wall thicknesses for nerve regeneration. J Biomed Mater Res A 2008.
218. Dardik H, Wengerter K, Qin F, Pangilinan A, Silvestri F, Wolodiger F, Kahn M, Sussman B, Ibrahim IM. Comparative decades of experience with

glutaraldehyde-tanned human umbilical cord vein graft for lower limb revascularization: an analysis of 1275 cases. J Vasc Surg 2002;35(1):64-71.
219. Li WC, Zhang HM, Wang PJ, Xi GM, Wang HQ, Chen Y, Deng ZH, Zhang ZH, Huang TZ. Quantitative analysis of the microstructure of human umbilical vein for assessing feasibility as vessel substitute. Ann Vasc Surg 2008;22(3):417-24.
220. Scharn DM, Dirven M, Barendregt WB, Boll AP, Roelofs D, van der Vliet JA. Human umbilical vein versus heparin-bonded polyester for femoro-popliteal bypass: 5-year results of a prospective randomized multicentre trial. Eur J Vasc Endovasc Surg 2008;35(1):61-7.
221. Mondalek FG, Lawrence BJ, Kropp BP, Grady BP, Fung KM, Madihally SV, Lin HK. The incorporation of poly(lactic-co-glycolic) acid nanoparticles into porcine small intestinal submucosa biomaterials. Biomaterials 2008;29(9):1159-66.
222. Truskey GA, Yuan F, Katz DF. Transport phenomena in biological systems. Upper Saddle River, NJ: Pearson Prentice Hall; 2004. 317-321 p.
223. Khalil E, Kretsos K, Kasting GB. Glucose partition coefficient and diffusivity in the lower skin layers. Pharm Res 2006;23(6):1227-34.
224. Prausnitz MR, Noonan JS. Permeability of cornea, sclera, and conjunctiva: a literature analysis for drug delivery to the eye. J Pharm Sci 1998;87(12):1479-88.
225. Pitkanen L, Ranta VP, Moilanen H, Urtti A. Permeability of retinal pigment epithelium: effects of permeant molecular weight and lipophilicity. Invest Ophthalmol Vis Sci 2005;46(2):641-6.
226. Cruysberg LP, Nuijts RM, Geroski DH, Gilbert JA, Hendrikse F, Edelhauser HF. The influence of intraocular pressure on the transscleral diffusion of high-molecular-weight compounds. Invest Ophthalmol Vis Sci 2005;46(10):3790-4.
227. Maher JF. Replacement of Renal Function by Dialysis: A Textbook of Dialysis: Kluwer Academic Publishers; 1989.
228. Awad HA, Butler DL, Harris MT, Ibrahim RE, Wu Y, Young RG, Kadiyala S, Boivin GP. In vitro characterization of mesenchymal stem cell-seeded collagen scaffolds for tendon repair: effects of initial seeding density on contraction kinetics. J Biomed Mater Res 2000;51(2):233-40.
229. Lode A, Bernhardt A, Gelinsky M. Cultivation of human bone marrow stromal cells on three-dimensional scaffolds of mineralized collagen: influence of seeding density on colonization, proliferation and osteogenic differentiation. J Tissue Eng Regen Med 2008;2(7):400-7.
230. Stolzing A, Coleman N, Scutt A. Glucose-induced replicative senescence in mesenchymal stem cells. Rejuvenation Res 2006;9(1):31-5.
231. Pottler M, Zierler S, Kerschbaum HH. An artificial three-dimensional matrix promotes ramification in the microglial cell-line, BV-2. Neurosci Lett 2006;410(2):137-40.
232. Cukierman E, Pankov R, Stevens DR, Yamada KM. Taking cell-matrix adhesions to the third dimension. Science 2001;294(5547):1708-12.
233. Walpita D, Hay E. Studying actin-dependent processes in tissue culture. Nat Rev Mol Cell Biol 2002;3(2):137-41.
234. Pankov R, Endo Y, Even-Ram S, Araki M, Clark K, Cukierman E, Matsumoto K, Yamada KM. A Rac switch regulates random versus directionally persistent cell migration. J Cell Biol 2005;170(5):793-802.

235. Yamada KM, Pankov R, Cukierman E. Dimensions and dynamics in integrin function. Brazilian Journal of Medical and Biological Research 2003;36:959-966.